STUDY ON SLOPE STABILITY OF PENANG ISLAND CONSIDERING EARTHQUAKE AND RAINFALL EFFECTS

Mastura Binti Azmi

March 2014

DECLARATION OF THESIS STATUS

I hereby declare that this thesis entitled 'STUDY ON SLOPE STABILITY OF PENANG ISLAND CONSIDERING EARTHQUAKE AND RAINFALL EFFECTS' has been presented and verified by a group of examiner as partial fulfilment of the requirements of degree of Doctoral of Engineering in Graduate School of Engineering, Kyoto University, Japan.

Professor Junji Kiyono

J. Kiyono

(Advisor)
Date: 28/01/2014

Associate Professor Aiko Furukawa

A. Furukawa

(Co-advisor)
Date: 29/01/2014

ABSTRACT

Vast development of hillsides especially in developing countries such as Malaysia always leads to landslides. Failure in design, construction negligence and external factors such as rainfall and earthquakes are usually the main reasons of failure in slopes. This study aims to understand this problem and tries to connect the possibility of landslide occurrence with regards to rainfall and earthquakes. Penang Island was chosen as site of interest as it was classified as highly susceptible of landslides by the government. Analyses start with probabilistic assessment of seismic hazard. Using probabilistic seismic hazard analysis, Peak Ground Acceleration (PGA) map for Penang Island was produced for several probabilities of occurrences. Then, analyses continued with probabilistic assessment on rainfall events. Using 60 years rainfall data, the best distribution function was selected to describe the probability of exceedance of rainfall for several return periods. Using this result, changes in groundwater level with regards to accumulated antecedent rainfall were then determined. Different groundwater levels were recorded for several return periods and these results are combined with the PGA results from the seismic analysis. In the last part of this study, all data collected in initial part of the study are used to check the stability of slopes using static and dynamic analyses. Results shown were based on return period of earthquake occurrences (98years, 475years, 975years and 2500years) and groundwater levels (1.25years, 2years, 5 years and 10years). The results shows that with higher groundwater levels and higher earthquake acceleration inputs, slopes are more susceptible to larger deformation.

ACKNOWLEDGEMENT

In the name of the Almighty God, I am ever grateful to Him to be able to finish my work. I also would like to express my gratitude to both my supervisors, Professor Junji Kiyono and Associate Professor Aiko Furukawa for their undivided attention and continuous help during the completion of this work.

I want to take this opportunity to thank my husband, Muhd Harris Ramli who never fails to encourage, support and always be there for me. To my children (Aiman and Aidan), my father, my stepmother and my mother in-law, my sister, families and friends, thank you for lending your shoulder and listen to my problems and encourage me to do my best.

I would also like to acknowledge and thank my colleagues who have provided sufficient help and data to ease my study and thank you to my scholarship provider, the Malaysian government and Universiti Sains Malaysia.

I am not who I am today without everybody's help so thank you so much from the bottom of my heart.

TABLE OF CONTENTS

LIST OF FIGURES

LIST OF TABLES

Chapter 1

INTRODUCTION

1.1 General Overview

In the world we are currently living where disasters and catastrophes are inevitable, it is important for us to really understand the impact of each event. Furthermore, individual disasters nowadays do not occur as a single event but usually as a combination of events. Earthquakes with landslides, earthquakes and tsunamis or typhoons with heavy flooding are some of the combinations of such terrifying events. Engineers and researchers always foresee these as a single event and try to solve them separately. But since large and major disasters occur in combination, further studies and rigorous research need to be done to overcome the problem.

Looking at the impact due to occurrences of disasters, it affects not only human lives but also the economic, social as well as well-being of the affected place. A larger disaster contributes a larger impact upon society. Human security is therefore an important criterion that needs to be taken into account when considering the impact of a disaster upon society.

A major disaster that has been given a lot of interest recently in geotechnical engineering is the earthquake-induced landslide. Landslides are one of the major disaster events that have caused a lot of impact not only to human lives but to the engineering aspect too. When landslides are combined with earthquakes the results are disasters that are hard to predict.

Landslide processes are part of the normal geomorphic cycles of landscape development. The term ‘landslide’ denotes the movement of a mass of rock, debris or earth down a slope. The recent intensification of land-use changes has raised the level of landslide susceptibility, particularly in mountainous regions. It is especially serious in developing countries where environmental protection and management are harder to sustain. Over 95% of all disasters and fatalities related to landslides in particular, and

mass movement in general, occur in developing countries.

All landslides have two things in common: (a) they are the result of the failure of the soil and rock materials that make up the hill slope and (b) they are driven by gravity, can be triggered by earthquakes, volcanic eruptions, soils saturated by heavy rain or groundwater rise, and river undercutting. An earthquake's shaking of saturated soils creates particularly dangerous conditions. Although landslides are highly localised, they can be particularly hazardous due to their frequency of occurrence.

Earthquakes on the other hand have always been associated with ground movement, sliding and liquefaction. In fact, earthquake-induced landslides have caused major casualties in recent years particularly when referring to the previous Chi-Chi earthquake or the 1970’s Peru earthquake.

In Southeast Asian countries like Indonesia, Malaysia, Thailand or the Philippines, monsoon seasons as well as tropical rainstorms bring heavy rainfalls that sometimes make slope stability critical and may lead to its failure. For some countries, such as Malaysia, rainfall-induced landslides are so significant and have always been a headline story all over the country. This is due to the fact that hundreds of lives have been taken due to this type of disaster.

With regards to landslide occurrences in Southeast Asia, prediction and hazard management is far from what most developed country can achieve. Developed countries, such as the United States as well as Japan, have been implementing rigorous hazard risk assessment and management through predictions as well as implementing it through laws and regulations, especially on hillside developments. Although it may sound impossible to use the same precision as has been conducted by developed countries there is still the need to provide early awareness to the public in order to reduce the impact of landslides in developing nations.

1.2 Overview of Landslides in Malaysia

Malaysia is a tropical country that experiences a lot of rainfall and most of the time this leads to landslides. Landslides commonly occur, especially in big cities where the development of hillside areas is uncontrollable and there are no strict regulations to guide the development. Mukhlisin[1] stated that the Malaysia Public Works Department (PWD) has identified more than 100 hillslopes around Malaysia as risky areas. In Malaysia, most landslides occur on man-made slopes due to lack of maintenance, construction negligence and design errors. On top of that, the biggest cause triggering landslides in Malaysia is heavy rainfall, especially during the monsoon season when Malaysia receives very high rainfall. Jamaludin[2] explains that shallow landslides are the most common landslide type to occur and are triggered due to heavy rainfall that lead to head loss in matrix suction areas in unsaturated areas.

The first recorded national landslide in Malaysia was in 1961[3]. Although it was not the first one officially recorded, it was the official first after Malaysian independence was achieved in 1957. The tragedy occurred at Ringlet, Pahang and resulted in 16 deaths. After that event, an increasing number of deaths due to landslide tragedies have occurred. From 1973 to 2000, about 440 landslides have been recorded with almost 600 lives claimed due to landslide catastrophes[3]. This is shown in Fig. 1.1 below. It can be seen that fatalities have increased after the 1990s. This was the time when development of hilly terrain and slopes was significant due to urbanisation.

It was due to the Highland Towers Tragedy on 11 December 1993, which claimed 48 lives that the government decided to set up several related agencies to form the special force to help mitigate the nation when disaster occurs. This was the time when not only the government but also the public started to notice the importance of landslide catastrophes. Another record of the highest fatality for a single landslide event occurred on 26 December 1996 when debris flow caused by Tropical Storm Gregg wiped out a few villages in Keningau, Sabah and claimed 302 lives.

Landslides do not only affect human lives but also the national economy. This can be seen through the losses of public infrastructure, such as road networks, and indirect

losses, such as business trips and interrupted schedules. Therefore, a landslide early warning system together with probability assessment of future landslides is important not only to predict landslides but also to plan future land-use.

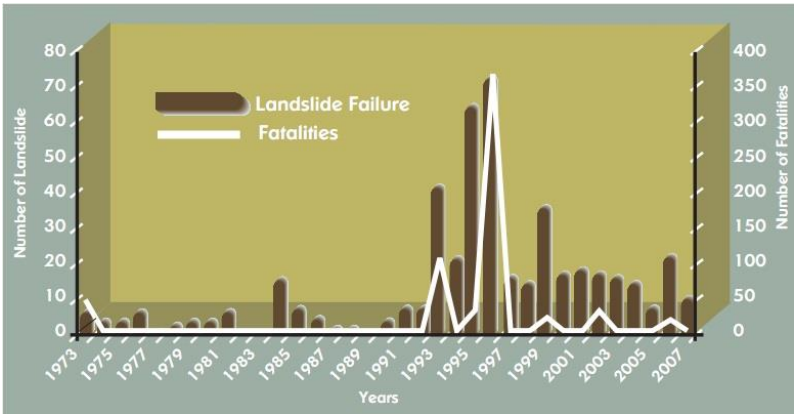

Fig. 1.1 Reported landslides and fatalities 1973-2007 (National Slope Master Plan, Public Works Department Malaysia[22])

Records of historical occurrences of landslides were compiled by Jaapar[4] and shown in Table 1.1. He listed all records of landslides which occurred from 1990-2004 and the record include date, location, fatalities, injuries and loss in monetary and property terms.

Table 1.1 List of major landslide events in Malaysia (Jaapar[4])

No	Date	Case	Fatalities	Losses
1	11 December 1993	Collapse of Highland Towers	48	1 apartment building collapse
2	30 June 1995	Genting Sempah Debris Flow	20 + 1 missing	Road closure
3	6 January 1996	Gunung Tempurung Slope Failure	1	Road closure
4	30 August 1996	Pos Dipang Debris Flow	44	Village
5	28 November 1998	Paya Terubong Rockslide	-	17 cars
6	7 February 1999	Sandakan Landslide	17	Houses
7	15 May 1999	Bukit Antarabangsa Landslide	-	Blocked route for 10,000 residents
8	28 January 2002	Ruan Changkul Landslide	16	Houses
9	20 November 2002	Taman Hillview Landslide	8	Houses
10	26 November 2003	Bukit Lanjan Rockslide	-	Highway closure for 6 months

Fig. 1.2 Some of landslide events in Malaysia (Jaapar[4])

1.3 Previous Study on Malaysian Landslide

There are 4 methods to assess slope hazard as mention by Varnes[5], such as from inventory analysis, the heuristic approach, the statistical method and the deterministic approach. In Malaysia, there are a lot of researchers doing research on landslides. Mukhlisin[1], Pradhan[6]–[8] and Huat[9] evaluate slopes using the GIS method. They use available mapping data and records to model landslide hazard. These studies cover large scale areas and this can predict the landslide hazard using land-use data. Lee *et al*[10] and Ng[11] studied the effect of rainfall on Malaysian slopes. They evaluated the amount of antecedent rainfall and the effect of rainfall infiltration on the suction envelope in slopes. The method uses limited equilibrium analysis to determine the safety of slopes in Malaysia.

Jamaludin and Ali[2] try to find empirical correlations between rainfall and shallow landslides in Malaysia. In that study, they discussed two empirical thresholds, such as Intensity-Duration and Intensity-Working Rainfall. The working rainfall is described as similar with accumulated antecedent rainfall by Crozier[12].

Some other researchers did research based on events, as mentioned by Jaapar[4], and studied the physical properties and failure mode of landslides for big landslides events in Malaysia.

1.4 Earthquakes in Malaysia

Malaysia is located on the stable Sunda Shelf with low to moderate seismic activity and is surrounded by active seismic faults. Although Malaysia has not experienced major earthquakes, recently tremors are repeatedly felt due to surrounding earthquake occurrences. Some of the earthquake tremors felt in Malaysia were due to large earthquakes originating from the intersection between the Eurasian and Indo-Australian plates near Sumatera while others are from the Great Sumatran fault.

Examples of earthquake occurrences that affected Malaysia are the magnitude 7.4 earthquake on 2nd November 2002 that caused cracks on buildings in Penang and also the magnitude 7.3 earthquake that occurred on 25th July 2004 in South Sumatera. The latter earthquake occurrence was more than 400km from Johor Bahru (south of Peninsular Malaysia) which caused cracks on some apartments there. Although no casualties were reported due to this earthquake it caused panic to people living near the scene. Some of the reported earthquake events felt in Malaysia are shown in Table 1.2 below.

Table 1.2 Earthquake shocks felt in Malaysia (National Slope Master Plan[22])

State	Frequencies	Maximum Intensity Observed (Modified Mercalli Scale)
Peninsular Malaysia (1909-2005)		
Perlis	2	IV
Kedah	9	V
Penang	31	VI
Perak	18	VI
Selangor/ Kuala Lumpur	37	VI
Negeri Sembilan	4	V
Melaka	9	V
Johor	21	VI
Pahang	4	III
Terengganu	1	IV
Kelantan	3	IV
Sabah & Sarawak (1923-2005)		
Sabah	24	VII
Sarawak	5	V

Table 1.3 shows a comparison between acceleration (*gal*) and other seismic intensities scales, such as the Modified Mercalli Intensity (MMI) scale, Japan Meteorological Agency (JMA) scale and the Medvedev-Sponheuer-Karnik (MSK) scale. It can be seen from Table 1.2, records of earthquakes felt on Penang Island are between 2-95gal.

In East Malaysia, earthquakes felt were of a small to moderate magnitude from a local origin and tremors originated from the southern part of the Eurasian and Phillipines

plates as mentioned by Hendriyawan[13]. Some of the examples of earthquake occurrences in East Malaysia were the 1976 Lahad Datu 5.8 magnitude earthquake that caused cracks on houses and buildings and also the 1991 Ranau earthquake with a magnitude of 5.2 that caused damage on housing quarters there[13].

Table 1.3 Comparison of various seismic intensities with acceleration [23], [24]

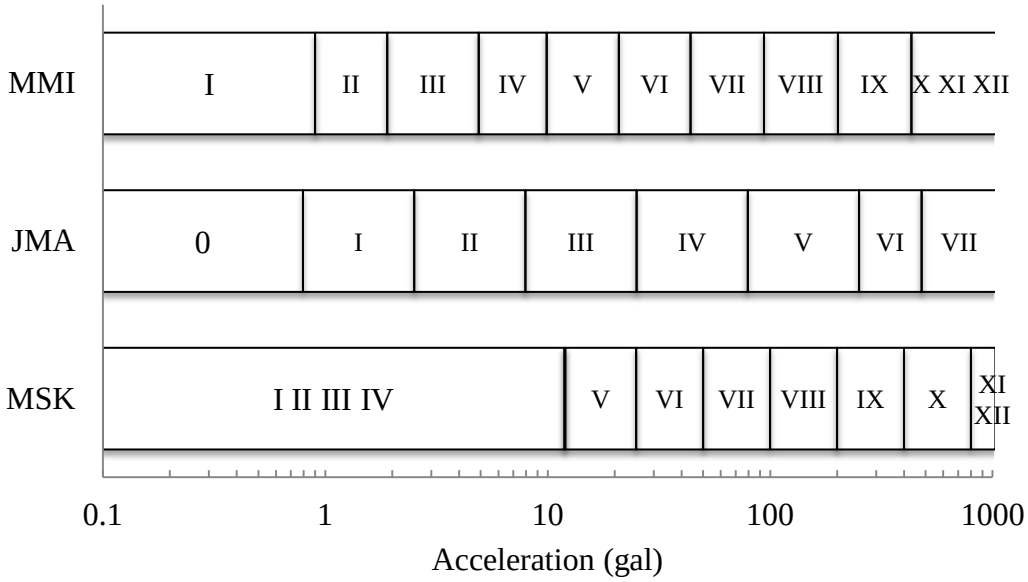

Research on the effect of earthquakes in Malaysia is not as good as other engineering fields. One of the main causes of this is the historical earthquake events in Malaysia are scarce and most research only relies on the records and experiences of earthquakes of neighbouring countries. But, there are several studies that try to look into earthquakes in Malaysia.

Taksiah *et al*[14][15] investigated the peak ground acceleration (PGA) values on several locations in Malaysia by using several attenuation relationships and tried to develop spectral acceleration using NERA software and based on the Uniform Building Code UBC (1997). Azlan *et al*[16] evaluated seismic hazard for Peninsular Malaysia by using the Gumbel distribution method. The outcome from the study is 10% and 2% probabilities of occurrences of earthquakes on Peninsular Malaysia. He also studied development of synthetic time histories for bedrock in Kuala Lumpur. Sherliza[17]

studied the effect of attenuation relationship on Malaysian soil and Hendriyawan[13] studied the PSHA method and the ground motions on Kuala Lumpur and Putrajaya.

The above mentioned researches are still not enough for Malaysia. There are still a lot of improvements that can be done in earthquake studies for the Malaysian condition. This study will be part of the development of the study about earthquakes in Malaysia and the future improvements required to be done continuously for Malaysia to be able to plan and prepare countermeasures for earthquake occurrences or tremors felt in Malaysia that affect the lives of its people.

1.5 Rainfall Studies in Malaysia

Malaysia is one of the blessed countries with very high amount of annual rainfall. The total annual rainfall amount is between 2,000 to 4,000mm and rainy days between 150 to 200 days yearly. Peninsular Malaysia is located on the equatorial line and experiences a tropical climate with monsoon seasons twice a year and sometimes experiences a dry climate due to warm ocean temperatures that cause extreme dry weather like El Nino.

The monsoon seasons of particular interest to this research are called the North East (NE) that usually occur between November to March and South West (SW) monsoons that usually occur between May to September.

Therefore, it is not new for Malaysian researchers to study the rainfall pattern in Malaysia. The Malaysian Meteorological Department played a very important role in providing a sufficient amount of data for research related to rainfall in Malaysia. The department recorded the first official observation in Malaysia in 1883 where observations of air pressure, temperature and rainfall were recorded in Penang and Malacca.

By 1971, the first automatic rain gauges were installed in Malaysia[18]. Since then there are hundreds of rain gauges installed all over Malaysia. Climatology and hydrological studies have been intensively investigated in Malaysia. The most prominent use of these

studies was directly contributed to the production of Urban Storm Water Management manual by the Department of Irrigation and Drainage Malaysia. The manual is used for guidelines for drainage design in Malaysia.

Local researchers also had played many important roles in research related to hydrology of rainfall, such as Zalina *et al*[18], Suhaila and Jemain[19] and Alias[20]. These researchers investigated the effect of extreme rainfall and adjoining wet days and used probability distribution analyses in their researches. From their results, a better understanding of rainfall patterns in Malaysia can be seen.

Part of this study also tries to determine the distribution of extreme rainfall with regards to accumulated antecedent rainfall. Mukhlisin[21] has studied the effect of antecedent rainfall on slope stability in Malaysia. He modelled the rain infiltration in slopes and determines the effect of pore-water changes in slope stability. His finding agrees that increases in pore water pressure leads to a reduction in factor of safety of a slope and increases the likelihood of slope failure.

1.6 Current Countermeasures on Landslide Susceptibility

In Malaysia, the government is the centre of all decisions that are being made related to either mitigating or controlling any hazard. It is undeniably true that the government needs to control all regulations related to the development of hill slopes. However, it is time to educate the public and private sectors that everybody is important in order to reduce the risk by increasing risk mitigation rather than spending more money on restoration. Developed countries have shown that the success of reducing landslide responsibilities relies not only on the government side but also the state and local authorities, private sectors, researches and non-profit community organisations.

In the disaster and restoration management cycle, the approach illustrated in Fig. 1.3 is well known worldwide and summarises the main actions to be carried out in relation to a disaster[3]. Four sectors in the cycle are used to differentiate what to be done before

and after a disaster. “Risk Control” is expected before any disaster occurs with certain preparedness and mitigation where else “Crisis Mitigation” are measures to be taken after the event stressing on the response and repair-restoration phase.

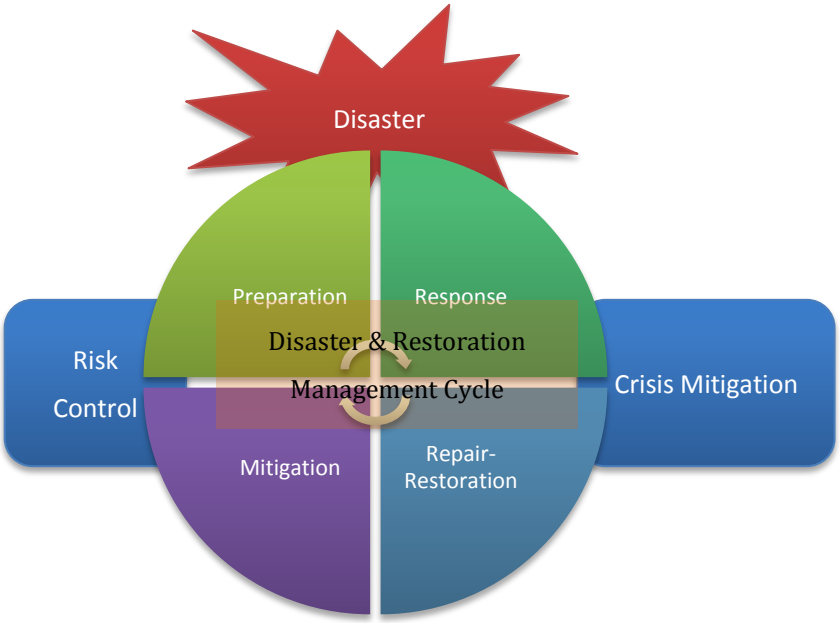

Fig. 1.3 Disaster & Restoration Management Cycle

Currently, there are very limited institutions that are looking into methods to reduce risk, monitoring potential risks and to educate public knowledge on landslide hazard awareness. Therefore, the government needs to play an important role to reduce considerably the economic damage and loss of human lives resulting from the occurrence of disastrous natural events.

Since the landslide event on December 1993 (The Highland Tower Landslide), the government has taken extra action to help reducing occurrences of big landslides[4]. After that event, a special committee was set up to study all matters regarding hazard response. The committee realies that the participation of authorities is not enough to impose regulations in order to achieve slope safety and they also imposes new regulations that all new development projects must prepare proposals with maps and

plans that detail the slope's physical characteristics and location of a buffer zone with tree sizes more than 150mm.

Following the Bukit Lanjan event in 2003, the Slope Engineering Branch was set up under the Public Works Department, Malaysia to manage road slopes and other slopes associated with government projects[4]. The functions of this branch are to reduce risk and fatalities due to landslides and to effectively use financial and manpower in repairing slopes and conducting maintenance work[4].

The Slope Engineering Branch since then has been proactive in helping the government to monitor landslide hazards. In 2009, the branch introduced the National Slope Master Plan which is being implemented from 2009 to 2023. The goal of this plan it to formulate a detailed, comprehensive and effective framework of policies, strategies and action plans to reduce risks from landslides and slopes nationwide. This plan also intends to include all activities at national, state and local levels as well as in the public and private sectors.

1.7 Malaysia Landslide Hazard Map

There are several locations in Malaysia which can be classified as high risk landslide areas (Fig. 1.4). Most of the areas have a high population density and with limited land. Thus, it can be seen that in these areas most houses are built at the toe of slopes and some are built on the slopes themselves.

A good landslide hazard map is needed in order to determine future probability of landslides in Malaysia. There are some current studies done by local researchers to provide those maps but there are still a lot of improvements that can be made. Such studies include using GIS software to provide susceptibility maps for Malaysian landslides[1] [6] [7].

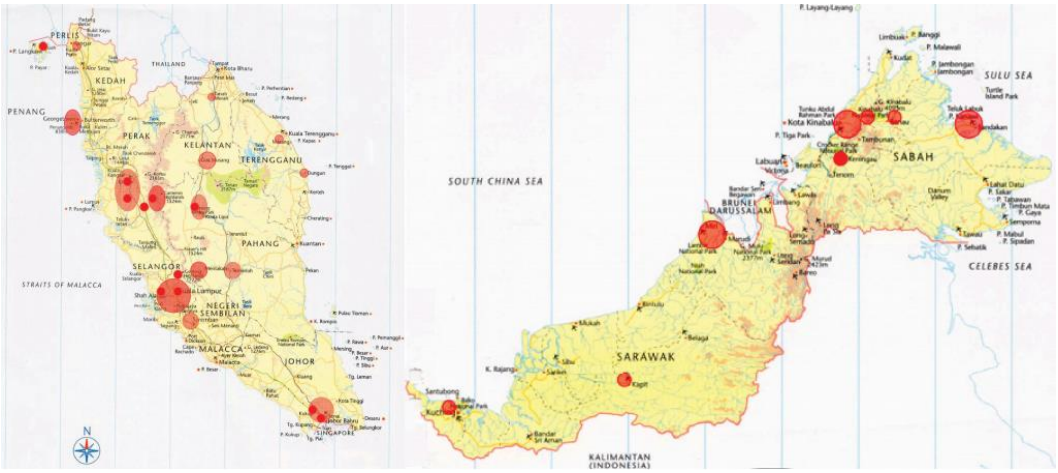

Fig. 1.4 Location of high landslide cases in Malaysia[25]

Most maps include an estimation of probability occurrences of landslides due to 1) rainfall effects; 2) geological soil type. But none of the maps cater for a combination of rainfall and earthquake effects on the probability of landslides. Therefore, this study will help to overcome this problem by introducing earthquake effects on Malaysian landslides.

The Malaysian peninsula, for example, is located about 400km from the nearest fault line in Sumatera, Indonesia and some of the earthquake tremors that happened there were also felt in Penang Island and Port Klang, Selangor. There were reports of cracks on buildings. This happened due to most structures in Malaysia not being built to sustain earthquakes.

1.8 Objectives of Study

In order to achieve the expected result, specific objectives need to be developed. An understanding on the distributions of landslides triggered by earthquakes and rainfall, its mechanisms and other associated subjects need to be addressed and carefully understood in order to forecast the landslides. This will help to evaluate the likelihood

of landslides and their impacts right after the occurrence of an earthquake or rainfall.

The actual results at the end of the study should at least be aimed towards the assessment of:

- Seismic hazard analysis of Penang Island, Malaysia.
- Rainfall distribution on Penang Island, Malaysia
- Combination of probabilistic analysis of earthquake and rainfall on Penang Island, Malaysia
- Effect of earthquake and rainfall on Penang Island slopes

1.9 Organisation of Thesis

Fig. 1.5 shows the flowchart of all chapters in this study. This thesis is composed of 6 chapters. The overall of the study includes several parts; analysis of earthquakes, analysis of rainfall, combination of earthquake and rainfall analysis and analysis of landslides. The detailed structure and content of the thesis are as follows:

Chapter 1 presents a general overview of the study and also detailed objectives and aims of the research. In this chapter reviews on previous studies related to earthquake and landslide occurrences in Malaysia are done. We also try to look into the current practices as well as researches in the field.

Chapter 2 details the probabilistic seismic hazard analysis of Penang Island. Using attenuation relationships, bedrock Peak Ground Acceleration (PGA) maps completed for Penang Island. Then, ground motion analysis using a nearby ground motion sensor as well as soil layers were used to determine the amplification factor. Using the amplification factor and bedrock PGA, hazard maps of several return periods for Penang ground are made using results from the analysis.

Chapter 3 includes analysis of probabilistic distribution of accumulated rainfall on Penang Island. Using 60 years of rainfall data collected from the local rainfall station on Penang Island, probabilistic distribution analyses were done using several methods and

goodness-of-fit was checked. The best fit distribution was selected to describe the return period of accumulated rainfall on Penang Island.

Chapter 4 describes the process of the combination of earthquakes and rainfall to the stability of a slope. In this chapter, using piezometer data, a relationship between rainfall and water heights was done. This process is important in order to do slope analysis in the next chapter. Also in this chapter, a critical location on Penang Island was chosen using GIS method. The most critical slope area with regards to a higher degree of slope was chosen as an area to be considered in the next step.

Chapter 5 shows the analysis of risk on Penang slopes due to earthquakes and rainfall. The analysis was done using results from chapters 3, 4 and 5. In this chapter, static analysis using limited equilibrium analysis was conducted followed by dynamic analysis and deformation analysis using Newmark's deformation method.

Chapter 6 summarises the results of this study

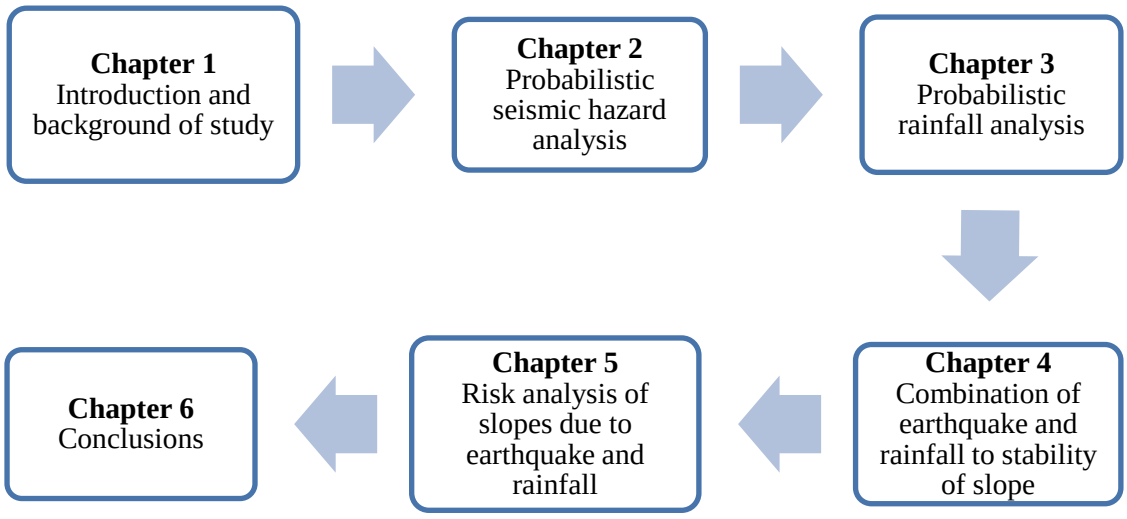

Fig. 1.5 Contents and structure of research

References

[1] M. Mukhlisin, I. Idris, A. S. Salazar, and K. Nizam, "GIS based landslide hazard mapping prediction in Ulu Klang, Malaysia," *ITB J. Sci.*, vol. 42, no. 2, pp. 163–178, 2010.

[2] S. Jamaludin and F. Ali, "An Overview of Some Empirical Correlations between Rainfall and Shallow Landslides and Their Applications in Malaysia," pp. 1429–1440.

[3] M. Azmi, J. Kiyono, and A. Furukawa, "Earthquake-induced landslide analysis for Batu Feringghi, Penang," in *Proceedings of the 31st Conference on Earthquake Engineering*, 2011, p. 5.

[4] A. R. Jaapar, "A Framework of A National Slope Safety System for Malaysia," The University of Hong Kong, 2006.

[5] D. J. Varnes, "Landslide Hazard Zonation," 1984.

[6] B. Pradhan and S. Lee, "Delineation of landslide hazard areas on Penang Island, Malaysia, by using frequency ratio, logistic regression, and artificial neural network models," *Environ. Earth Sci.*, vol. 60, no. 5, pp. 1037–1054, Jul. 2009.

[7] S. Lee and B. Pradhan, "Probabilistic landslide hazards and risk mapping on Penang Island, Malaysia," *J. Earth Syst. Sci.*, vol. 115, no. 6, pp. 661–672, Dec. 2006.

[8] B. Pradhan, "Remote sensing and GIS-based landslide hazard analysis and cross-validation using multivariate logistic regression model on three test areas in Malaysia," *Adv. Sp. Res.*, vol. 45, no. 10, pp. 1244–1256, May 2010.

[9] S. Jamaludin, B. B. K. Huat, and H. Omar, "Evaluation of slope assessment systems for predicting landslides of cut slopes in Granitic and Meta-sediment formations," *Am. J. Environ. Sci. 2*, vol. 2, no. 4, pp. 135–141, 2006.

[10] L. M. Lee, N. Gofar, and H. Rahardjo, "A simple model for preliminary evaluation of rainfall-induced slope instability," *Eng. Geol.*, vol. 108, no. 3–4, pp. 272–285, Oct. 2009.

[11] K. Y. Ng, "Rainfall-induced landslides in Hulu Kelang area, Malaysia," Universiti Tunku Abdul Rahman, 2012.

[12] K. Hennrich and M. J. Crozier, "A hillslope hydrology approach for catchment-scale slope stability analysis," *Earth Surf. Process. Landforms*, vol. 29, no. 5, pp. 599–610, May 2004.

[13] Hendriyawan, "Seismic Macrozonation of Peninsular Malaysia and Microzonation of Kuala Lumpur City Center and Putrajaya," 2007.

[14] T. Majid, S. S. Zaini, F. Mohd Nazri, M. R. Arshad, and I. F. Mohd Suhaimi, "Development of design response spectra for northern Peninsular Malaysia based on UBC 97 code," *J. - Inst. Eng. Malaysia*, vol. 68, no. 4, pp. 23–29, 2007.

[15] M. N. Fadzli and A. M. Taksiah, "Peak Ground Acceleration (PGA) for Georgetown due to Sumatran Subduction and Fault Zones," in *National Seminar on Civil Engineering Research (SEPKA)*, 2006, no. December, pp. 1–7.

[16] A. Adnan, A. Marto, and Hendriyawan, "Lesson learned from the effect of recent far field Sumatra earthquakes to Peninsular Malaysia," in *13th World Conference on Earthquake Engineering*, 2004, no. 416.

[17] S. Zaini Sooria, S. Sawada, A. Adnan, and H. Goto, "An investigation on the attenuation characteristics of distant ground motions in Peninsular Malaysia by comparing values of recorded with estimated PGA and PGV," *Malaysian J. Civ. Eng.*, vol. 22, no. 1, pp. 38–52, 2010.

[18] M. D. Zalina, K. Lumpur, and A. Mechanics, "Selecting a probability distribution for extreme rainfall series in Malaysia," no. 1991, pp. 63–68, 1993.

[19] J. Suhaila and A. A. Jemain, "Investigating the impacts of adjoining wet days on the distribution of daily rainfall amounts in Peninsular Malaysia," *J. Hydrol.*, vol. 368, no. 1–4, pp. 17–25, Apr. 2009.

[20] N. E. Alias and K. Takara, "Probability distribution for extreme hydrological values-series in the Yodo river basin, Japan and Kuala Lumpur, Malaysia," in *2nd International Conference on Water Resources*, 2012.

[21] M. Mukhlisin and M. R. Taha, "Numerical Model of Antecedent Rainfall Effect on Slope Stability at a Hillslope of Weathered Granitic Soil Formation," *J. Geol. Soc. India*, vol. 79, pp. 525–531, 2012.

Chapter 2

PROBABILISTIC SEISMIC HAZARD ANALYSIS

2.1 Introduction

Penang Island is located in the northwest of Peninsular Malaysia. The capital city of the island is Georgetown; this is a historic city with notable buildings built over 500 years of colonial reign (Fig. 2.1). Almost two-thirds of Penang Island is hillside and forest. However, because of rapid development and modernisation, the hillsides are used for housing development, roads built to connect the east and west of the island and a dam to provide water supply.

This chapter evaluates the probability of seismic hazards on Penang Island. The Island is located in a region of low seismicity with low-to-moderate seismic activity, depending on the distance from the reporting site to the epicentre (Fig. 2.2). However, recently, a number of earthquakes have affected the island, including the Great Sumatran-Andaman earthquake of 2004, which generated a tsunami as well as severe shaking on high ground. The Malaysia Meteorological Agency and mass media reported swaying of tall buildings in Georgetown itself.

Peak ground acceleration data for bedrock can be determined using probabilistic seismic hazard analysis (PSHA) and suitable empirical attenuation relationships and historical data for nearby locations. This mathematical approach can predict the potential for earthquakes. Assessment of ground responses during an earthquake, under ideal conditions, is based on the assumption that such responses are based on upward propagation of stress waves from the bedrock. Factors affecting ground responses include soil conditions and geologic features, such as the depth of soil, the bedding planes of soils overlying bedrock, changes in soil types, and faults crossing soil deposits.

The main objective in this chapter is to be able to assess and investigate the behaviour of seismicity on Penang Island by using a statistical method and to produce a map that can represent seismicity activity on the island.

Fig. 2.1 Location of Penang Island

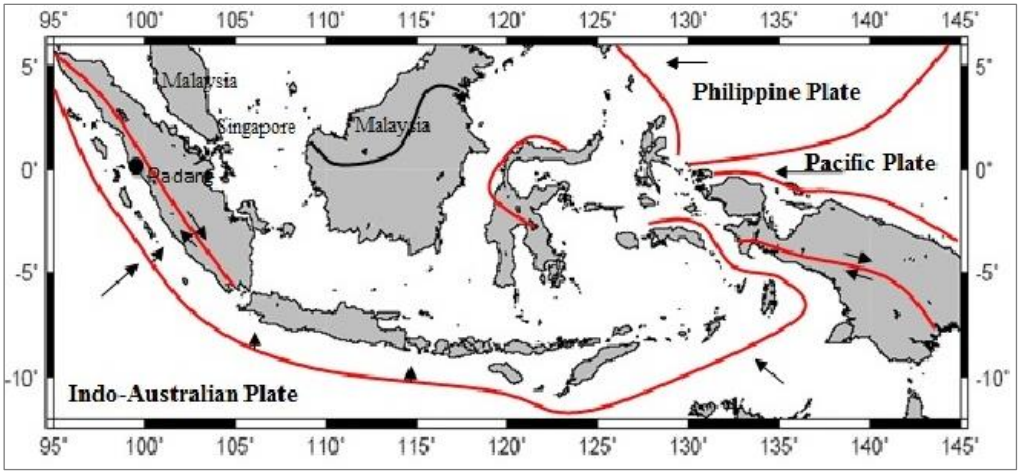

Fig. 2.2 Subduction zone surrounding Malaysia[15]

2.2 Chapter Overview

This chapter tries to evaluate the probabilistic seismic hazard analysis of Penang Island. Since data is scarce, evaluations are based on historical records from sources outside

Malaysia. Data acquisition not only include historical records but also soil layer and nearby ground motion records. The next step in this chapter is the attenuation relationship analysis. This study uses 4 attenuation relationships that are detailed in proceeding sub-chapters. Following that step, estimation of Peak Ground Acceleration (PGA) on bedrock is conducted. A map is constructed using GIS software (Manifold). Then, ground motion analysis is done using a nearby ground motion record. Using results from the bedrock PGA and ground motion analysis, estimation of PGA for local ground is completed and another map is produced. Fig. 2.3 shows the steps in this chapter.

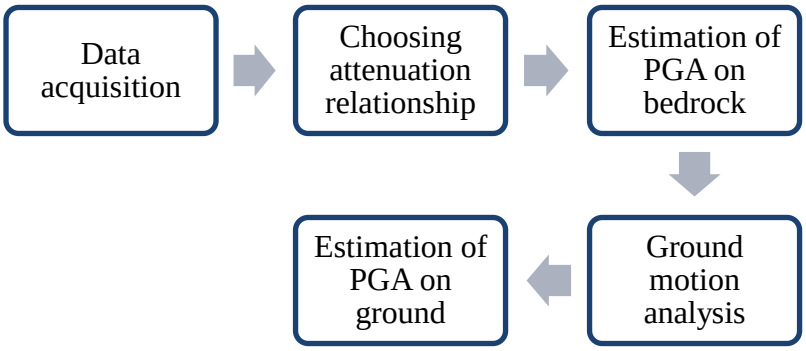

Fig. 2.3 Flowchart of chapter 2

2.3 Probabilistic Seismic Hazard Analysis (PSHA)

Probabilistic Seismic Hazard Analysis from its name uses the probabilistic approach for the analysis. The objective of PSHA is to determine the rate of exceedance of various ground motions at the site given all possible earthquake magnitudes. The probabilistic and deterministic approaches have a lot of differences[1]. For example, the deterministic approach is limited to a single specific type of earthquake. In order to use the deterministic approach, the site must behave similarly with the past records used to model the behaviour of the site of interest. The result usually has lower probability to exceed than what is expected from the analysis. In the probabilistic method, the analysis incorporates uncertainties and randomness of earthquake location as well as its

occurrences and a ground motion estimation process. This is important to allow engineers to determine the effect of an earthquake that is similar to the site of interest and determines the risk and also plans for countermeasures in the case where earthquakes might occur.

The PSHA method is a mathematical method that can quantify uncertainties in the extent of shaking and can be used to understand site behaviour during an earthquake. PSHA can map the distribution of future shaking using historical earthquake data from a particular area. The basic steps in the PSHA method are usually divided into several stages[1]. The steps include identifying all earthquake sources that are capable of producing damaging ground motion within a certain distance. Next, characterising these earthquakes and the distributions of source-to-site distances associated with potential earthquakes. Then, predicting the distribution of ground motion intensity as a function of these magnitudes and distances, and, finally, combining all uncertainties using a total probability approach.

2.3.1 Identifying earthquake sources and distances

The first step in the PSHA method is identification and characterisation of seismic sources[2]. A seismic source represents a region of the earth's crust where the characteristics of earthquake activity are recognised to be relatively different than those of the adjacent crust[1].

Peninsular Malaysia is located within the stable Sunda plate with low to moderate seismic activity levels and is characterised by low seismicity and strain rates[1][3][4]. Penang Island is located in the northwest of Peninsular Malaysia. The island has 295km^2 of land area and relevant earthquake events occur within 600km of the island (Fig.2.4). Past records showed that the island experienced tremors and tsunamis created by large earthquakes up to 450km from the island. There were about 13 earthquakes with magnitudes ranges from 5.6 to 9.0 in the last 170 years originated from the Sumatera subduction zone felt in Malaysia[1]. Examples include the 1996 earthquake with 5.4 magnitude at about 300km from coast of Perak shaken the island. The infamous magnitude 9.0 earthquake in 2004 at about 161km from west coast of

Sumatera Island also affected Penang Island and Kedah. About 68 lives were lost and 100 people were injured due to tsunami produced by the earthquake.

As most large earthquakes in Sumatra are located about 600km from the island, all historical records of earthquakes of magnitude 4.0 or more within the 600km radius were collected for analysis. The target area of this study was the area from 100.26E to 100.35E in longitude and 5.48N to 5.25N in latitude, which was divided into 49 grids (Fig.2.5). Earthquake records for magnitudes larger than 7.0 and within 600km radius from the area selected are shown in Table 2.1.

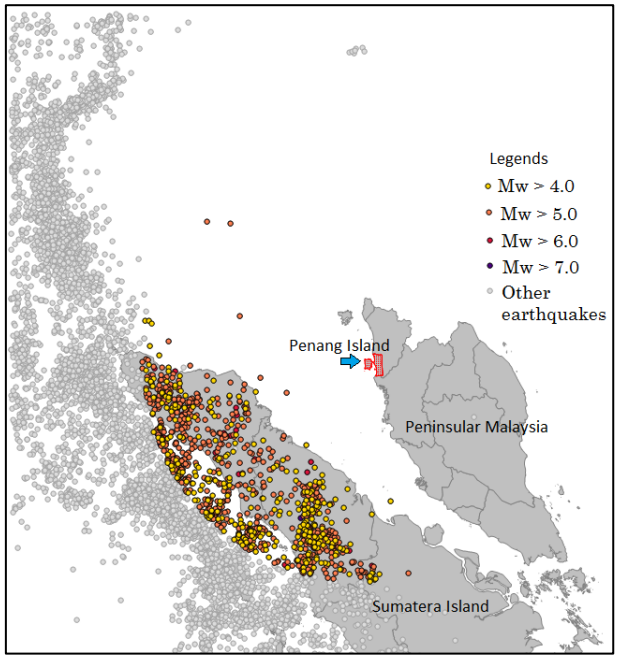

Fig. 2.4 Earthquake events within 600km (in colours) from Penang Island from 1871 to 2011

Table 2.1 Earthquake records for magnitude larger than 7.0 and distances within 600km radius from Penang Island

Date	Latitude	Longitude	Magnitude	Magnitude type	Distance
20/6/1976	3.40	96.32	7.0	MsGS	524.05
2/11/2002	2.82	96.08	7.4	MwGS	576.48
26/12/2004	3.30	95.98	9.1	Mw011	563.09
28/3/2005	2.09	97.11	8.6	MwHRV	529.97
20/2/2008	2.77	95.96	7.4	MwUCM	590.84
6/4/2010	2.38	97.05	7.8	MwGCM	514.00
9/5/2010	3.75	96.02	7.2	MwUCM	541.03

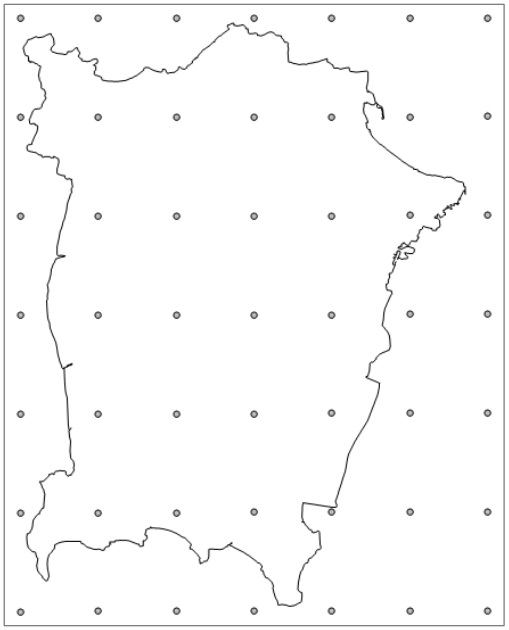

Fig. 2.5 Penang Island is divided into 49 grids

2.3.2 Earthquake catalogues and magnitudes

Estimations of the probability of earthquake occurrences are based on historical data; these are some of the important inputs if predictions are to be made. However, such data

are scarce. For this study, data were acquired from the US Geological Survey and the Indonesia Meteorology Agency (BMG). The data include historical records on earthquakes including dates, locations, magnitudes, and depths; from 1871 to 2011. There are more than 1,000 records collected for the analysis (within 600km radius). Baker[2] considers that if individual faults are not identifiable then earthquake sources can be described regionally. For Malaysia, many uncertainties on fault parameters are evident, so for this paper, an areal source model are adopted that employs only historical earthquake data. All records are converted to moment magnitudes[5].

2.4 Development of Attenuation Models and Estimation of PGA on Bedrock

2.4.1 Attenuation models suitable for Penang Island

The next step in the PSHA method is to determine the ground motion parameters at a particular site. Quantification of ground motion is important to understand the behaviour of any site during an earthquake and to do this, attenuation relationship is used in the analysis. Attenuation models are used to predict the probability distribution of ground-shaking intensity, as a function of variables including earthquake magnitude, distance from the site, the faulting mechanism, and near-surface site conditions. The attenuation model or relationship is a simple mathematical model that relates all ground motion parameters and earthquake source parameters. The mathematical models were derived by using results from seismograms records as well as previous earthquake records. The ground motion is simulated and a regression analysis was done. The regression equation represents the ground motion relationship based on the characteristics of the input parameter. In order to use the attenuation relationship, the relationship parameters and the parameters used for the analysis should be similar if not identical, such as distance for source-to-site and magnitudes range.

In the present study, four attenuation relationships were chosen for analysis. The equations used outputs of the attenuation relationships derived by Megawati *et al.*[6], Young *et al.*[7], Petersen *et al.*[8], and Atkinson and Boore[9]. These four equations are

widely used in PSHA and allow analysis of subduction zone earthquakes of M_w > 5.0 at distances ranging from 10 to 1,500 km to be analysed depending on the assumptions made and rock types. These characteristics of parameters are similar to the records gathered for Penang Island.

(a) Megawati *et al.*[6] attenuation model

This attenuation relationship was built for the Sumatran-fault segment based on larger magnitude earthquakes. This attenuation tries to reproduce the response spectra which were not covered by other attenuation models for sites near the Sumatran subduction zones. The relationship can be used for sites between 200 and 1,500km from the epicenter and an earthquake's moment magnitude up to M_w = 9.0. The equation is as described below where Y (cm/sec^2) is the geometric mean of horizontal peak ground acceleration (PGA), peak ground velocity (PGV) or response spectrum analysis (RSA) values (5% damping ratio) at various natural periods.

$$\ln Y = a_0 + a_1(M_w - 6) + a_2(M_w - 6)^2 + a_3 \ln(R) + (a_4 + a_5 M_w)R + \varepsilon_{\ln(Y)} \quad (2.1)$$

with $a_2(M_w - 6)$ is to show that the corner period of the earthquake source spectrum increases when distance and magnitude increase, a_3 is the geometrical attenuation rate, a_4 and a_5 are the inelastic attenuation, $\varepsilon_{ln(Y)}$ is the variation in PGA, PGV and RSA due to randomness in source parameters considered in the simulations, R is the distance from site to epicenter and the parameters for PGA calculation is a_0 = 3.8220, a_1 = 1.8988, a_2 = -0.1174, a_3 = -1.0, a_4 = -0.001741, a_5 = 0.00007760, $\varepsilon_{ln(Y)}$ = 0.2379. The parameters from a_0 to a_5 are determined to best fit the regression equation and are calculated based on the least square method.

(b) Young *et al.*[7] attenuation model

This attenuation model is a regression of recorded ground motions from inter-plate earthquakes occurring in subduction regions of Alaska, Chile, Cascadia, Japan, Mexico, Peru and Solomon islands. This relationship valid for moment magnitude, $M_w \geq 5.0$ and distance, R from 10 to 500km and is shown in Eq. (2.2) with Y is in g.

$$\ln Y = 0.2418 + 1.414M + C_1 + C_2(10 - M)^3 + C_3 \ln(R + 1.7818e^{0.554M}) + 0.00607H + 0.364Z_T \quad (2.2)$$

with standard deviation $\varepsilon_{ln(Y)} = C_4 + C_5 M$ and $C_1 = 0$, $C_2 = 0$, $C_3 = -2.552$, $C_4 = 1.45$, $C_5 = -0.1$. H is the focal depth in kilometre; Z_T is source type with 0 for interface and 1 for intraslab. These parameters are for rock type.

(c) Petersen *et al.*[8] attenuation model

This attenuation model was built based on the Sumatran earthquakes, and the data used are suitable for calculation of seismic intensity for Peninsula Malaysia. The equation for this model is for distances beyond 200km and was modified using Young *et al.*[7] attenuation model. The relationship is as follows;

$$\ln Y = \ln Y_{YOUNGS}(M, R) + [-0.0038 * (R - 200)] \quad (2.3)$$

ln Y_{YOUNGS} is the same equation in section (b) for PGA calculation (rock).

(d) Atkinson and Boore[9] attenuation model

The Atkinson and Boore[9] attenuation relationship was developed using a stochastic method for a tectonically stable region of Eastern North America (ENA). This model can be applied for distance, R from 10 to 500km and from moment magnitude, M_w from 4.0 to 7.5. The function is represented as;

$$\ln Y = f_1(M_w, R) + f_2(S) \quad (2.4)$$

with Y (gal) is horizontal component of PGA, and

$$f_1(M_w, R) = c_1 + c_2(M_w - 6) + c_3(M_w - 6)^2 - \ln R + c_4 R \quad (2.5)$$

$$f_2(S) = c_5 S_{deep} \quad (2.6)$$

with $c_1 = 1.8410$, $c_2 = 0.6860$, $c_3 = -0.1230$, $c_4 = -0.0031$, $c_5 = 0$, S_{deep} is 30m velocity in m/sec = 1 and $\varepsilon_{ln(Y)} = 0$ (not applicable).

2.4.2 Analysis of attenuation model

Using the dataset of the Malaysian Meteorological Agency[10], records were retrieved from the interval May 2004 to July 2007. This interval contained data on 15 interplate earthquake events of $M_w \geq 5.0$ and of shallow hypocentral depth, thus $h_{hypo} \leq 40$ km. The dataset used had initially been analysed by Sherliza *et al.*[10] and was then reduced because of distance constraints on all four attenuation relationships.

The magnitudes chosen for analysis were $M_w = 6.3$, $M_w = 6.7$, and $M_w = 8.6$. Although Gutenberg and Richter[11] suggested that choice of more magnitudes might be appropriate, the limited number of recorded PGAs caused us to choose only three. The dataset[10] revealed that the minimum PGA value was 0.3gal (March 6, 2007; $M_w = 6.3$) and the maximum 20gal (March 28, 2005; $M_w = 8.6$). Fig. 2.6 shows the four attenuation relationships for $M_w = 6.3$. It may be noted that the attenuation model of Young *et al.*[7] fitted the data well; Malaysia's records fell within the predictive range.

In Fig. 2.6 middle picture, the attenuation models of Young *et al.*[7] and Atkinson and Boore[9] predicted values very close to the Malaysian dataset for $M_w = 6.7$ events and, in Fig. 2.6 bottom picture, the attenuation model of Petersen et al.[8] predicted a value that fitted closely to those of the dataset for $M_w = 8.6$ events. The reason why most attenuation models do not accurately represent or closely fit datasets is because the ranges of distance and maximum earthquake magnitude are considerably less than the optimum values for these models, except in the attenuation model of Megawati *et al.*[6].

In Fig. 2.6, it can be seen that the attenuation models of Young *et al.*[7], Atkinson and Boore[9], and Petersen *et al.*[8], estimated PGA values very accurately. Most observed or recorded PGA values were predicted by the models. However, for earthquakes of magnitudes less than 8.0, the model of Young *et al.*[7] should be used; the model considers the depth of the earthquake, h_{hypo}, and the distance, R_{hypo}. For earthquakes of M_w of over 8.0, Fig. 2.6 bottom picture shows that the attenuation model of Petersen *et al.*[8] fits recorded data well, but the model remains unsuitable because the attenuation relationship is based on an earthquake of maximum $M_w = 8.2$.

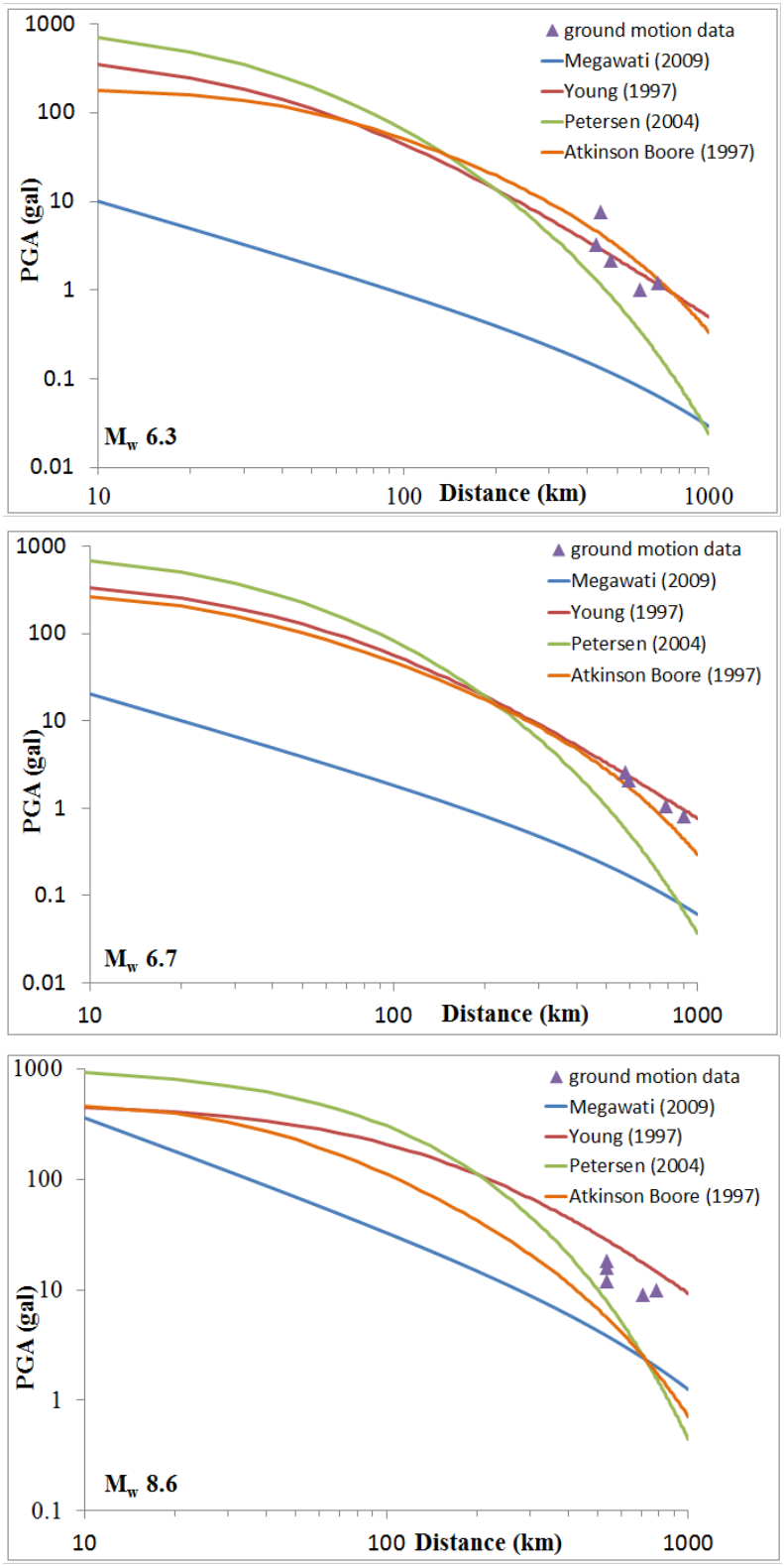

Fig. 2.6 Comparison of estimated and recorded PGA values of the magnitude of earthquake moment, Mw = 6.3 (top); Mw = 6.7 (middle); Mw = 8.6 (bottom).

2.5 Peak Ground Acceleration (PGA) on Bedrock

The next step in PSHA is to combine the uncertainties on earthquake location, size and ground motion parameters prediction to obtain the probability that the ground motion parameters will be exceeded during a particular time period[1] [2].

Using the total probability approach, a hazard map for Penang Island was constructed. Eq. (2.7) was used to calculate total probability:

$$\upsilon = \sum_{i=1}^{N} \upsilon_{M_{min}} \int\int P(Y > y|m, r) f_{M_i}(m) f_{R_i}(r) dm dr \quad (2.7)$$

Where $P(Y>y|m,r)$ is a term from the ground motion attenuation model, and $f_M(m)$ and $f_R(r)$ are probability density functions of magnitudes and distances; these are ultimately integrated. Such integration sums the conditional probabilities of overestimation associated with all possible magnitudes and distances. Manifold is GIS software and was used to produce the bedrock PSHA map for Penang Island.

Fig. 2.7 shows a PSHA map of the Penang Island bedrock area developed using Eq. (2.7). The map shows the probabilities of seismic occurrences at the 40%, 10%, 5%, and 2% levels, over 50 years. Fig. 2.7 shows that, in terms of a 40% probability of an event in 50 years (thus, in a 98-year return period), the highest PGA for Penang bedrock is 56.45gal and the lowest 49.55gal. For a 10% probability of an event in 50 years (thus, in a 475-year return period), the highest PGA value is 101.92 gal and the lowest 85.06 gal. In fig. 2.7, for a 5% probability of an event in 50 years (a 975-year return period), the highest PGA value is 130.91 gal and the lowest 108.06 gal. For a 2% probability of an event in 50 years (a 2,500-year return period), the highest PGA value is 177.82 gal and the lowest 145.09 gal.

From Fig. 2.7, it can be seen that for all 4 maps, larger values of PGAs are concentrated in the southwest of Penang Island. This is because; most input data, especially higher earthquake magnitude records, came from that area. If in the future big earthquakes come from another area, the map will change accordingly.

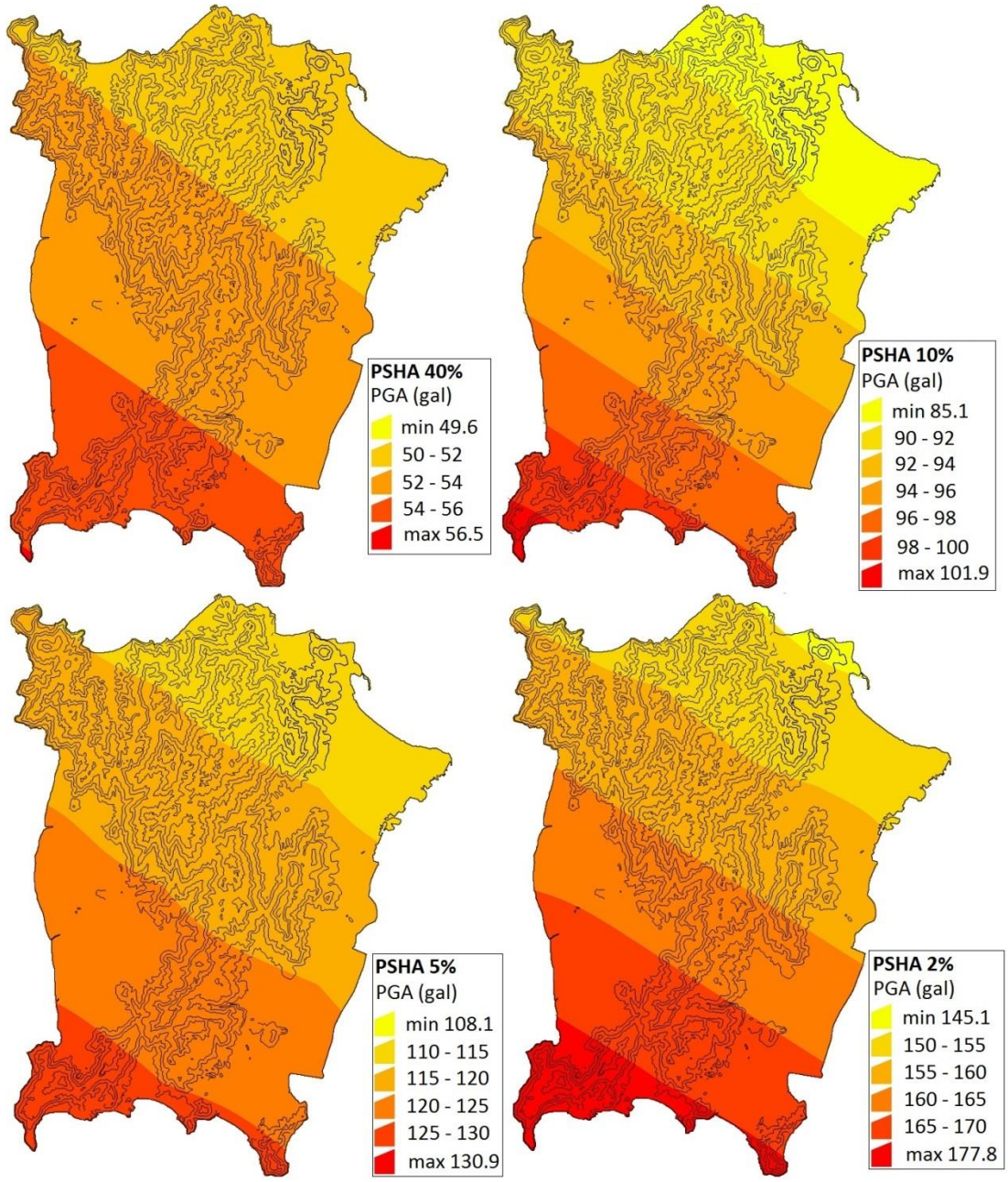

Fig. 2.7 PSHA maps of Penang Island showing the probabilities of events at the 40%, 10%, 5% and 2% in 50 years (bedrock)

2.6 Ground Motion Analysis

To develop a surface PGA map, ground response analysis was used to determine surface ground motion at a specific site. This analysis also is used to determine the stability of earth retaining structures with regards to earthquake forces in next chapter.

For purposes of simplification, this study simply uses the data to determine ground motion; the responses are not described. Ground response analysis can determine surface motion influenced by the soil layer beneath the surface[12]. The ground response on the particular site is influenced by the stress moved from the bedrock layer underneath and also the soil that lies beneath the particular site. A schematic representation to compute the effects of stress wave and local soil condition is shown in Fig. 2.8.

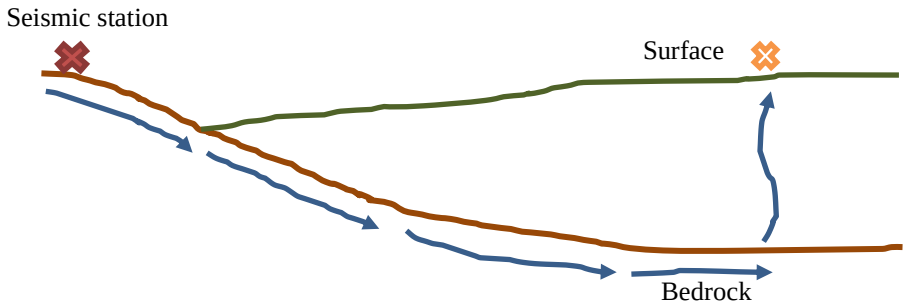

Fig. 2.8 Schematic presentation on wave movement from seismic station to surface at site

In ground response analysis, one-dimensional analysis (either linear, equivalent linear or non-linear) is carried out by using the rock motions as input motion and time series at the surface can be computed. This time series from the ground response analysis can be used to represent the ground surface motions.

When an earthquake happens, fault rupture occurs below the earth's surface and a body wave travels from the source in all directions. When the wave reaches boundaries of different geologic condition, it is reflected and refracted. The wave propagation

velocities of shallow materials are lower and incline rays that strike horizontal layer boundaries are usually reflected in a vertical direction. When the rays reach the surface, the multiple refractions have bent to a nearly vertical direction.

The secondary wave (S wave) arrives at the observation station after the propagation of the primary body wave. The S wave generates a significant amount of horizontal motion, it is considered as the most important cause of seismic damage.

Factors affecting the ground response include shear wave velocity, density and layer thickness. The depths of soil deposits and bedrock play important roles in determining the amplification of waves from bedrock to the surface. The amplification is a phenomenon where the local soil acts as filter and modifies the ground characteristics. The amplification factor is the key parameter that needs to be known in this subchapter in order to determine the ground surface response.

To analyse ground motion, soil profiles are required and a record of ground motion should be used. This study adopted the 1-D analysis method, so the effect of ground surface irregularity is not considered. One-dimensional ground response analysis is based on the assumption that all boundaries are horizontal and the response of a soil deposit is predominantly caused by SH-waves that propagates vertically from bedrock. The bedrock is assumed to extend infinitely in horizontal direction and the response of the soil deposit is caused by shear waves that are propagating vertically from bedrock. This assumption is in agreement with responses in many cases as mentioned by Kramer[13].

2.6.1 Input ground motion

In this study, ground motion triggered by a nearby earthquake was analysed. Input ground motion is used in the study to show amplification effect using a transfer function. The ground motion data was collected from the seismic station of the Malaysian Meteorological Agency located in Serdang, Kulim, Kedah (latitude 5.29, longitude 100.65). The distance from Penang Island to this station is about 50 km and the station is on the top of a mountain; the station is thus assumed to be on bedrock. The input

ground motion used was imparted by an earthquake of M_w 8.6 that occurred on 28 March 2005 in Pulau Bangkaru, Indonesia (latitude 2.09, longitude 97.11). Sherliza *et al.*[10] has made the corrections needed before ground motion data can be used in analysis. Fig. 2.9 shows the ground motion record that was analysed.

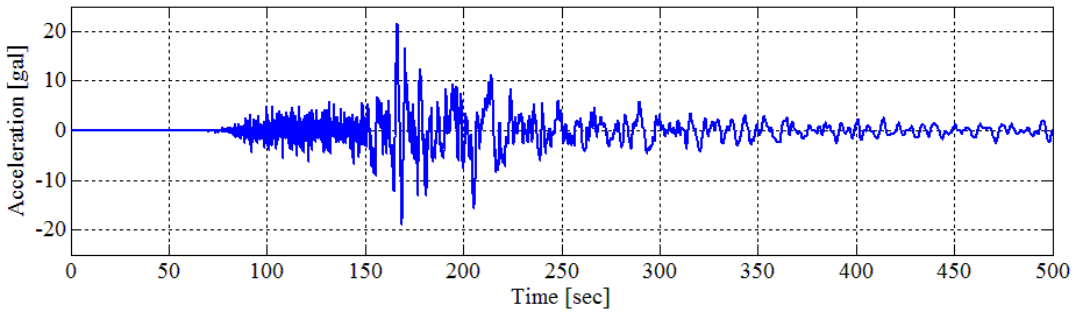

Fig. 2.9 The earthquake record, in the N-S direction, recorded on 28 March 2005 in Indonesia (latitude 2.09, longitude 97.11)

2.6.2 Soil profile

Penang Island soil profiles were collected from local consultants engaged in several projects on Penang Island. The soil profiles were collected during site investigations. Standard Penetration Tests (SPTs) were performed for each borehole; N numbers were recorded; and soil samples were taken. The test sites were Batu Ferringhi and Tanjung Bungah. A total of 24 records of soil profiles were available (Appendix A), layer types were determined and shear-wave velocities calculated. An example of a borehole is shown in Fig. 2.10. This borehole was located in Batu Ferringhi 52m from the shore. Bedrock (granite) was met at 12.6m. Most boreholes reached bedrock at 10m if on hilltops and at 15-20m otherwise.

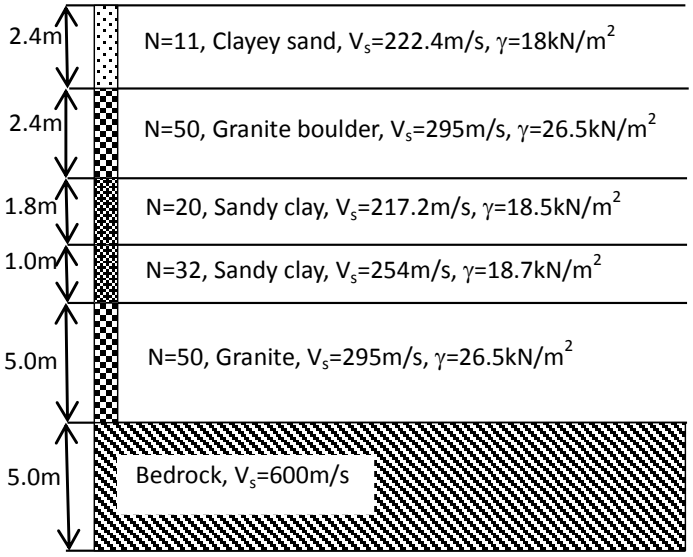

Fig. 2.10 The borelog for borehole BH5, Batu Ferringhi

2.6.3 Ground response analysis

Prediction of ground responses involves several steps. First, the characteristics of motion likely to develop in rock formations underlying the site must be explored. Maximum acceleration, the predominant period, and effective duration, are the important parameters. An empirical relationship between these parameters and the distance from the fault to the site is determined[12].

Next, using soil profile information (the *N*-numbers) from the SPT, the dynamic properties of each soil layer are determined. In this study, a damping factor of 5% was applied to all soil types. Many ways of relating shear-wave velocity and SPT *N*-number are available and, in this study, the Japanese Highway Bridge Design Code was adapted; this is in general use in Japan[14] and the defined relationship between *N*-number and shear-wave characteristics is easy to adopt. Such analysis yielded results similar to those obtained by seismic refraction analysis performed in past experience. Eq. (2.8) and Eq. (2.9) show the relationships between shear-wave velocity and N-numbers for sandy and clayey soils:

$$V_s = 80N^{1/3}\ for\ sand \tag{2.8}$$

$$V_s = 100N^{1/3} for\ clay \tag{2.9}$$

Next, by reference to soil parameters (unit weight, shear-wave velocity, and the depth of each layer), computation was used to determine the responses of the soil deposits to base-rock motion. In this chapter, we used the multiple reflection analysis to determine the ground response. Transfer function is used in 1-D ground response analysis with time series at the rock as the input and the frequency domain is represented by Fourier series. Each term in the Fourier series is multiplied by the transfer function.

Taking one borehole (BH5) in Batu Ferringhi as an example, the ground response is as shown in Fig. 2.11. The blue line represents the time series for bedrock and the red line that for the surface. The differences between the peaks of each point on these time series are amplification factors for the site. The amplification factor for BH5 is shown in Fig. 2.12. For this borehole, the amplification factor was set at 1.7 to estimate PGA on the surface, with reference to the highest possible amplification that could occur in the borehole. Amplification results for other boreholes as mentioned in the preceding sub-chapter are shown in Appendix B.

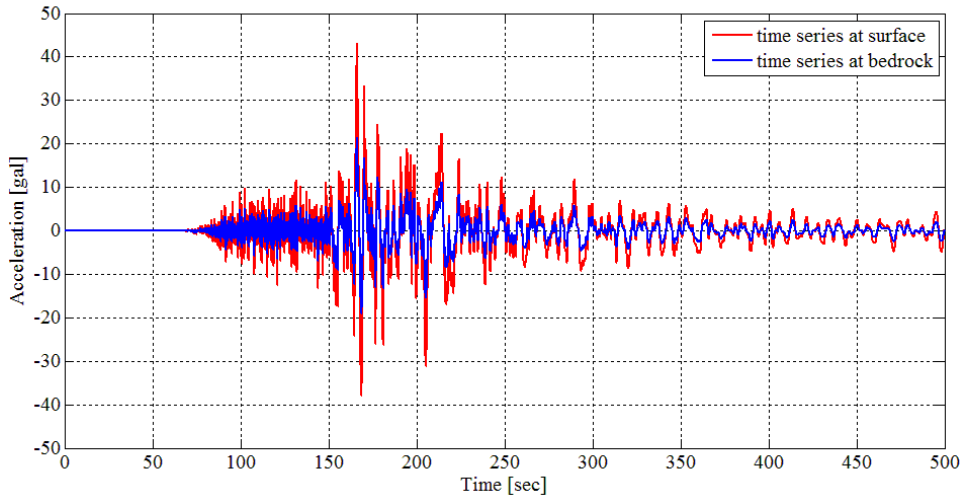

Fig. 2.11Ground motion for borehole BH5, Batu Ferringhi, Penang

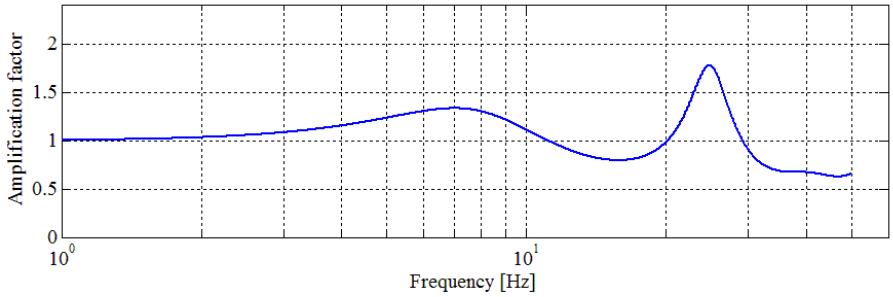

Fig. 2.12 Amplification factor for borehole BH5, Batu Ferringhi, Penang.

2.7 Expected Peak Ground Motion for Penang Island

From PSHA analysis, each location on the contour line was amplified. The idea was that the soil layers at the tops of hills in Penang Island were the same and amplification was considered to be the same as the bedrock PSHA values when heights were higher than the heights of available records. By plotting all results for every borehole, two sets of groups can be seen as in Fig. 2.13. Two regression equations were shown in the figure. When the lines are projected, it can be seen that both intersect each other at 50m height.

From Fig. 2.13, slopes higher than 50m are interpreted as having 1.5 amplification factors. It means that the PGA value for the ground is the same as PGA value at bedrock and for slopes lower than 50m, the following equation was used to determine the amplification factor.

$$y = -0.0144x + 2.2926 \tag{2.10}$$

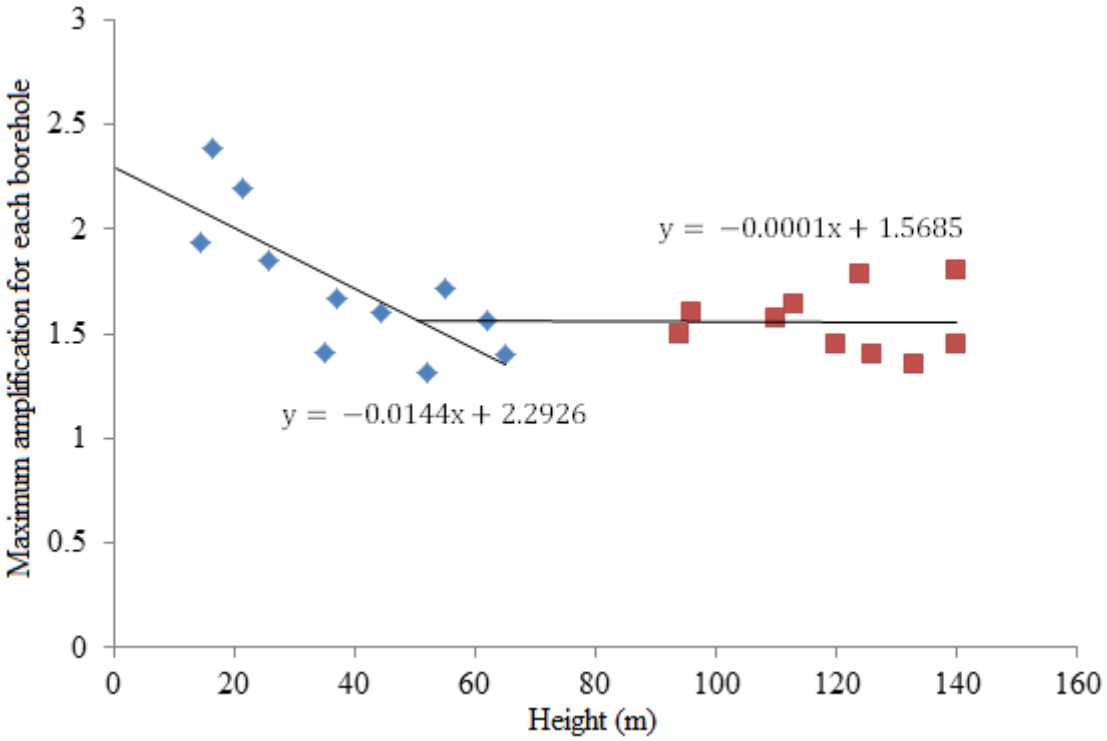

Fig. 2.13 Relationship between amplification factors and slope height

Using Eq. (2.10), a map was made. Fig. 2.14 shows that for a 40% probability of an event in 50 years (a 98-year return period), the highest value of PGA was 110gal and the lowest 46.4gal. In Fig. 2.14, for a 10% probability of an event in 50 years (a 475-year return period), the highest value of PGA was 200gal and the lowest 135gal. For a 5% probability of an event in 50 years (a 975-year return period), the highest value of PGA was 255gal and the lowest 168.8gal. For a 2% probability of an event in 50 years (a 2,500-year return period), the highest PGA value was 340gal and the lowest 255gal.

In Fig. 2.14, the distributions of peak ground accelerations are highly concentrated in the lowlands, especially near the coast. This is because amplifications on lowlands are higher than on hillsides. The values are relatively small if compared to those of regions of higher seismicity but effects will still be felt on Penang Island if seismic activity occurs within 600km radius. Since the area is located on lowland, it can be seen that for all probability of occurrences, the PGAs prediction for lowland areas are at the maximum value. This shows there is effect on seismicity on the historical city. Although

it is not as large as what other historical cities in the world anticipate, there are still some risks in case bigger earthquakes happen in the future. Since the amplification was obtained by 1-D analysis, which cannot take into account the complex shape of the hill, we will investigate the 3-D effect in future analysis. Further investigation should focus on what would happen if an earthquake coincided with heavy rainfall, which is the main cause of landslides on the Island.

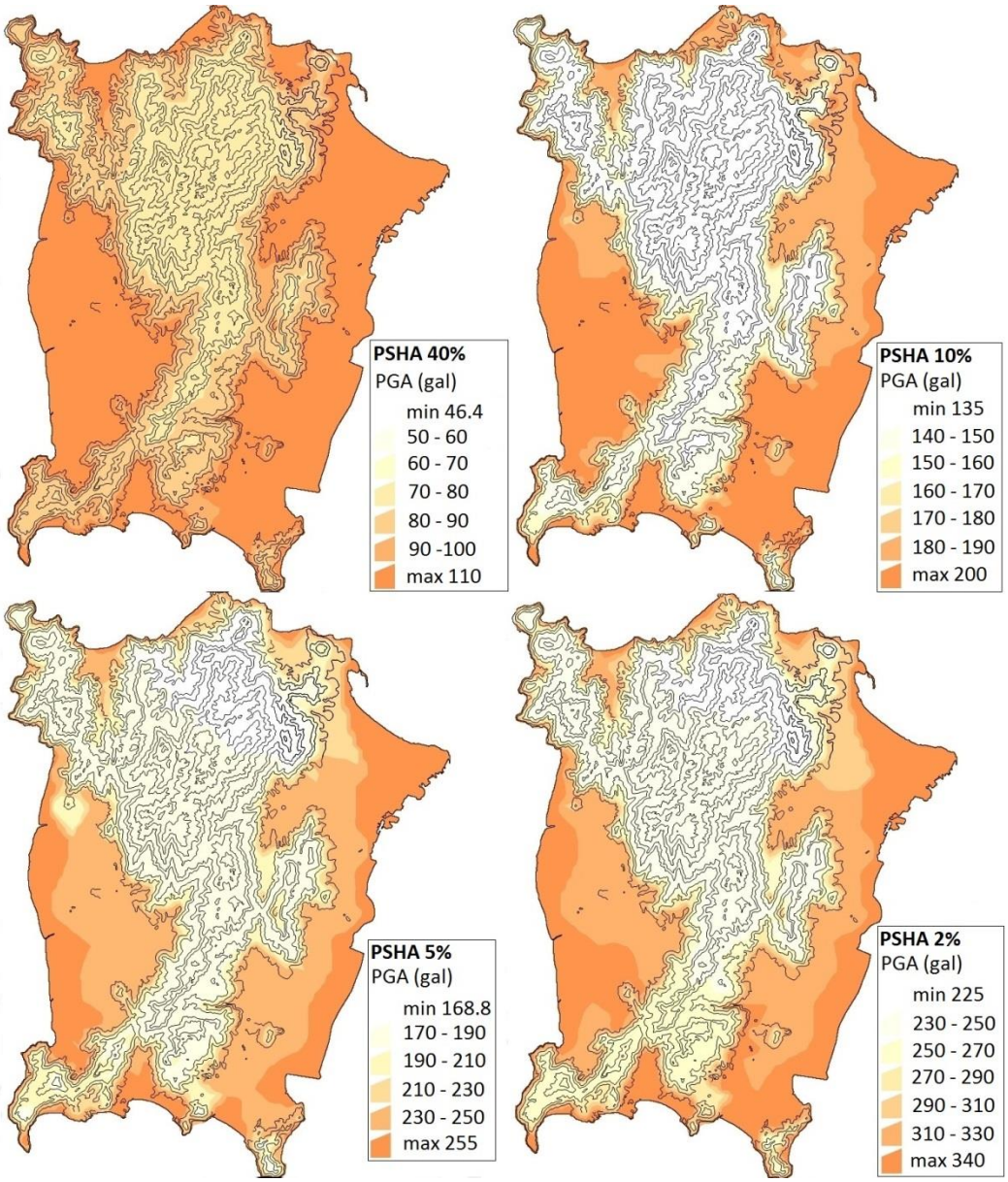

Fig. 2.14 PSHA maps of Penang Island showing the probabilities of events at the 40%, 10%, 5% and 2% in 50 years (surface)

2.8 Conclusions

In this chapter, behaviour of seismicity on Penang Island was assessed and by using a statistical method, peak ground acceleration map for Penang Island were mapped based on 40%, 10%, 5%, and 2% probabilities of events in 50 years (98-, 475-, 975-, and 2,500-year return periods, respectively). Historical data were used since Malaysian earthquake records are very scarce. Then, a suitable attenuation relationship was chosen to be used in producing the PGA map. The PGA bedrock map was done by using results from total probability theorem.

The next step in the chapter is ground motion analysis by using a nearby ground motion record. Ground response analysis can determine surface motion influenced by the soil layer beneath the surface. From the analysis, a PGA map for the ground was made.

The final results shows that the distributions of peak ground accelerations are highly concentrated in the lowlands, especially near the coast. This is because amplifications on lowlands are higher than on hillsides. It can be seen that the implications are less than those in highly seismic regions. Lowland areas are at higher risk; they contain softer soils that amplify earthquake motion more than do the soil types of higher ground. This is because the soil layers are shallow, and the bedrock (granite) is located at shallow depths (high level) on the tops of hills, yielding lower amplification factors, which in turn yield lower PGA values.

The result from this chapter will be used in Chapter 5 for analysis of slope failure due to earthquake and rainfall. The PGA value is one of the main parameters in the slope analysis and prediction of slope failure that can be made for Penang Island.

References

[1] Hendriyawan, “Seismic Macrozonation of Peninsular Malaysia and Microzonation of Kuala Lumpur City Center and Putrajaya,” 2007.

[2] J. W. Baker, “An introduction to Probabilistic Seismic Hazard Analysis (PSHA),” 2008.

[3] T. Majid, S. S. Zaini, F. Mohd Nazri, M. R. Arshad, and I. F. Mohd Suhaimi, "Development of design response spectra for northern Peninsular Malaysia based on UBC 97 code," *J. - Inst. Eng. Malaysia*, vol. 68, no. 4, pp. 23–29, 2007.

[4] A. Adnan, Hendriyawan, and M. Irsyam, "The effect of latest Sumatra earthquake to Malaysia Peninsular," *J. Kejuruter. Awam (Journal Civ. Eng.*, vol. 15, no. 2, 2002.

[5] T. C. Hanks and H. Kanamori, "A Moment Magnitude Scale," *J. Geophys. Res.*, vol. 84, no. B5, pp. 2348–2350, 1979.

[6] K. Megawati and T. Pan, "Ground-motion attenuation relationship for the Sumatran megathrust earthquakes," *Earthq. Eng. Struct. Dyn.*, no. October 2009, pp. 827–845, 2010.

[7] R. R. Youngs, B. S. J. Chiou, W. J. Silva, and J. R. Humphrey, "Strong ground motion attenuation relationships for subduction zone earthquakes," *Seismol. Res. Lett.*, vol. 68, no. 1, pp. 58–73, 1997.

[8] M. D. Petersen, J. Dewey, S. Hartzell, C. Mueller, S. Harmsen, A. Frankel, and K. Rukstales, "Probabilistic seismic hazard analysis for Sumatra, Indonesia and across the Southern Malaysian Peninsula," *Tectonophysics*, vol. 390, no. 1–4, pp. 141–158, Oct. 2004.

[9] G. M. Atkinson and D. M. Boore, "Ground-motion relations for Eastern North America," *Bull. Seismol. Soc. Am.*, vol. 85, no. 1, pp. 17–30, 1995.

[10] S. Zaini Sooria, S. Sawada, A. Adnan, and H. Goto, "An investigation on the attenuation characteristics of distant ground motions in Peninsular Malaysia by comparing values of recorded with estimated PGA and PGV," *Malaysian J. Civ. Eng.*, vol. 22, no. 1, pp. 38–52, 2010.

[11] B. Gutenberg and C. . Richter, "Frequency of earthquakes in California," *Bull. Seismol. Soc. Am.*, vol. vol. 34, no. no 4, pp. 185–188, 1944.

[12] P. B. Schnabel, J. Lysmer, and H. B. Seed, "SHAKE - A Computer Program for Earthquake Response Analysis of Horizontally Layered Sites," 1972.

[13] S. L. Kramer, *Geotechnical Earthquake Engineering*. 1996, pp. 438–439.

[14] I. Towhata, *Geotechnical Earthquake Engineering*. Berlin, Heidelberg: Springer Berlin Heidelberg, 2008, pp. 134–135.

Chapter 3

PROBABILISTIC RAINFALL ANALYSIS

3.1 Introduction

Peninsular Malaysia is located on the equatorial line and experiences a tropical climate with monsoon seasons twice a year and sometimes experiences a dry climate due to warm ocean temperatures that cause extreme dry weather like El Nino. The monsoon seasons in particular interest with this research are called the North East (NE) that usually occur between November to March and South West (SW) monsoons that usually occur between May to September. These monsoons bring heavy rains that contribute to high annual rainfall in Malaysia, which is between 2,000 to 4,000mm. The rainy days in Malaysia are usually between 150 and 200 days annually[1]. The duration between the two monsoons (April and October) is referred to as the inter-monsoon season[2].

The Malaysian Meteorological Department reported that during the northeast monsoon season, the east coast of Peninsular Malaysia, western Sarawak and northeast coast of Sabah experience heavy rains. The maximum amount of rainfall occurs during this period. For the rest of the peninsula, except the southwest area, primary monthly rainfall reaches a maximum from October-November and secondary rainfall amount occurs between April-May. On north-western region areas, such as Penang Island, the primary minimum occurs in January to February and secondary minimum occurs between June to July.

There are several triggering factors that can lead to landslides and in Malaysia, heavy rainfall is the most common cause that leads to slope failure. Past cases of landslides in Malaysia were shown in Chapter 1 and will not be discussed again in this chapter. The mechanism of rainfall-induced slope failure is explained by Lee *et al.*[3]; rainfall infiltration results in reduction of matric suction in soil, which leads to a reduction in shear strength in soil and subsequently can trigger slope failure. During heavy rainfall, water infiltrates into soil and increase the water table height. This will increase positive

pore-pressures and therefore decrease the effective strength of the soil and will result in a higher risk of slope failure.

There are several types of rainfall that are usually studied by researchers. One is antecedent rainfall. Any rainfall that precedes a landslide event is defined as antecedent rainfall[4]. Antecedent rainfall is an accumulated amount of rainfall that might trigger slope failure. It varies depending on the amount of rainfall that may initiate the slope failure and it may be between 1 – 120days[5]. For example, in New Zealand, the antecedent rainfall duration may be around 10-days and in Singapore, studies found that 5-day antecedent rainfall can initiate slope failure[4][6].

The main objectives in this chapter are to be able to assess and investigate the behaviour of rainfall pattern on Penang Island by using the statistical method and to determine the appropriate distribution function that can represent the antecedent rainfall on Penang Island.

3.2 Chapter Overview

This chapter includes analysis of probabilistic distribution of accumulated rainfall on Penang Island. Using 60 years of rainfall data collected from a local rainfall station on Penang Island, probabilistic distribution analyses were conducted using several methods and goodness-of-fit was checked. The best fit distribution was selected to describe the return period of accumulated rainfall on Penang Island.

This chapter discusses analysis of probabilistic distribution of accumulated antecedent rainfall on Penang Island. Daily rainfall data from a rainfall station were collected from the Department of Irrigation and Drainage Malaysia. Then, several probability distribution functions were chosen for the analysis. Data collected were compared with these functions and using goodness-of-fit tests, the best distribution function is chosen to represent the return period of accumulated antecedent rainfall in Penang Island.

Fig. 3.1 shows the flowchart of this chapter. Results from this chapter will be used in the proceeding chapter 4, which incorporate the rainfall amount and its return period with the water height.

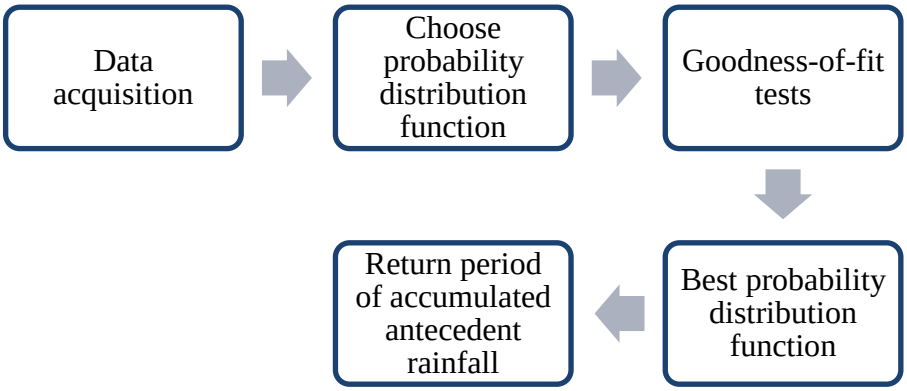

Fig. 3.1 Flowchart for chapter 3

3.3 Rainfall Pattern and Antecedent Rainfall

According to Chow[7], there are about four conditions that are necessary for production of the observed amounts of rainfall (1) mechanism to produce cooling of the air, (2) mechanism to produce condensation, (3) mechanism to produce growth of cloud droplets and (4) mechanism to produce accumulation of moisture with sufficient intensity to account for observed rates of rainfall. Simultaneous occurrences of these mechanisms are sufficient to produce heavy rainfall.

Rainfall may occur at any time of the day and may occur within a few hours or may extend for several days. There are about 3 main types of rainfall: convective rainfall, orographic rainfall or frontal rainfall. Convectional rainfall usually occurs in tropical areas where the climate is hot. This rain type occurs when the ground surface warms up causing moisture in the ground to evaporate and rise up. When water vapour rises, it condenses into clouds and eventually rain and if the water vaporises too quickly, this will lead to thunderstorms[1].

Frontal rainfall occurs when two air masses with different densities (warm and cool air) meet and the hot air is pushed up over the cold air. When the warm air cools, it condenses into water and falls as raindrops. Orographic rainfall occurs when hot air is forced to rise over a higher altitude range (mountain). The hot air cools down when it reaches a higher level and becomes rain[1]. Even though there are different types of rainfall the distribution of rainfall shall be treated equally in this study. Rainfall can be measured using radar rainfall or by point measurement depending on the size of the study area. The most common rainfall measurement is taken using rain gauges that measure the amount of rainfall and can be monitored continuously. In Malaysia, the precipitation data are usually collected by the Malaysian Meteorological Agency and the data are in hourly and daily (24-hour) increments and can be retrieved by applying from the agency.

In tropical countries with high amounts of rainfall like Malaysia, Singapore, Indonesia etc., landslides usually occur after a certain duration of heavy rainfall occurrences. Frattini and Tsaparas[8][9] conforms that rainfall is one of the most recognised triggering factors of landslides. Infiltration of rainwater into unsaturated soil will decrease the matric suction, thus reducing the shear strength of the soil and can cause slope failure[10].

Antecedent rainfall is defined as rains that fall in the days preceding a landslide event[4]. There are many researchers who try to determine the rainfall threshold and found that landslides are related to antecedent rainfall with different durations[4]–[6]. Although some researchers do not find any relationship between antecedent rainfall with landslide occurrences, Rahardjo[4] has proved from his study of slope responses (pore-water pressure distribution) using comprehensive instrumentation that 5-day accumulated antecedent rainfall can affect the stability of slopes in Singapore and Tsaparas *et al.*[9] conducted a study on the factors that control rainfall-induced slope failure including antecedent rainfall. Rahimi *et al.*[4] studied the effect of antecedent rainfall pattern on the stability of slopes. These studies were done based on the Singaporean soil condition, which is almost the same as Malaysian soil condition as well as rainfall amount.

Therefore, in this chapter, 5-day accumulated antecedent rainfall is adopted as the number of days that may initiate slope failure in Malaysia.

The Antecedent Water-Status model was introduced by Crozier[6] and the fundamental assumption is that a critical water content is needed to initiate failure. He also introduced an important premise in critical water content that it is composed of two components: antecedent soil water and event water. In the model, accumulated antecedent rainfall is calculated from excess rainfall. Excess rainfall is decayed and accumulated over a given period and it was calculated as follows:

$$r_{a_0} = kr_1 + kr_2 + .. + kr_n \tag{3.1}$$

where r_{a_0} = antecedent daily precipitation, based on maximum regional precipitation values (mm) for day 0, k = constant representing the outflow of the regolith, and r_n = maximum regional precipitation (mm) on the nth day before 0. Crozier and Eyles used k = 0.84 based on Ottawa (U.S) streamflow data.

3.4 Statistical Analysis for Rainfall Distribution in Malaysia

As explained by Chow[7], in hydrologic investigation, the quantitative analyses are based on hydrologic data and the measurement are expanded and the amount of data is large. Statistics are able to deal with the computation of these data and are able to deal with the measure of likelihood and chances. Using the past records and data, probabilistic studies can solve hydrology problems and determine future probabilities of occurrences.

To determine the amount of rainfall that can influence the level of water that leads to slope failure, a comprehensive study using laboratory equipment was done by Rahardjo[4], [11] which is the best method to analyse the changes. However, since it is unfeasible to do the same procedure for this study, statistical analysis is adopted. A

sufficient amount of data was provided by the Department of Irrigation and Drainage, Malaysia.

The statistical method is one of the common methods used by hydrological researchers to determine the distribution of rainfall patterns since in statistical analysis there is the possibility of statistically combining several variables (in this study rainfall and earthquakes), this study will use this method for analysis.

In statistical analysis, frequency of occurrences is important and distribution fitting is usually done to predict and forecast magnitude of occurrences in certain intervals. By using several distributions, observed data is compared with several distribution functions and the function that fitted closely to the observed data is chosen to represent the distribution of the data. Previous studies by local researchers have been done for the Malaysian condition and common distribution functions have been tested based on local conditions[1][12]. This study will use the previous researchers' works as background for comparison of methods used in selection of distribution functions that best represent rainfall distribution on Penang Island.

In the analysis, several steps were done prior to fitting the distribution, such as determining the aim of the analysis. In this chapter, evaluation on the probability of occurrences of 5-days accumulated antecedent rainfall over a certain period is needed and to do this, several probability distribution functions were chosen. Using these distributions, probability of occurrences over certain periods is determined. EasyFit is statistical software used in this study to fit the distributions in this study.

Data used for analysis of this chapter is 5-days accumulated rainfall amount, which was observed randomly daily at a rainfall station on Penang Island. The rainfall station is located at Tali Air Besar Sungai Pinang (Station ID 5302001) (latitude 5.39, longitude 100.21) and the data was in daily rainfall (mm) from 1953 to 2012. The total amount of data used was about 1,770 data and was collected based on daily amount rainfall (24-hour reading) and all data are real numbers which means considerations are made based on continuous distributions.

3.5 Analysis of Probability on Random Event

Hydrologic data can be treated as statistical variables. The whole collection of objects is called population in statistics. The characteristics in population are called variables and denoted as *X* where else an individual observation, *x* of any variable *X* is known as variate. For example, in hydrologic phenomena, the depth of rainfall is *X* and the amount of rainfall is *x* (for example 100mm rainfall).

The observation of hydrologic phenomena in a certain period is considered as a trial and by this trial, the rainfall depth, for example is obtained as a random variable. Since the values of the rainfall depth are non-negative values, the sample space is infinite. There are two types of random variables, the discrete and continuous random variables. The discrete random variable has finite sample space and the sample space of the continuous random variable has real numbers. An example as explained by Chow[7], the number of rainy days is discrete but the depth of rainfall is continuous. In this study, the amount of rainfall is the major concern and therefore a continuous random variable is chosen.

Fitting probability distribution means analysing data using a valid model that can represent the frequency of occurrences. There are a lot of functions that can be used with each probability distribution in order to evaluate the probability of various outcomes, such as Cumulative Distribution Function (CDF). For a continuous random variable, the probability of a variate can be considered as the probability *p(x)* of a discrete value grouped in the range from *x* to $x + \Delta x$. As *x* is a continuous value or Δx becomes dx, the probability *p(x)* becomes a continuous function called probability density. The cumulative probability or CDF indicates probability of random event, *X* to happen less or equal to a certain limit, *x*

$$\mathrm{F(x)} = \mathrm{P(X \leq x)} = \int_{-\infty}^{x} f_X(t)dt \tag{3.2}$$

To determine that *X* takes on value more than *x*, the following function can be used.

$$\mathrm{P(X > x)} = 1 - \mathrm{P(X \leq x)} = 1 - \mathrm{F(x)} \tag{3.3}$$

By plotting *P(X > x)* for every distribution, the probability of certain amount of accumulated antecedent rainfall to happen over a period of time can be determined.

3.6 Probability Distribution Function

In order to understand the behaviour of each distribution function, the distribution pattern should be taken into consideration. If the data is asymmetrically distributed, the suitable distribution fitting should be chosen between normal distribution, logistic distribution and Student's t-distribution. If data is skewed to the right, selection can be chosen from log-normal, log-logistic, Gumbel, exponential, Pareto, Weibull or Frechet[7]. Detailed explanations for each distribution are widely discussed and therefore will not be described further in this chapter. In this study, when data is tabulated, as in Fig. 3.1, it can be seen that the distribution of data is skewed to the right. Therefore, the following distributions are chosen for the analysis.

3.6.1 Normal distribution function

The Normal distribution function is the oldest distribution function and is frequently used. It is symmetric at the mean value and is unbounded. Although this distribution does not represent well with the distribution of rainfall data observed, it is still chosen just to ensure that the basic distribution function is selected. Parameters in Normal distribution include mean value, μ (as the location of peak of distribution) and σ as scale parameter (σ > 0). Since Normal distribution is unbounded, x will be $-\infty<x<+\infty$ and the probability density function (PDF) will be

$$f(x) = \frac{exp\left(-\frac{1}{2}\left(\frac{x-\mu}{\sigma}\right)^2\right)}{\sigma\sqrt{2\pi}} \tag{3.4}$$

Probability distribution function is shown in Fig. 3.1 and the *P(X > x)* plot of accumulated rainfall for this distribution is shown in Fig. 3.2.

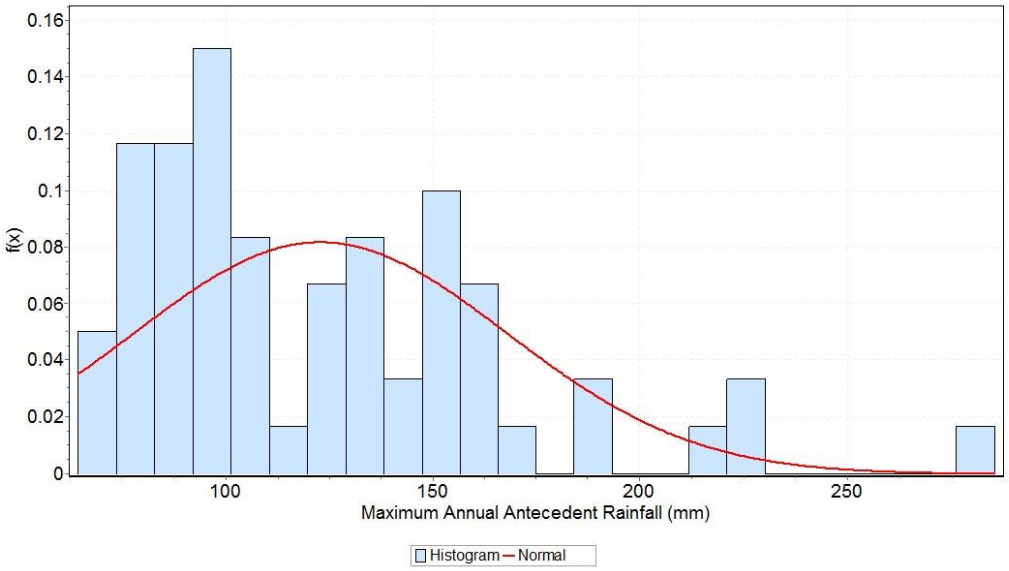

Fig. 3.2 Probability density function for Normal distribution

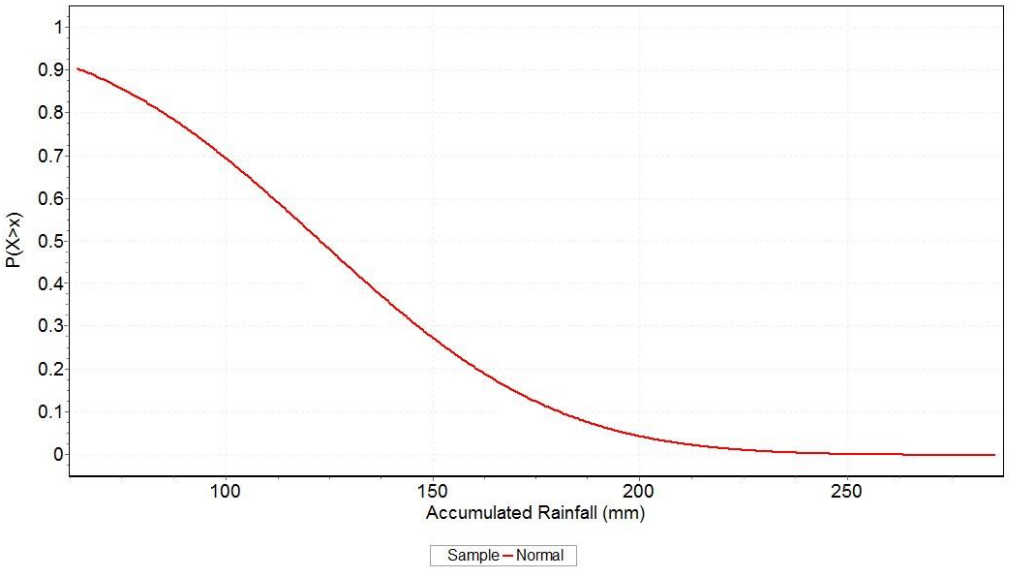

Fig. 3.3 Probability of exceedance for Normal distribution

3.6.2 Extreme value distribution

The antecedent rainfall is not a daily event and the analysis usually takes into account the maximum amount of rainfall at a specified time interval. In extreme conditions, separate analysis should be done to represent the worst or extreme events. In statistics, extreme value theory is based on the usage of three types of distribution that model extreme cases of an event.

These three theories are needed to model maximum and minimum values of a collection of random observations from the same distribution. In this study, the antecedent daily rainfall is assumed as the maximum amount of rainfall (in mm) in a specific time interval (5 days). The three distributions that can describe extreme events are Gumbel, Frechet and Weibull distribution. Combining these three distributions gives General Extreme Values (GEV), which is a widely known distribution used in risk management study.

(a) Gumbel distribution function

A German scientist (Gumbel) was one of the earliest scientists that applied the extreme value theory. He studied the extreme event of flood flows and therefore applied the extreme value theory to his study. Gumbel distribution, also known as Extreme Value Type I, is an unbounded distribution and has the following probability density function:

$$f(x) = \frac{1}{\sigma} exp\big(-z - exp(-z)\big) \tag{3.4}$$

where $z = (x - \mu) / \sigma$, μ is location parameter and σ is the distribution scale. Probability distribution function for Gumbel is shown in Fig. 3.3 and the $P(X > x)$ plot of accumulated rainfall for this distribution is shown in Fig. 3.4.

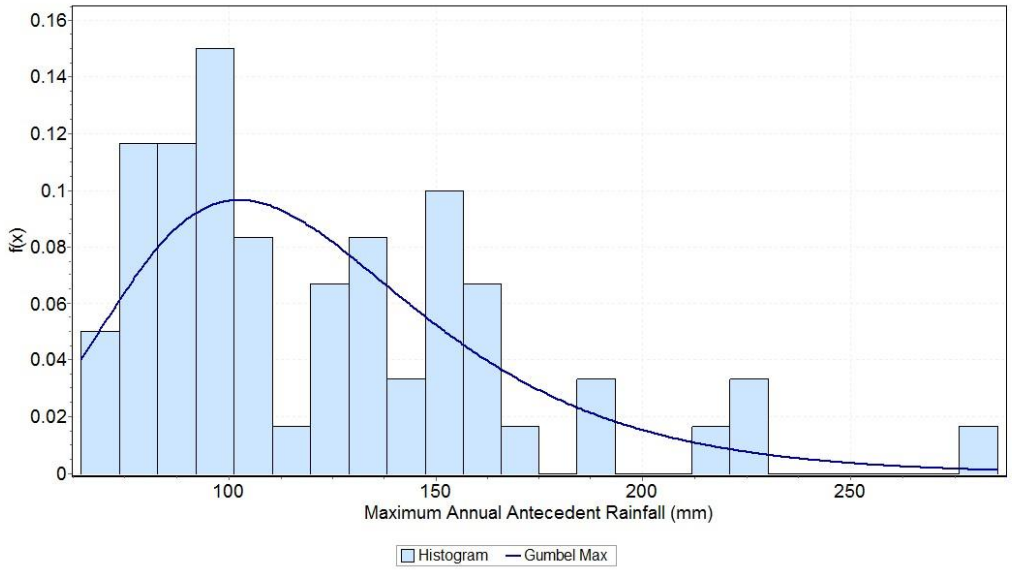

Fig. 3.4 Probability density function for Gumbel distribution

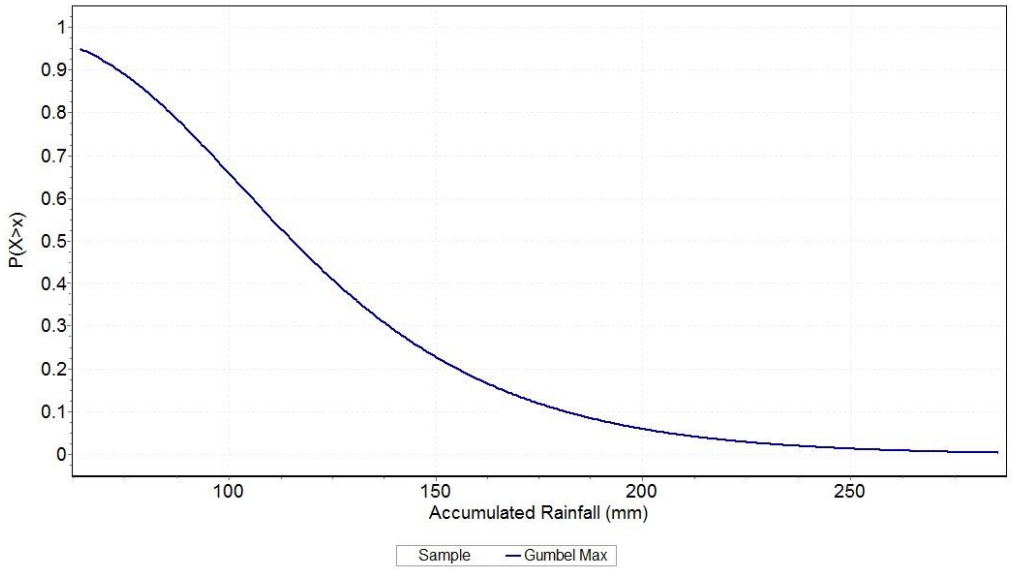

Fig. 3.5 Probability of exceedance for Gumbel distribution

(b) Frechet distribution function

This distribution was introduced by a French mathematician named Maurice Frechet and is commonly used in extreme value analysis, such as annual maximum rainfall or in

river discharges. He identified limited distribution in his study and Frechet distribution is also known as Extreme Value Type II. The distribution is defined as:

$$f(x) = \frac{\alpha}{\beta}\left(\frac{\beta}{x}\right)^{\alpha+1} exp\left(-\left(\frac{\beta}{x}\right)^{\alpha}\right) \tag{3.5}$$

where α is shape parameter, β is scale parameter and the distribution is bounded on lower side *(x > 0)*. Eq. (3.5) when plotted in probability distribution function is shown in Fig. 3.5 and the *P(X > x)* of accumulated rainfall for this distribution is shown in Fig. 3.6.

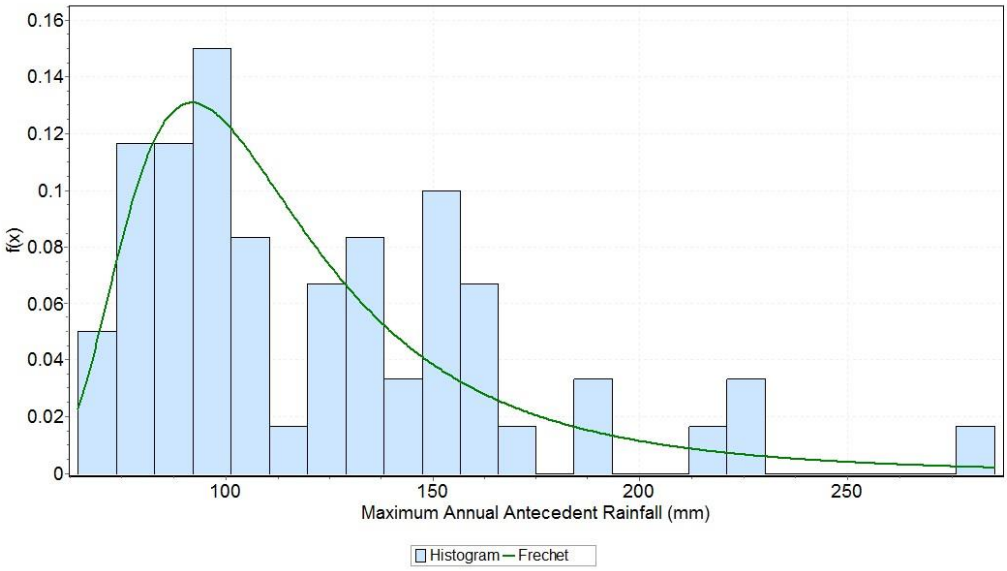

Fig. 3.6 Probability density function for Frechet distribution

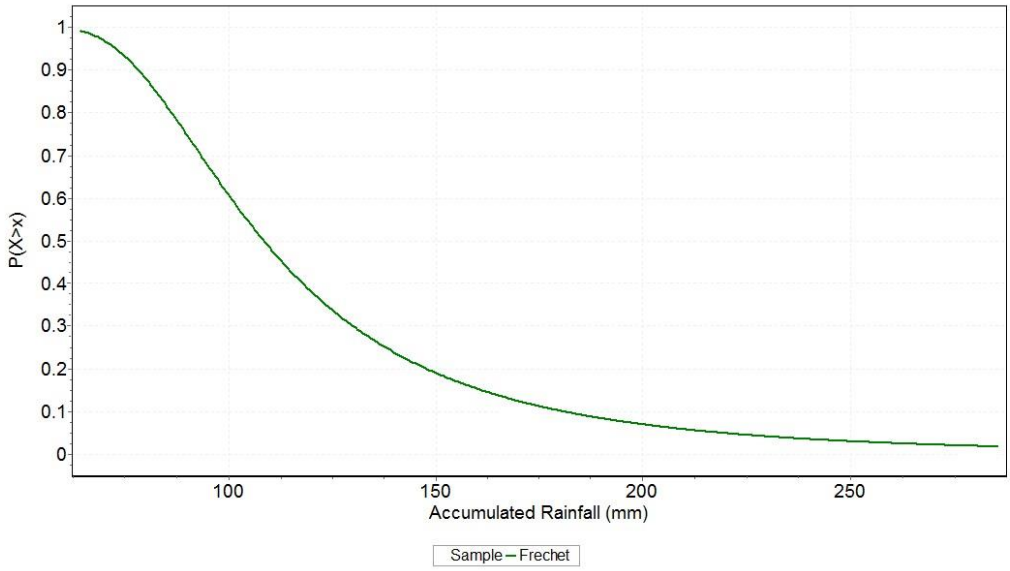

Fig. 3.7 Probability of exceedance for Frechet distribution

(c) Weibull distribution function

Waloddi Weibull, a Swedish engineer, introduced this distribution, which is also known as Extreme Value Type III. The probability density function is defined as:

$$f(x) = \frac{\alpha}{\beta}\left(\frac{x}{\beta}\right)^{\alpha-1} exp\left(-\left(\frac{x}{\beta}\right)^{\alpha}\right) \tag{3.6}$$

This distribution is defined for $x > 0$ and both distribution parameters (α-shape and β-scale) are positive. Probability distribution function is shown in Fig. 3.7 and $P(X > x)$ of accumulated rainfall for this distribution is shown in Fig. 3.8.

(d) Generalised Extreme Value distribution function

The GEV distribution is developed by combining three distributions (Gumbel, Frechet and Weibull). It is a flexible three-parameter model and has the following PDF:

$$f(x) = \begin{cases} \frac{1}{\sigma} exp\left(-(1+kz)^{-1/k}\right)(1+kz)^{-1-1/k} \ , for\ k \neq 0 \\ \frac{1}{\sigma} exp\left(-z - exp(-z)\right), for\ k = 0 \end{cases} \tag{3.7}$$

where $z = (x - \mu) / \sigma$ and k = shape parameter, σ = scale parameter, and μ = location parameter. The scale must be positive, and shape and location can be any real numbers. The range definition of GEV depends on the shape parameter, k:

$$\begin{matrix} 1+k\frac{(x-\mu)}{\sigma}>0 \; for \; k \neq 0 \\ -\infty<x<+\infty \; for \; k=0 \end{matrix} \tag{3.8}$$

When fitting GEV to sample data, shape parameter, k will indicate one of the three models that best describes the random process. Probability distribution function is shown in Fig. 3.9 and $P(X > x)$ of accumulated rainfall for this distribution is shown in Fig. 3.10.

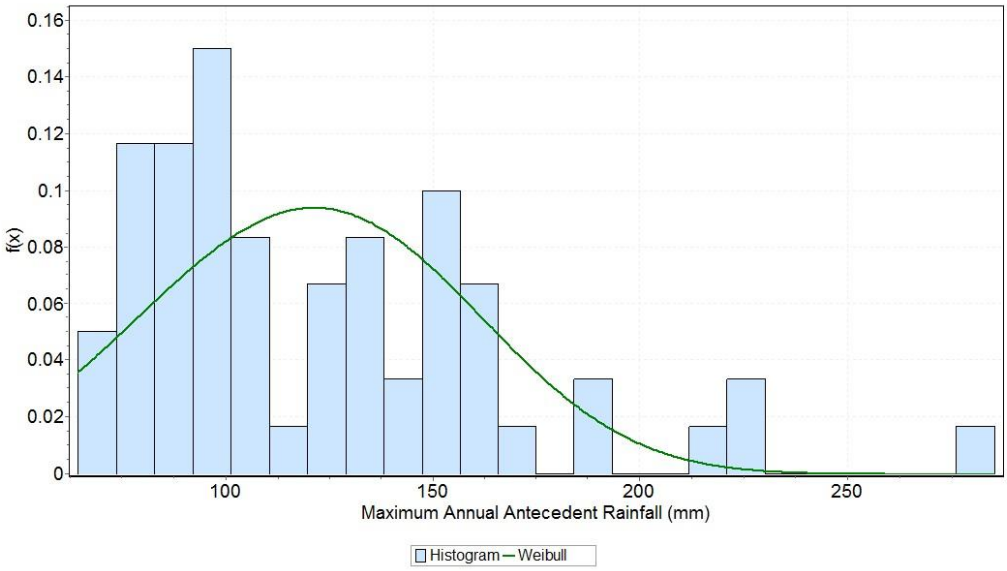

Fig. 3.8 Probability density function for Weibull distribution

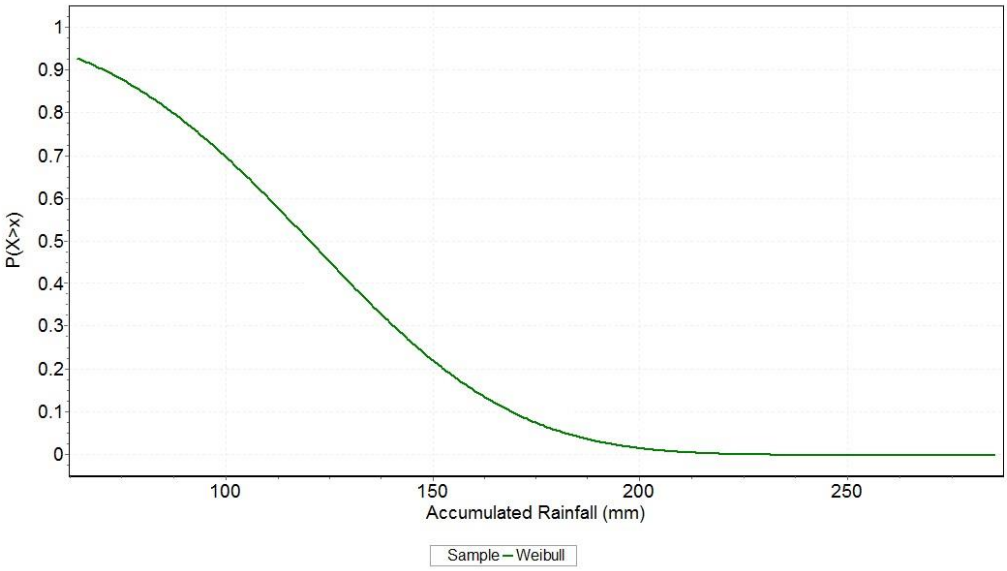

Fig. 3.9 Probability of exceedance for Weibull distribution

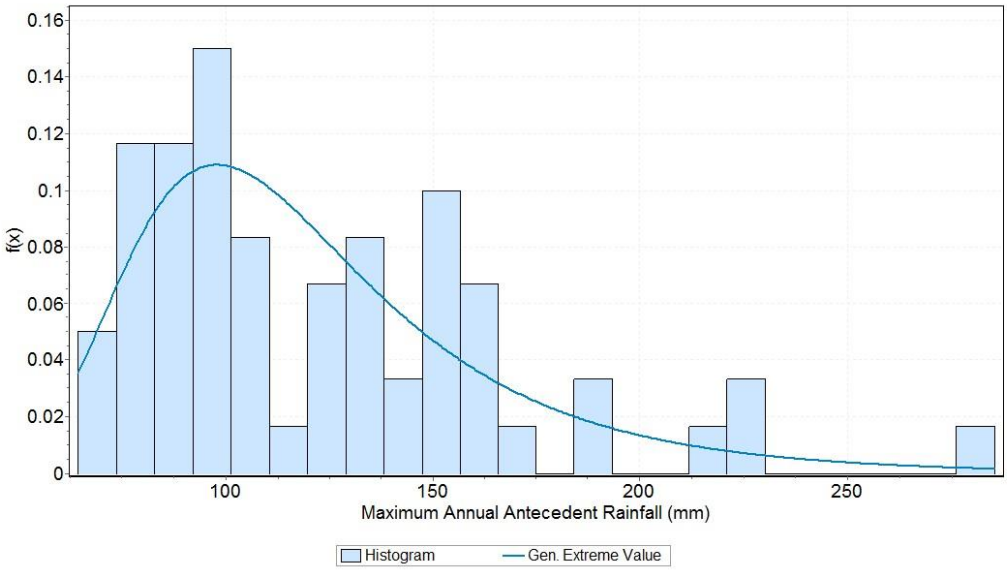

Fig. 3.10 Probability density function for GEV distribution

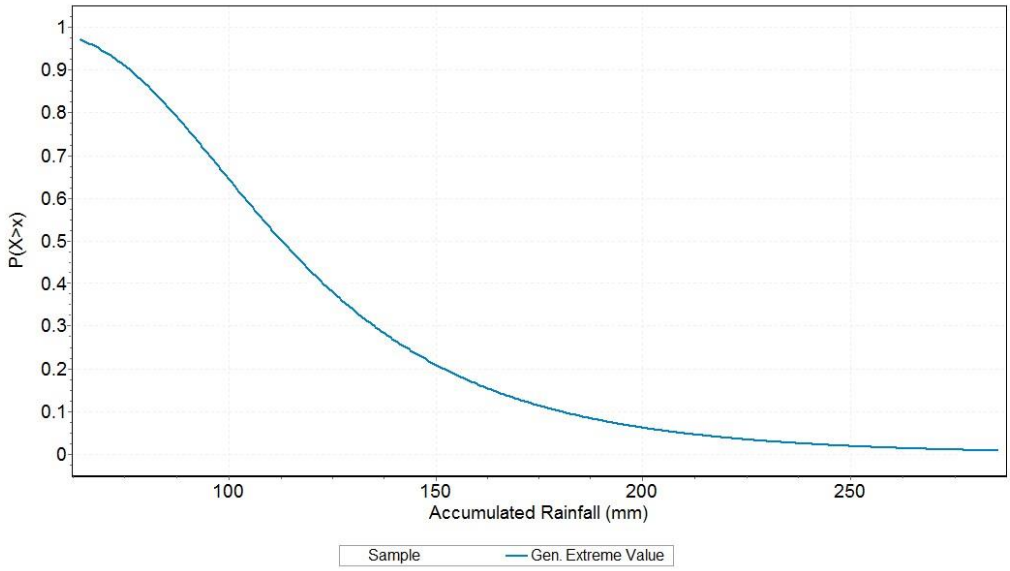

Fig. 3.11 Probability of exceedance for GEV distribution

3.6.3 Goodness-of-fit tests

In order to determine which distribution is the most valid model to be used with the data, goodness-of-fit tests are done. The goodness-of-fit (GOF) tests are used to measure distance between data and the distribution chosen and compare the distance to a threshold value. The distance is called a test statistic and if it is less than the threshold value (critical value), the fit is considered as good.

Three GOF tests include Kolmogrov-Smirnov, Anderson-Darling and Chi-Squared tests. Using these three tests, the best distribution that model this study's data can be seen.

(a) Kolmogorov-Smirnov test

This test is used to decide if sample comes from hypothesised continuous distribution. This test is based on empirical CDF and assumed random sample $x_1, \ldots, x_n$ from some continuous distribution with CDF $F(x)$. Empirical CDF is as follows

$$F_n(x) = \frac{1}{n}[\text{number of observations } \leq x] \tag{3.9}$$

$$F_n(x) = \frac{1}{n}\sum_{i=1}^{n} I(x_i \leq x) \tag{3.10}$$

With I = 1 if true and 0 if false. Kolmogorov-Smirnov statistic is based on the largest difference between $F(x)$ and $F_n(x)$ and is given as in equation below

$$D_n = \sup_x |F_n(x) - F(x)| \quad (3.11)$$

(b) Anderson-Darling test

This is a general test to compare fit of an observed continuous distribution function to empirical distribution function. The Anderson-Darling test gives more weight to the tails than Kolmogorov-Smirnov test and is given by the following equation

$$A^2 = -n - \frac{1}{n}\sum_{i=1}^{n}(2i-1).\left[\ln F(X_i) + \ln\left(1 - F(X_{n-i+1})\right)\right] \quad (3.12)$$

(c) Chi Squared test

The Chi-Squared is used to determine if sample comes from population with specific distribution. The test is applied to bin data and it compares how well theoretical distribution with empirical distribution. The test equation is given as follows

$$x^2 = \sum_{i=1}^{k}\frac{(O_i - E_i)^2}{E_i} \quad (3.13)$$

Where O_i is the observed frequency value for bin i and E_i is the expected frequency for bin i.

$$E_i = F(x_2) - F(x_1) \quad (3.14)$$

F is the cumulative distribution function of probability being tested and x_1 and x_2 is the limits for bin i.

3.6.4 Selection of the best distribution function

The Previous subchapter 3.6.3 shows the whole distribution functions chosen for this study. The results for every return period for 5-days accumulated antecedent rainfall for the particular station on Penang Island are shown in Table 3.1. The return period is an important indicator, as mentioned in Chapter 2, to represent the probability of

occurrences of the event with regards to very high accumulated antecedent rainfall. From the return periods, the total amount of rainfall can be predicted and countermeasures or preparedness can be done in the case of catastrophic events.

In this study, the 1.25 years, 2 years, 5 years and 10 years return period were chosen for the next step of analysis. The probability of occurrence of accumulated antecedent rainfall for the return periods are 0.8, 0.5, 0.2 and 0.1 for 1.25, 2, 5 and 10 years respectively. The total amounts of rainfall in Penang Island for all probabilities are shown below.

Table 3.1 Total amount of accumulated rainfall in 1.25 years, 2 years, 5 years and 10 years return period

Distribution	1.25 years	2 years	5 years	10 years
GEV	86.40mm	112.60mm	151.91mm	180.62mm
Gumbel	85.73mm	115.32mm	155.14mm	181.50mm
Frechet	86.05mm	108.36mm	147.77mm	181.50mm
Normal	84.81mm	122.72mm	160.64mm	180.46mm
Weibull	87.11mm	120.15mm	152.59mm	168.92mm

It can be seen from the table above that the range for rainfall amount for all distributions are almost the same. In order to choose the best distribution function to represent the accumulated antecedent rainfall in Penang Island, the goodness-of-fit tests were done and the result are shown in Table 3.2.

Table 3.2 Ranking for probability distribution using goodness-of-fit tests

Distribution	Test ranking position					
	Kolmogorov-Smirnov		Anderson-Darling		Chi-Squared	
	Statistic	Rank	Statistic	Rank	Statistic	Rank
GEV	0.09753	1	0.48254	1	6.8902	5
Gumbel	0.10719	2	0.60676	2	5.8395	3
Frechet	0.11061	3	0.61102	3	2.6587	1
Normal	0.13469	4	1.6611	4	5.864	4
Weibull	0.1398	5	1.8554	5	3.2812	2

The test statistic numbers for the study were computed for 5 types of probability distributions. The probability having first ranked together with the statistic number is presented as in table 3.2. It can be observed that using the Kolmogorov-Smirnov test and the Anderson-Darling test, the Generalised Extreme Value (GEV) obtained the first rank for the amount of rainfall for 5-days accumulated antecedent rainfall. Using the Chi Squared test, the Frechet distribution function obtained first rank. In this study, the GEV distribution function will be used in the following chapter. This is because the GEV distribution function gave the best result when tested with the goodness-of-fit tests. The Kolmogorov-Smirnov test shows that GEV rank is number 1 and this shows that the sample comes from hypothesised continuous distribution and the Anderson-Darling test shows that the observed CDF is fit when compared with the empirical CDF. The Anderson-Darling test also gives more weight to the tail of the graph (right side of the histogram) than the Kolmogorov-Smirnov test.

3.7 Conclusions

The aim of this chapter was to be able to determine the probability rainfall analysis for Penang Island. In order to accomplish that, several steps of procedure were done which

included collection of rainfall data for Penang Island, determination of the suitable distribution functions that can best represent the rainfall pattern on Penang Island, testing of the distribution functions and finally selection of the best function.

Five distribution functions were selected based on work from previous researchers in Malaysia[1][12][13] and they are the normal distribution and extreme condition distributions (Gumbel, Frechet, Weibull and Generalised Extreme Value). The extreme condition distribution is chosen since the data used for analysis represent extreme rainfall conditions for Penang Island. Results for each distribution are shown in sub-chapter 3.6.2. From these graphs, probability of occurrences of accumulated antecedent rainfall can be obtained. In this study, the 1.25 years, 2 years, 5 years and 10 years return periods were chosen for further analysis. The results for every probability for each distribution function are shown in Table 3.1.

To determine the best distribution function that can represent accumulated antecedent rainfall for Penang Island, goodness-of-fit tests were done. The Kolmogorov-Smirnov test, the Anderson-Darling test and the Chi Squared test were chosen for the analysis. These tests are most commonly used and are accepted as appropriate tests for the analysis based on previous researchers' works. Results for these tests are measured by the statistic number and are ranked as shown in Table 3.2.

From Table 3.2, it can be seen that the suitable distribution functions that can represent accumulated antecedent rainfall for Penang Island are the GEV distribution and the Frechet distribution. However, from previous researchers results[12][13], it can be concluded that GEV is the best distribution functions to be used for the Penang Island condition.

By using the GEV distribution function, the probability exceedance per annum for 0.8(1.25 years), 0.5(2years), 0.75(5 years) and 0.1(10years) corresponds with 86.4mm, 112.60mm, 151.91mm and 180.62mm rainfall. This function is considered suitable for this study since it represents extreme conditions and is based on a combination of the other three distribution functions (Gumbel, Frechet and Weibull) and will be used in the next chapter analysis.

References

[1] J. Suhaila and A. A. Jemain, "Investigating the impacts of adjoining wet days on the distribution of daily rainfall amounts in Peninsular Malaysia," *J. Hydrol.*, vol. 368, no. 1–4, pp. 17–25, Apr. 2009.

[2] N. S. Muhammad, "Probability Structure and Return Period Calculations for Multi-Day Monsoon Rainfall Events at Subang, Malaysia," Colorado State University, 2013.

[3] L. M. Lee, N. Gofar, and H. Rahardjo, "A simple model for preliminary evaluation of rainfall-induced slope instability," *Eng. Geol.*, vol. 108, no. 3–4, pp. 272–285, Oct. 2009.

[4] A. Rahimi, H. Rahardjo, E. Leong, and M. Asce, "Effect of Antecedent Rainfall Patterns on Rainfall-Induced Slope Failure," no. May, pp. 483–491, 2011.

[5] F. Guzzetti, P. Reichenbach, M. Cardinali, M. Galli, and F. Ardizzone, "Probabilistic landslide hazard assessment at the basin scale," *Geomorphology*, vol. 72, no. 1–4, pp. 272–299, Dec. 2005.

[6] M. J. Crozier, "Prediction of rainfall-triggered landslides: a test of the Antecedent Water Status Model," *Earth Surf. Process. Landforms*, vol. 24, no. 9, pp. 825–833, Aug. 1999.

[7] V. Te Chow, *Handbook of Applied Hydrology*. McGraw-Hills Companies, 1964.

[8] P. Frattini, G. Crosta, and R. Sosio, "Approaches for defining thresholds and return periods for rainfall-triggered shallow landslides," vol. 1460, no. March, pp. 1444–1460, 2009.

[9] I. Tsaparas, H. Rahardjo, D. G. Toll, and E. C. Leong, "Controlling parameters for rainfall-induced landslides," vol. 29, pp. 1–27, 2002.

[10] G. B. Crosta and F. Agliardi, "How to obtain alert velocity thresholds for large rockslides," *Phys. Chem. Earth*, vol. 27, no. July, pp. 1557–1565, 2002.

[11] H. Rahardjo, E. C. Leong, and R. B. Rezaur, "Effect of antecedent rainfall on pore-water pressure distribution characteristics in residual soil slopes under," vol. 523, no. October 2007, pp. 506–523, 2008.

[12] M. D. Zalina, K. Lumpur, and A. Mechanics, "Selecting a probability distribution for extreme rainfall series in Malaysia," no. 1991, pp. 63–68, 1993.

[13] N. E. Alias and K. Takara, "Probability distribution for extreme hydrological values-series in the Yodo river basin, Japan and Kuala Lumpur, Malaysia," in *2nd International Conference on Water Resources*, 2012.

Chapter 4

CRITERIA OF CRITICAL LOCATION AND COMBINING EARTHQUAKE AND RAINFALL EFFECTS

4.1 Introduction

This chapter explains identification of slopes and the characteristics for Penang Island. There are 4 methods to assess slope hazard as mentioned by Varnes[1], such as from inventory analysis, the heuristic approach, the statistical method and the deterministic approach. In the deterministic approach, analysis can be done by using site-specific characteristics to determine the stability of a slope. The method to determine the factor of safety of a slope takes into account the physical appearance of the slope, the water level condition, soil characteristics as well as external factors, such as rainfall infiltration or seismic activity. It is the best method to analyse stability of a slope but it is limited to site-specific problems and the effect of homogeneity cannot be counted.

When it comes to analysis of an area without engineering parameter records, historical records play an important role and thus came along the statistical approach in analysing landslides or slope failures. Also in the case where the study area is too large and collecting each soil sample is impossible, the statistical approach is the most suitable method to analyse slope condition. In this study, the soil record for Penang Island is also limited to a certain area and therefore, consideration and assumptions need to be taken to ensure investigation of the slope condition can be done without jeopardising the accuracy of the analysis.

4.2 Chapter Overview

In chapter 2 and 3, probabilistic analyses were done with respect to earthquakes and rainfall on Penang Island. In this chapter, the analysis was divided into 2 parts. The first part tries to identify areas that are critical with the highest number of slopes and the Geographical Information System (GIS) method was used. Data, such as an elevation map of Penang Island, were collected from a local researcher at the Universiti Sains

Malaysia. By using ArcGIS10, Digital Elevation Model (DEM) and TIN (Triangulated Irregular Network) a model was created and spatial analysis conducted to produce a map that shows the slopes in degrees and in percentage (%). From there, a specific location can be chosen for the next chapter analysis.

The second part of the chapter shows the effect of 5-day accumulated rainfall on Penang Island slopes. Data used for this part are the piezometer test data and rainfall amount data from a nearby rainfall station. The piezometer data were taken from a site in the Universiti Sains Malaysia and data was collected from March 2005 to February 2006. For the same period, daily rainfall data were collected from Kolam Takungan Air Hitam Rainfall Station. The data collected were converted into 5-days accumulated antecedent rainfall as mentioned in chapter 3. Using rainfall data and combining it with piezometer test result, water level changes can be monitored and this result will be used for the next chapter when analysis on the slope failure will be done.

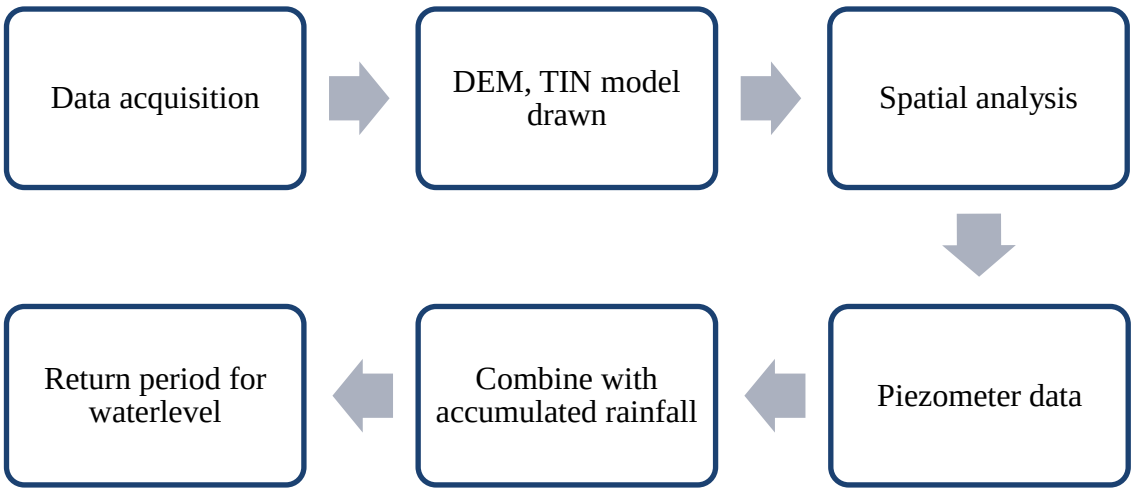

Fig. 4.1 Flowchart of chapter 4

4.3 Slopes Distribution in Penang Island

4.3.1 Introduction

Penang Island is almost 60% covered with slopes and hillsides (Fig. 4.2). Lee and Biswajeet[2] reported that Penang Island is covered with slopes ranging from 25° to 87°. The highest point from sea level is about 840m and some of the hills are developed for housing and infrastructure. From Fig. 4.2, it can be seen that higher elevations are concentrated at the centre of the island. The bedrock of the island is granite and since there are limited flat surfaces on the island, a lot of residential areas are built especially on the east part of the island, which is close to the capital city of Penang, Georgetown.

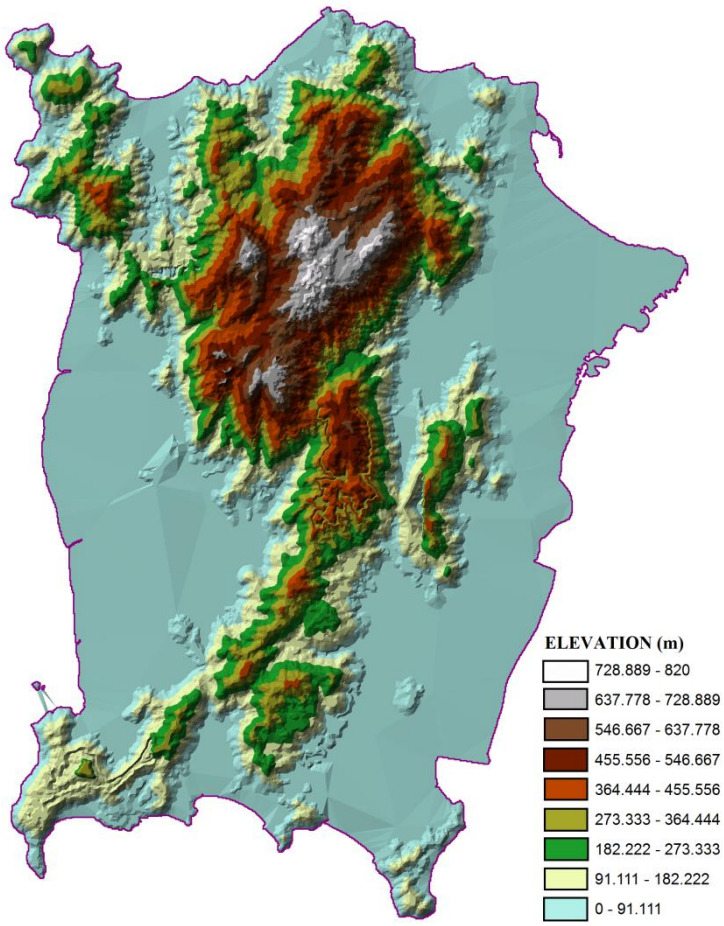

Fig. 4.2 Elevation map of Penang Island

In order to identify areas that are critical with the highest number of slopes and near to housing and important infrastructure, an aerial map is used with remote sensing analysis. There are several factors that contribute to landslides, such as the slope physical features (angle), the soil types, groundwater condition and external factors, such as rainfall and seismicity. Using the Geographical Information System these factors are transformed into a vector-type spatial database, such as by creating a Digital Elevation Model (DEM).

4.3.2 Geographical Information System (GIS) for slope analysis

The usage of GIS-mapping is to produce geographical data that can simplify the view of characteristics of the area of study. All data are schematised to give a proper view of the whole area and enabling us to visualise the landscape of the study area.

In this study an elevation map of Penang Island was obtained from local expertise in the Universiti Sains Malaysia. The 20-meter interval contours elevation map was then converted into DEM using ArcGIS10 (Fig. 4.3).

The DEM is then converted into TIN (Triangulated Irregular Network) model in order to be analysed using 'SLOPE' function under the Spatial Analyst command. Using square windows, spatial analysis was done to filter discretised, continuous surface and compute a new value for each central cell of the square windows[3]. This operation is known as *convolution*. In smoothing (low-pass) filter, value for the centre cell of the window is computed as a simple arithmetic average value of the other cells.

Slopes for each cell are the rate of change in the value from each cell to its neighbours and since the gridded surface has been discretised, derivatives are approximated either by computing differences within each square filter or by fitting a polynomial to the data within the filter. Burrough and McDonnell[3] defined a slope as a plane tangent to the surface as modelled by the DEM at any given point and comprises two components GRADIENT (maximum rate of change of altitude) and ASPECT (compass direction of this maximum rate of change).

Fig. 4.3 DEM models of Penang Island

Gradient is usually measured in percent, degrees or radians and aspect in degrees. Percent is considered as the rise divided by run, multiplied by 100. When the angle is 45 degrees, the rise is equal to run and it will be 100 percent. As slope angle approaches vertical (90 degrees), the percent will reach infinity.

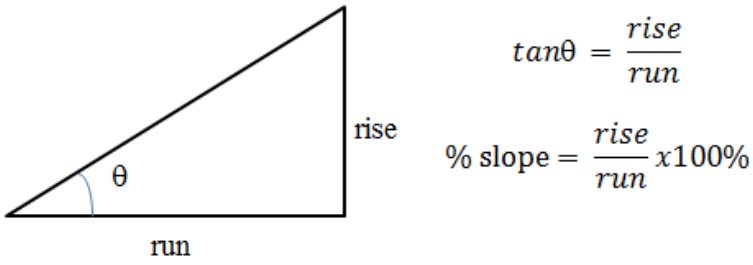

Fig. 4.4 Illustration on slope angle calculation on ArcGIS10

4.3.3 Estimation of slope

Using ArcGIS10, slopes can be determined from the rates of change of surface in the horizontal (*dz/dx*) and vertical (*dz/dy*) directions from the centre cell[4]. The rate of change for x- and y- direction was taken from Horn[5], a method which is a third-order finite difference estimator using all eight outer points of the window;

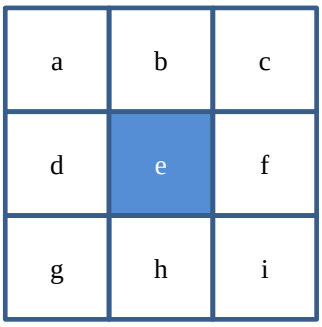

Fig. 4.5 Neighbourhood window for each cell at x- and y- direction

For the east-west gradient, the rate of change function will be

$$\left[\frac{dz}{dx}\right] = \frac{\left((c+2f+i)-(a+2d+g)\right)}{(8*cell\ size\ at\ x-direction)} \tag{4.1}$$

and for the south-north gradient, the rate of change function will be

$$\left[\frac{dz}{dy}\right] = \frac{\left((g+2h+i)-(a+2b+c)\right)}{(8*cell\ size\ at\ y-direction)} \tag{4.2}$$

To calculate the slope in degrees, the equation will be

$$Slope\ in\ degrees = \tan^{-1}\left(\sqrt{\left(\frac{dz}{dx}\right)^2+\left(\frac{dz}{dy}\right)^2}\right) x\,\frac{180}{\pi} \tag{4.3}$$

From Eq. (4.3), using spatial analyst command in ArcGIS10, each centre cell for each window is assigned with degrees and percent values. New map showing location of slope on Penang Island is then constructed as shown in Fig. 4.6 and 4.7.

4.3.4 Slope map for Penang Island

Fig. 4.6 and 4.7 show the slope map for Penang Island with different cell sizes. In order to produce better results, a smaller cell size should be chosen to represent the ideal condition of the slope formation. Using ArcGIS10 Spatial Analyst command, 2 cell sizes were chosen for this study to represent Penang Island slopes, 10-unit and 50-unit. The map for 10-unit cell size shows better prediction on Penang Slope than 50-unit. Lee and Pradhan[2] [6] mentioned in their papers that angle of slopes on Penang Island range from 26° to 87°. From Fig. 4.6, it can be seen that the highest angle on Penang Island is 86.6° and this is almost the same as reported by previous researchers. One of the reasons of different maximum slope angles between the two cell sizes is that a bigger size gives a larger mean value for the cell height (*dz* values), therefore, the calculation proceeding section from there will give lower values of slope angle.

By choosing a smaller cell size, it can be seen that the resolution of the map is better than a bigger cell size. This is due to the effect of smoothing and filtering. The cell size 10-unit map resolutions are better and more detailed analysis showing the slope angle and the location of critical slopes can be seen.

In Fig. 4.6, it can be seen that almost 70% of the total area on Penang Island is governed with slopes with more than 16° angle and reach up to 86.6°. This shows that there are a lot of hillsides and slopes on the island and probability of landslide occurrences is high.

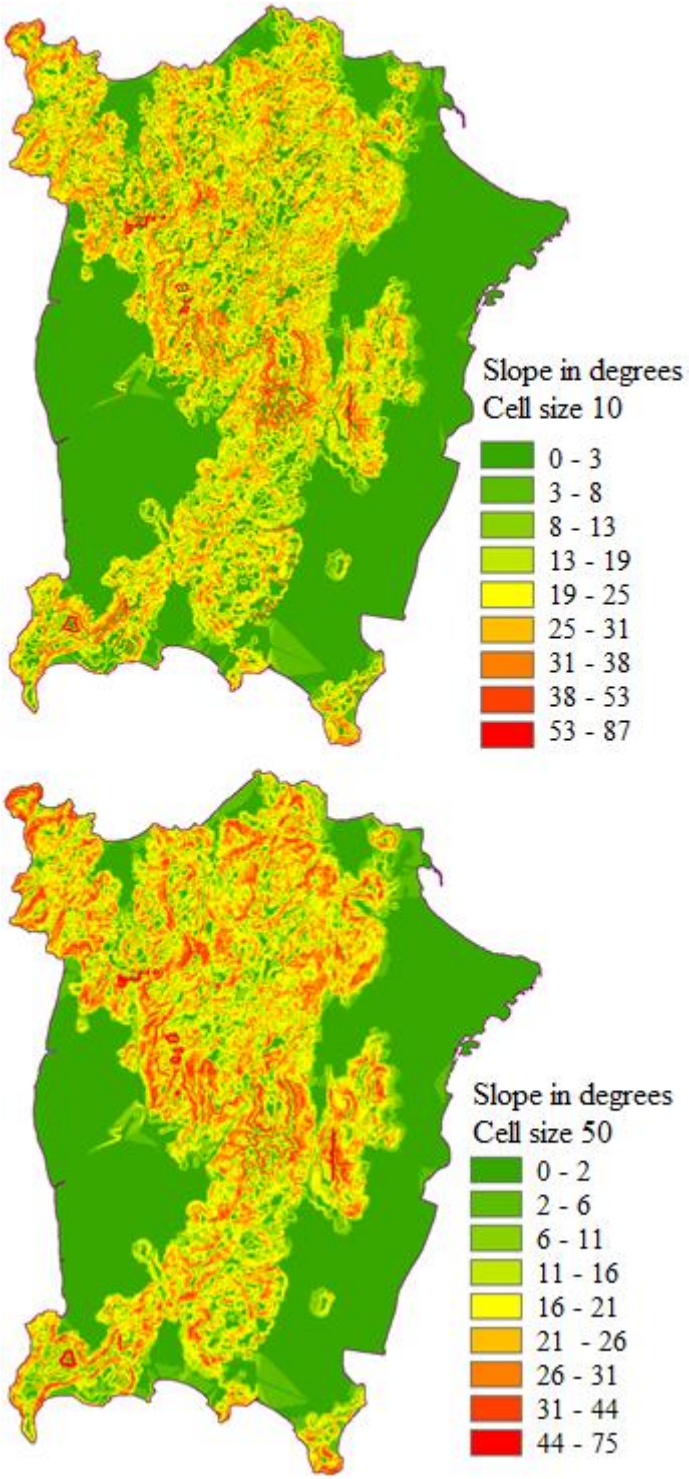

Fig. 4.6 Penang Island map showing slope in degrees for cell size 10 units (top) and 50 units (bottom)

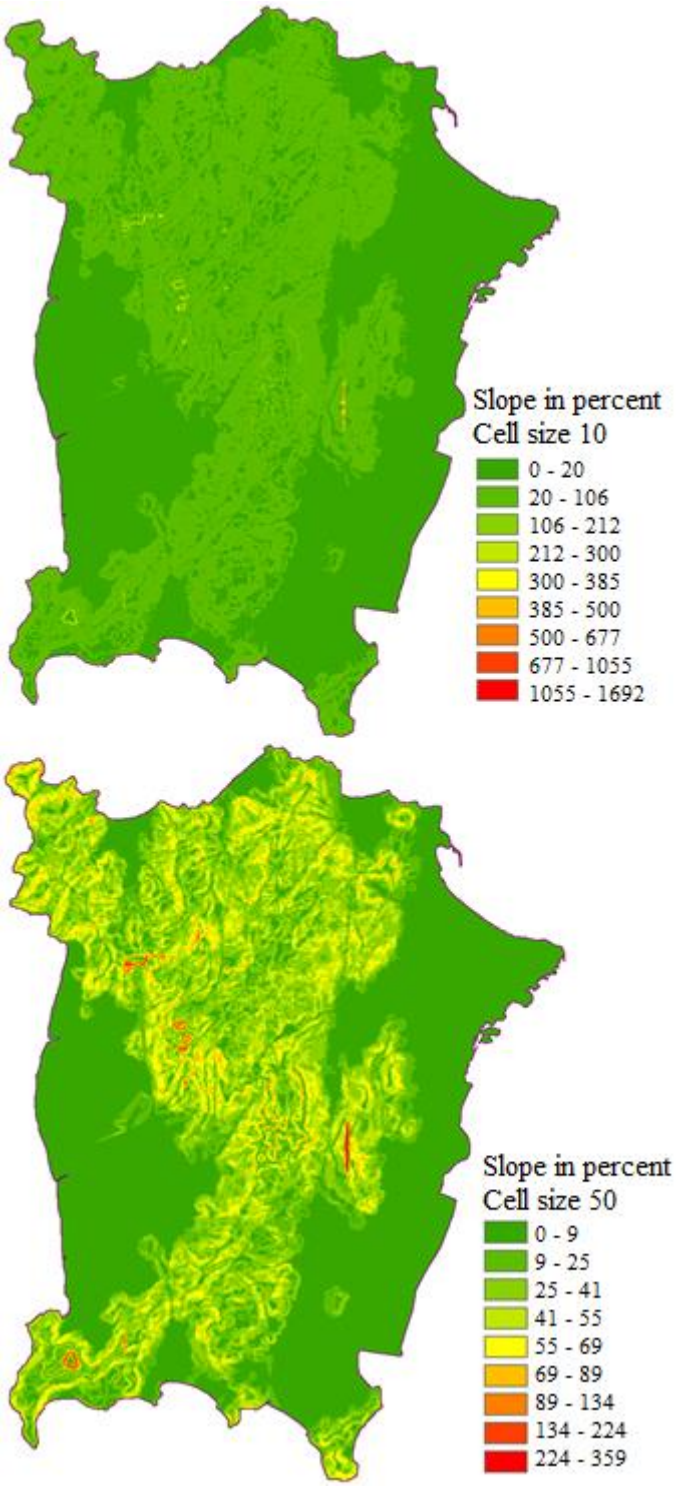

Fig. 4.7 Penang Island map showing slope in percent for cell size 10 units (top) and 50 units (bottom)

To specify the location of an area that is more critical, several attributes should be taken into account. For example, a location with a higher density of population as well as important infrastructure and located near to critical slopes should be considered as a risky area. In Fig. 4.8, important locations are shown and some of these locations are important in the next chapter analysis. All locations are numbered as seen in the figure with number 1, which is the capital city of the island, Georgetown (latitude 5.42, longitude 100.33). It is worth mentioning that although the capital city is far from hills and slopes, there are important old buildings in the city as Georgetown has been regarded by UNESCO as a historical site in 2008.

Location number 2 is Batu Ferringhi (coastal along latitude 5.47, longitude 100.25) which is located on the north of the island. Here, residential properties and hotels are built near the seashore as well as on the hillsides. Next, number 3 location is Tanjung Bungah (latitude 5.46, longitude 100.29), which also like Batu Ferringhi is a tourist attraction for sightseeing and sea-bathing.

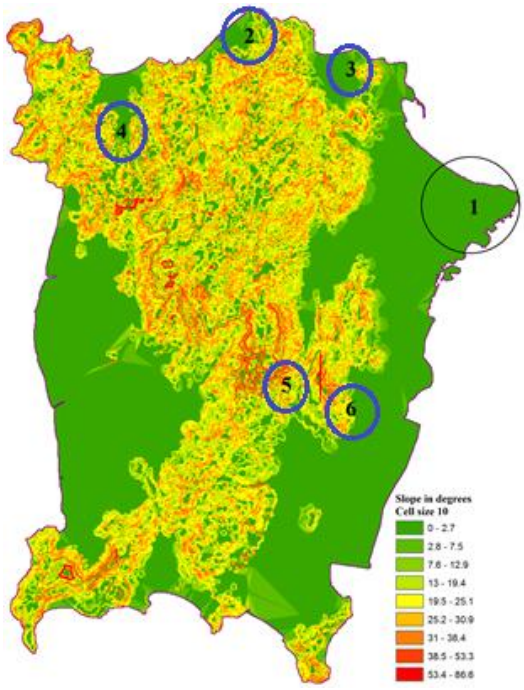

Fig. 4.8 Important location on Penang Island

At point number 4 a dam is located that supplies water for the island, the Telok Bahang Dam and surrounding the dam there are a lot of roads that connect between the east and west of the Island. Location 5 is Air Hitam. In Fig. 4.7, for cell size 10-unit map, few spots with higher slope percentages can be seen. The red strip on the map on the centre of the island is the location of Paya Terubong. Although there is a limited number of residences there, but in the next part of this chapter, rainfall data from there is used for the next analysis. Location 6 is the Universiti Sains Malaysia where piezometer data was taken and will be used in the next part of this chapter.

In the next chapter, deterministic analysis will be done by combining the earthquake data and rainfall data. Since there is a limitation on data acquisition, the analysis will be limited to certain areas on Penang Island. Soil parameters are the most important entities used in the slope analysis in the next chapter and for this study, the soil parameters available only applied to Batu Ferringhi and Tanjung Bungah. Since these are some of the most important locations on Penang Island, it is assumed to be sufficient enough to be chosen as the study area for the next chapter analysis.

4.4 Changes in Groundwater Level

4.4.1 Mechanism of rainfall-induced landslides

Landslides may occur due to many triggering factors, such as earthquakes and rainfall. In Malaysia, annual precipitations are almost up to 2,500mm and therefore become one of the most important triggering factors of slope failure. Ng[7] describes an overview of the mechanism of rainfall-induced landslides in tropical residual soil slopes. During rainfall events, the shear strength of soil is reduced due to matric suction loss in unsaturated zones and this may lead to a landslide event. Previous researchers and studies have shown that reduction in shear strength in soil is the most important factor that leads to reduction in safety factor of the slope resulting in landslide[8]–[11].

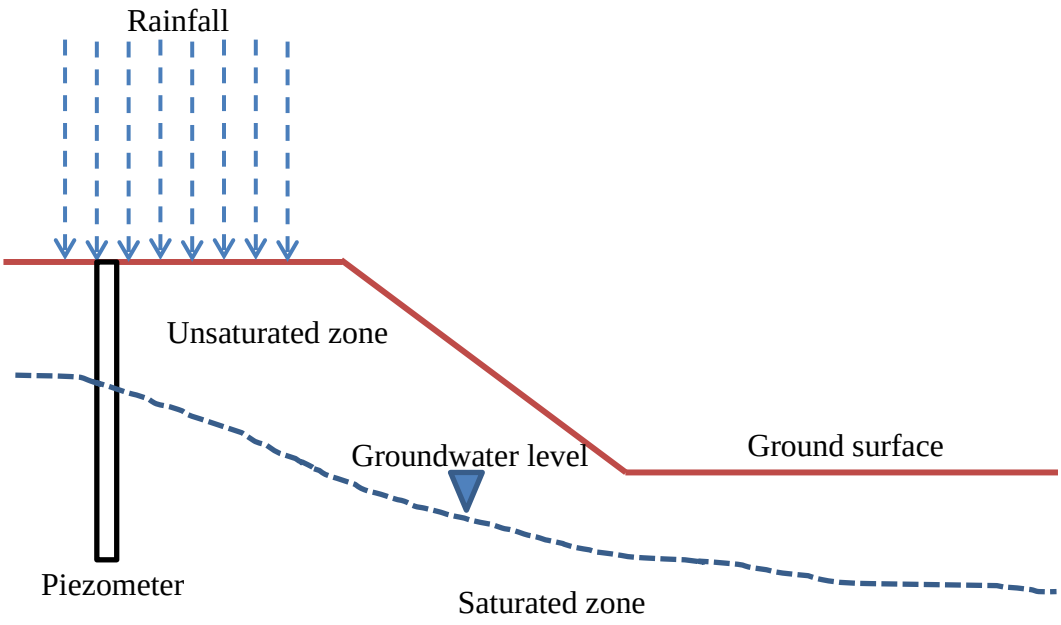

Fig. 4.9 Mechanism of rainfall-induced landslide

4.4.2 Monitoring groundwater changes

Since groundwater changes are the most important parameters that contribute to slope failure, it is important to monitor its changes to understand the behaviour of water underground. Groundwater monitoring is a constant process and each change should be taken into account. One of the methods to monitor groundwater changes is by installing a piezometer. A piezometer is a device used to measure static liquid pressure by measuring the height of water or liquid that rises against the gravity in a column constructed by excavation. The readings are in frequency (*hz*), since the reader is a vibrating wire, and then converted into pressure values by applying calibration factors. These pressure values, which are in mH_20 units, are equal to the height of water.

By referring to Fig. 4.9, when a piezometer is installed in the excavated column, it should be below the existing groundwater level, which represents the saturated area underneath the ground. The water level at the saturated level is already in a certain pressure depth so any water changes above the saturated level (which is the unsaturated area) means an uplift pressure from water in the saturated area; thus is equal to height.

For this study, the piezometer data was taken from a site in the Universiti Sains Malaysia (location 5 in Fig. 4.8) from March 2005 to February 2006. Details of the piezometer test pit can be seen in Fig. 4.10.

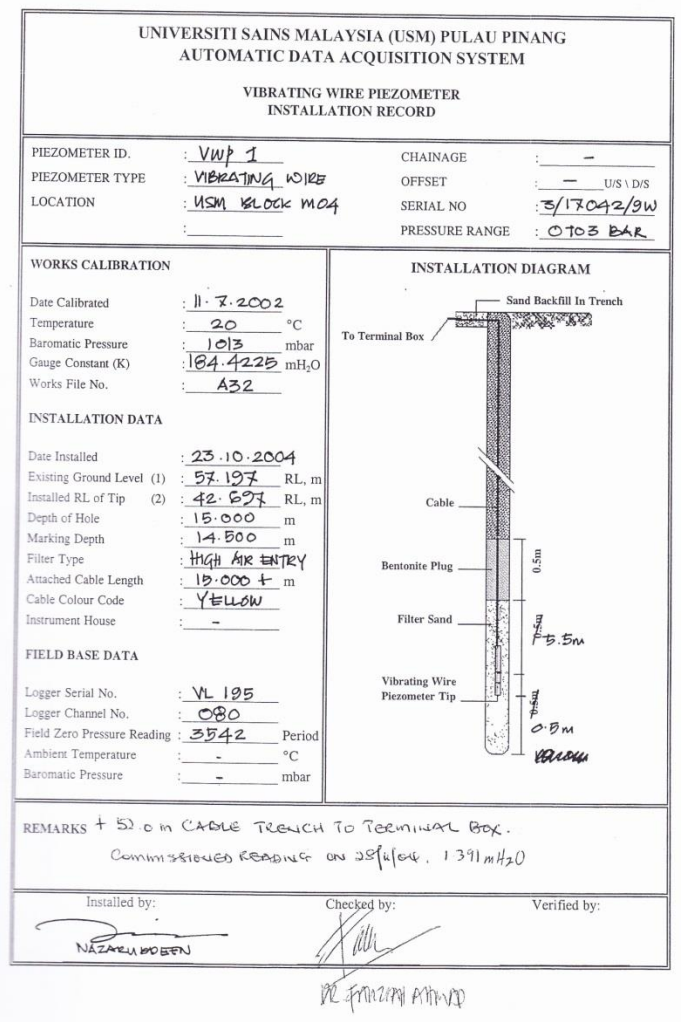

UNIVERSITI SAINS MALAYSIA (USM) PULAU PINANG
AUTOMATIC DATA ACQUISITION SYSTEM

VIBRATING WIRE PIEZOMETER
INSTALLATION RECORD

PIEZOMETER ID.	: VWP 1	CHAINAGE	: -
PIEZOMETER TYPE	: VIBRATING WIRE	OFFSET	: — U/S \ D/S
LOCATION	: USM BLOCK M04	SERIAL NO	: 3/17042/9W
	:	PRESSURE RANGE	: 0 TO 3 BAR

WORKS CALIBRATION

Date Calibrated	: 11.7.2002	
Temperature	: 20	°C
Baromatic Pressure	: 1013	mbar
Gauge Constant (K)	: 184.4225	mH_2O
Works File No.	: A32	

INSTALLATION DATA

Date Installed		: 23.10.2004	
Existing Ground Level	(1)	: 57.197	RL, m
Installed RL of Tip	(2)	: 42.697	RL, m
Depth of Hole		: 15.000	m
Marking Depth		: 14.500	m
Filter Type		: HIGH AIR ENTRY	
Attached Cable Length		: 13.000 +	m
Cable Colour Code		: YELLOW	
Instrument House		: -	

FIELD BASE DATA

Logger Serial No.	: VL 195	
Logger Channel No.	: 080	
Field Zero Pressure Reading	: 3542	Period
Ambient Temperature	: -	°C
Baromatic Pressure	: -	mbar

INSTALLATION DIAGRAM

REMARKS + 52.0 m CABLE TRENCH TO TERMINAL BOX.
COMMISSIONED READING ON 25/4/06. 1.391 mH_2O

Installed by: NAZARUDEEN
Checked by:
Verified by:

Fig. 4.10 Detail on piezometer data in the Universiti Sains Malaysia

Fig. 4.11 shows the soil layer for the borehole that was constructed for piezometer installation. The total depth of the hole was 15m and the impermeable layer was granite from 7.5m downward. Usually the piezometer data is also read with rainfall data. A rainfall gauge is usually installed next to the piezometer and reading can be done together. However, the rainfall gauge used with this piezometer was broken and thus no reliable data can be used for this study. In order to simplify the next step analysis, another rainfall gauge is used with the piezometer data and is explained next.

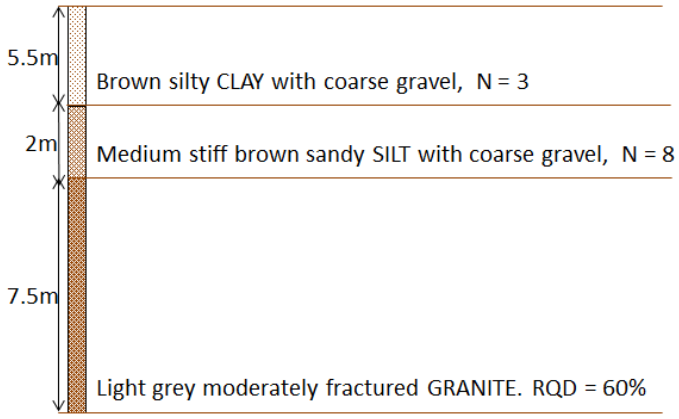

Fig. 4.11 Soil layer for piezometer pit

4.4.3 Combine piezometer data with rainfall data

The nearest available rainfall gauge is at Kolam Takungan Air Hitam (lat 5.23 long 100.15), which is near location 5 in Fig. 4.8. It is situated about 5.5km from the piezometer and data is taken by the Malaysian Meteorological Department. The rainfall data was in daily measurement and the piezometer data was in hourly so conversion on piezometer data was done to match the rainfall data. Several assumptions were made to simplify the analysis, such as the effect of evapo-transpiration, as well as water flow was neglected. The rainfall data was converted into 5-days antecedent rainfall amount. Explanation on the antecedent data is the same as in Chapter 3.

Data was then plotted as Fig. 4.12 to show the relationship between rainfall occurrence and water level. It can be seen that with an increase of rainfall, the water table becomes higher and unsaturated areas become shallower. Infiltration of rainwater into saturated soil will decrease the matric suction, thus reducing the shear strength of the soil. This will lead to slope failure.

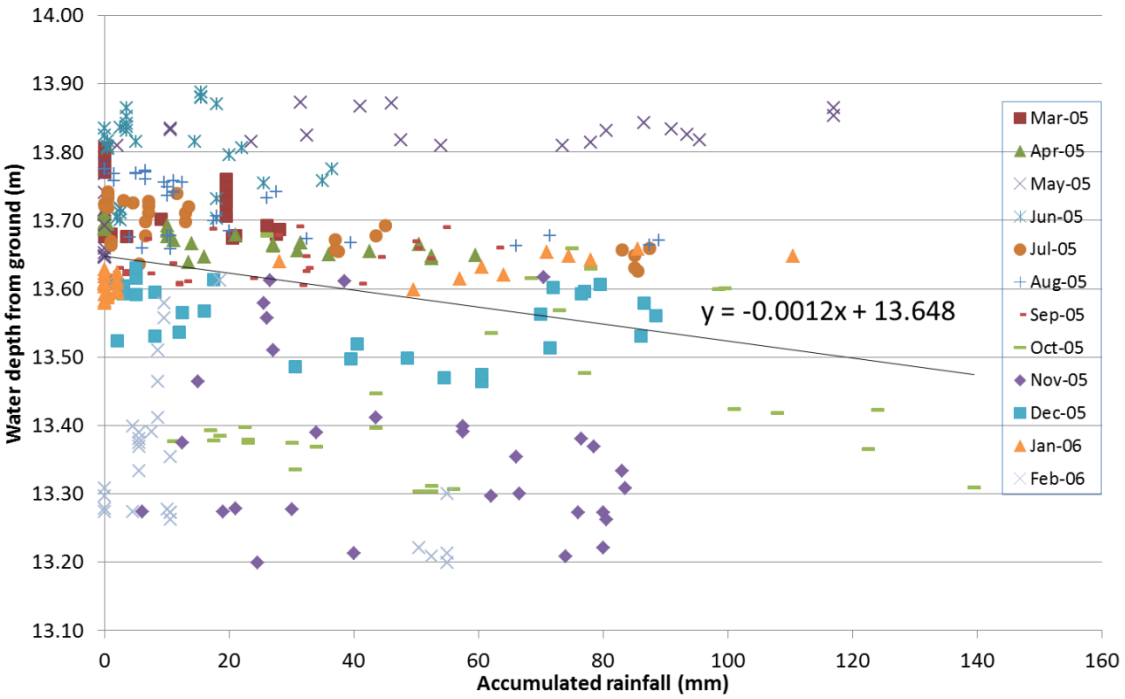

Fig. 4.12 Relationship between average water heights with 5-days accumulated rainfall

Fig. 4.13 and Fig. 4.14 show the relationship between average water heights with 5-days accumulated rainfall for dry months (June – September) and wet months (October – December). The definition for dry and wet months is given by the Malaysian Meteorological Agency and the figures show the relationship for the two seasons.

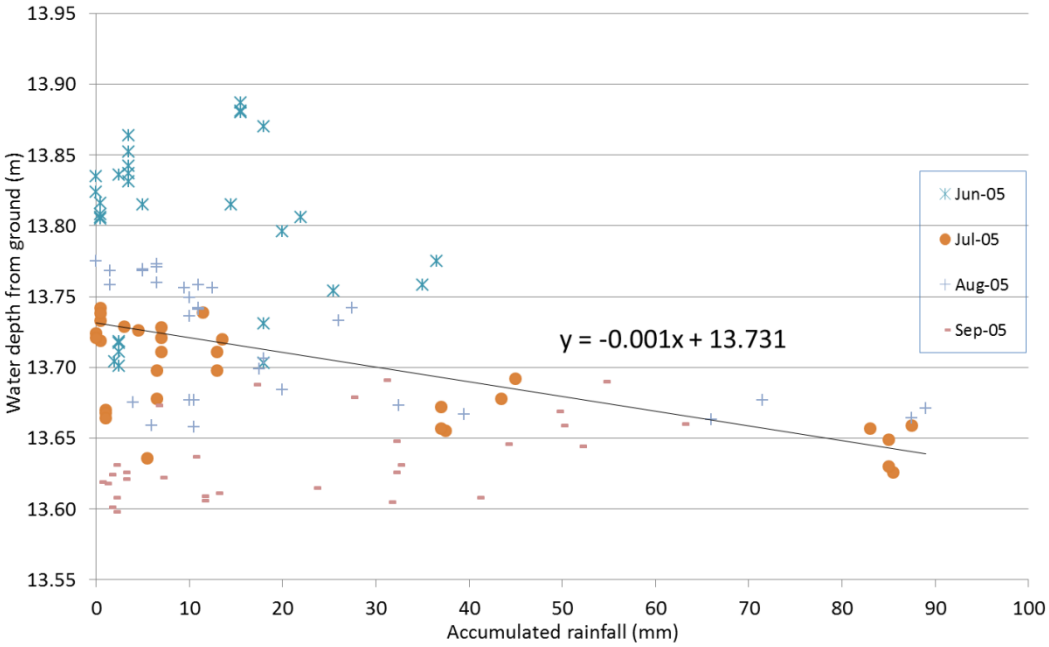

Fig. 4.13 Relationship between average water heights with 5-days accumulated rainfall for dry months (June to September)

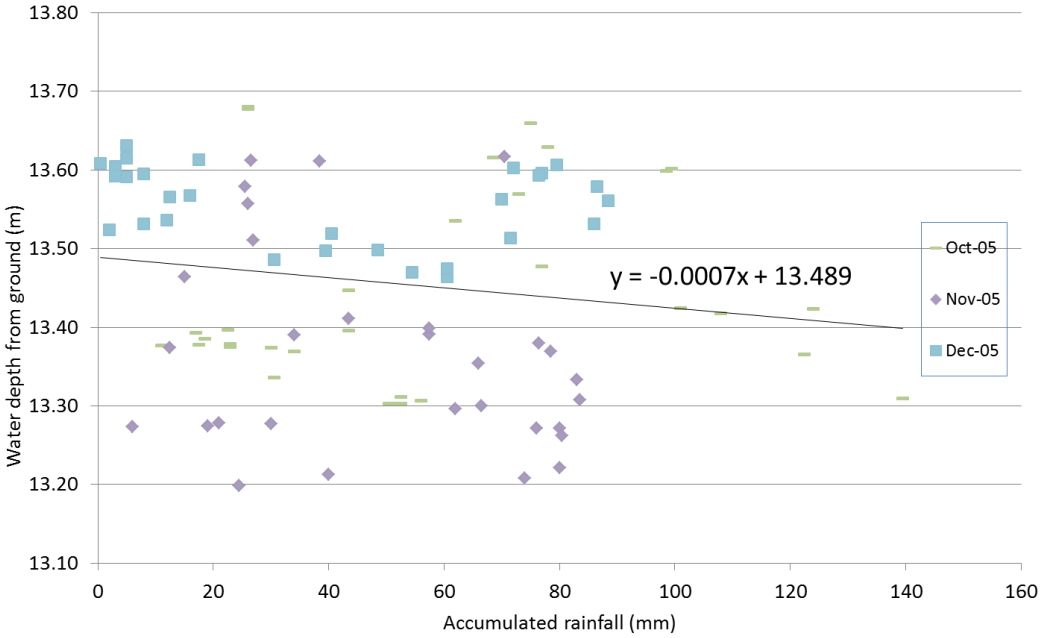

Fig. 4.14 Relationship between average water heights with 5-days accumulated rainfall for wet months (October to December)

Dryer months show lower accumulated rainfall, which leads to a deeper water table. Higher accumulated rainfall can be seen on wet months and the water table can be seen at shallower depths. Some months on wet seasons show less accumulated rainfall but still a higher water table. This may be due to heavy rainfall on higher areas from the rainfall station and the piezometer pit.

In Fig. 4.12, it can be seen that the results are combined for all seasons. The regression equation for the relationship between water heights with 5-days accumulated rainfall is as below

$$Y = -0.0012X + 13.648 \tag{4.4}$$

With Y = water height and X = 5-days accumulated rainfall in *mm*.

The data in Fig. 4.12 are mostly scattered therefore multiple regression analysis is done to check the regression in Eq. (4.4). Multiple regression analysis was done and the multiple regression equation is as follows

$$Y = 13.83893 - 0.0315X_1 - 0.00069X_2 \tag{4.5}$$

With Y = water height, X_1 = month in sequence order and X_2 = 5-days accumulated rainfall in *mm*. When results from Eq. (4.5) is plotted (Fig. 4.15), the regression equations becomes

$$Y = -0.0012X + 13.647 \tag{4.6}$$

This is almost similar to Eq. (4.4). Therefore, it can be concluded that Eq.4.4 can represent the relationship between water heights to 5-days accumulated rainfall.

From Chapter 3, three important return periods have been selected for analysis in Chapter 5, which would be used to estimate the slope failure due to rainfall and earthquake. The return periods are 1.25 years, 2 years, 5 years and 10 years. For 1.25 years, the rainfall amount is 75mm, for 2 years return period, the rainfall amount is

112.5mm, 5 years return period (151.88mm) and for 10 years return period (181.25mm). All rainfall results are 5-days accumulated antecedent rainfall. The water heights from ground level for all three return periods are 13.56m (1.25years), 13.51m (2 years), 13.47m (5 years) and 13.43m (10 years). These results will be used during the analysis of slope failure in the next chapter.

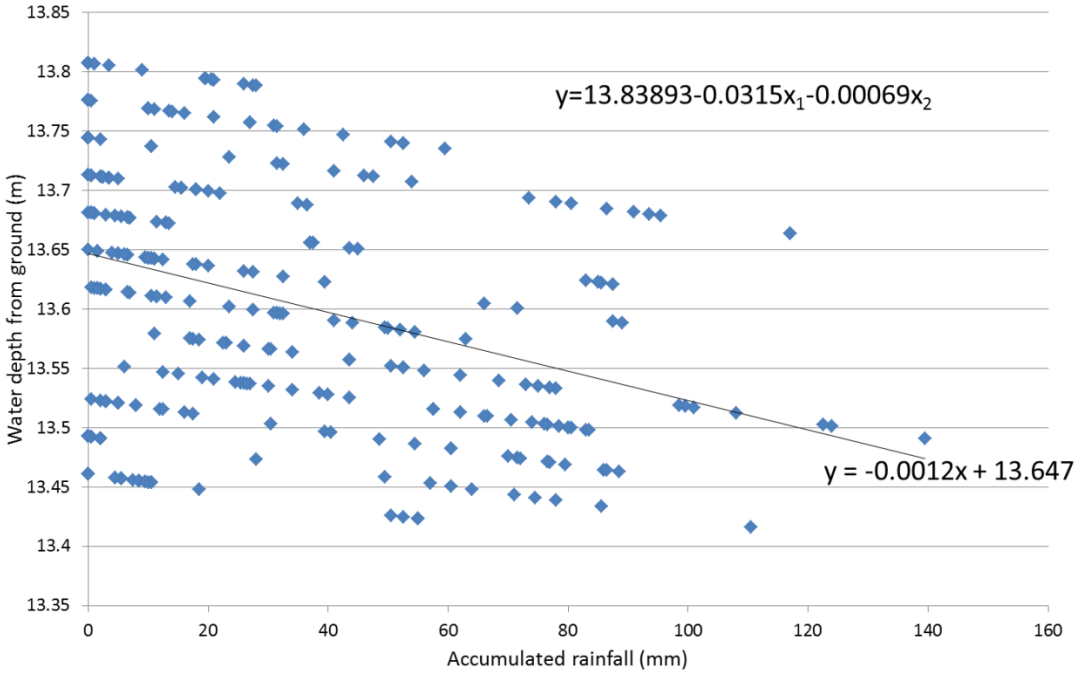

Fig. 4.15 Relationship between water levels with 5-days accumulated rainfall from multiple regression analysis

The initial groundwater level from the piezometer record is 14.5m from the ground. For the next chapter analysis, the differences between the initial height and the new groundwater level for different return periods shall be determined as in Table 4.1. The groundwater level differences shall be the same for each return period for all slope analyses in the next chapter.

Table 4.1 Differences between the initial groundwater level and groundwater level for different return periods

Return period	Probability of exceedance	Water level from ground	Differences
1.25 years	0.8	13.59m	+0.91m
2 years	0.5	13.63m	+0.88m
5 years	0.2	13.66m	+0.84m
10 years	0.1	13.67m	+0.83m

4.4.4 Probability distribution function for water heights

To determine the probability of water level changes due to heavy rainfall, Eq. (4.6) is used. The Cumulative Distribution Function (CDF) for the water height was calculated and two types of distribution have been chosen; Normal distribution and Generalised Extreme Value (GEV). Detail description of these distributions can be seen in the preceding chapter. Fig. 4.16 shows the probability of exceedance curve for both distributions.

Goodness-of-fit was done to both functions using 3 different methods, the Kolmogorov-Smirnov test, the Anderson-Darling test and the Chi-Squared Test. Detailed descriptions for all these tests are discussed in Chapter 3. The best distribution to be used to determine the probability of water height changes is the GEV (Fig.4.16).

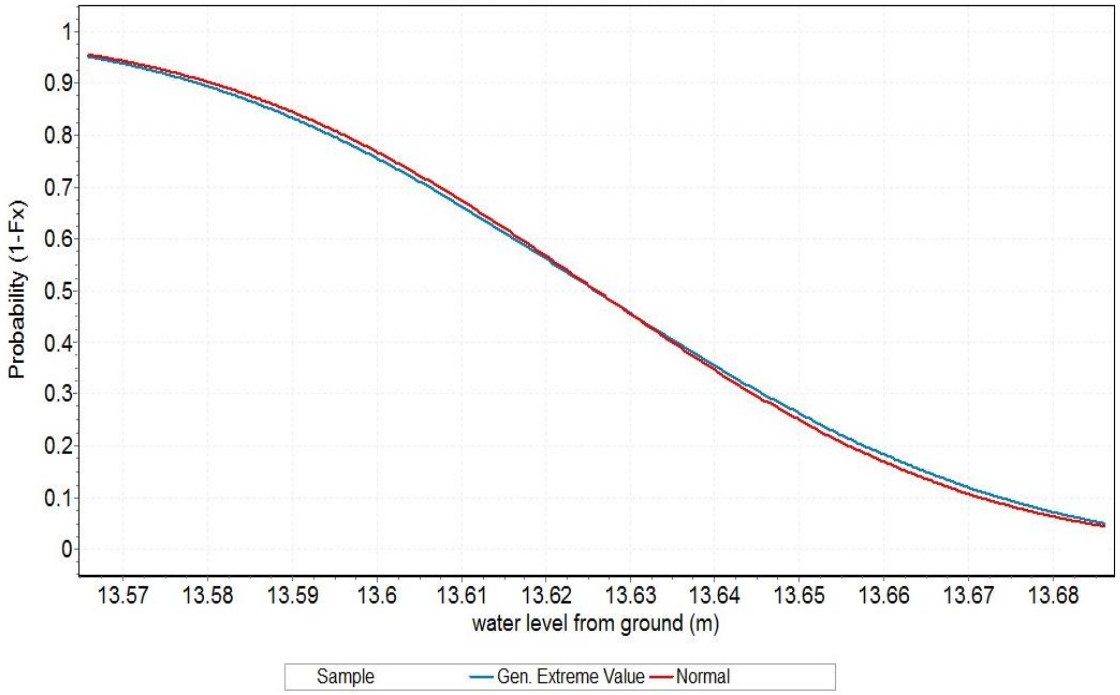

Fig. 4.16 Probability of exceedance function for water height

4.5 Combination Earthquake and Rainfall

In chapter 2, probabilistic seismic analysis was determined for a return period of 98years, 475years, 975years and 2,500years. For groundwater level, analysis was based on a return period of 1.25years, 2years, 5 years and 10years. Earthquake events and rainfall events are independent and based on a multiplication rule, the combination of both events will be

$$P(E \cap R) = P(E)\,P(R) \tag{4.7}$$

Where *P(E)* is the probability of earthquake occurrence and *P(R)* is the probability of groundwater levels.

To calculate the probability of exceedance for 40%, 10%, 5% and 2% in 50 years (earthquakes), the following equations are used. *n* is the number of earthquake occurrences. It is assumed that the rate of occurrence in time is governed by Poisson's

process as in Eq. (4.8) and the exceedance probability of 0 occurrences per year is e^{-n}. To determine the annual probability, *P*, Eq. (4.8) is used;

$$\mathrm{P}(x) = \frac{(\nu t)^x}{x!} e^{-\nu t}, with\ x = 0,1,2,3 \tag{4.8}$$

$$\mathrm{P}(x > 0) = 1 - e^{-\nu t} \tag{4.9}$$

Using Eq. (4.9), the probability of exceedance for 40%, 10%, 5% and 2% in 50 years are 0.01, 0.002, 0.001 and 0.0004 respectively.

For probability of exceedance of groundwater levels, the following equation was used.

$$\mathrm{P}(\mathrm{R}) = \frac{1}{Y} \tag{4.10}$$

Using Eq. (4.10), probability of exceedance of groundwater level based on accumulated antecedent rainfall for 1.25years, 2years, 5years and 10years return period are 0.8, 0.5, 0.2 and 0.1 respectively. Combining both events using Eq. (4.7) will give results of the annual probability of exceedance as in Table 4.1. Results from these probabilities are used in Chapter 5 for slope analysis for static and dynamic.

Table 4.2 Probability of occurrences for combination of earthquake and groundwater level

		Groundwater level (return period)			
		1.25 years	2 years	5 years	10 years
Earthquakes	40% in 50 years (98 years return period)	0.008	0.005	0.002	0.001
	10% in 50 years (475 years return period)	0.0016	0.001	0.0004	0.0002
	5% in 50 years (975 years return period)	0.0008	0.0005	0.0002	0.0001
	2% in 50 years (2500 years return period)	0.00032	0.0002	0.00008	0.00004

4.6 Conclusions

This chapter provided the identification of areas that are critical with the highest number of slopes; the Geographical Information System (GIS) method was used. By using ArcGIS10, Digital Elevation Model (DEM) and TIN (Triangulated Irregular Network) model were created and spatial analysis was done to produce a map that shows the slopes in degrees and in percentage (%).

Fig. 4.6 and 4.7 shows the slope map for Penang Island with different cell sizes. Smaller cells represent the ideal condition of the slope formation. 2 cell sizes were chosen for this study to represent Penang Island slopes, 10-unit and 50-unit. The map for 10-unit cell size shows better prediction on Penang slopes than 50-unit. From Fig.4.6, it can be seen that the highest angle on Penang Island is 86.6° and this is almost the same as reported by previous researchers[6]. In Fig. 4.7, it can be seen that almost 70% of the total area on Penang Island is governed with slopes with more than 16° angle and reaches up to 86.6° angle. This shows that there are a lot of hillsides and slopes on the island and probability of landslide occurrences is high.

The second part of this chapter discussed the relationship between 5-days accumulated antecedent rainfall with water heights. Using piezometer data and rainfall data from a local rainfall station, a graph has been plotted (Fig. 4.12) and provided regression equation (Eq. (4.4)) that will give an idea on water height when a certain rainfall amount occurred. Combining results from probability rainfall analysis in Chapter 3, gives water height results to be used in the next chapter. Cumulative Distribution Function analysis was also conducted in this chapter and the most suitable method to represent the water height changes is the GEV method (Fig. 4.17).

In the last part of the chapter, a combination of probabilities of earthquake and groundwater changes were determined and using these probabilities, a calculation for static and dynamic analysis to check the slope stability of Penang Island in the next chapter can be done.

References

[1] D. J. Varnes, “Landslide Hazard Zonation,” 1984.

[2] S. Lee and B. Pradhan, “Probabilistic landslide hazards and risk mapping on Penang Island, Malaysia,” *J. Earth Syst. Sci.*, vol. 115, no. 6, pp. 661–672, Dec. 2006.

[3] P. A. Burrough and R. A. McDonnell, *Principles of geographical information systems*. Oxford University Press, 1998.

[4] J. Iwahashi, S. Watanabe, and T. Furuya, “Landform analysis of slope movements using DEM in Higashikubiki area, Japan,” *Comput. Geosci.*, vol. 27, no. 7, pp. 851–865, Aug. 2001.

[5] B. K. P. Horn, “Hill shading and the reflectance map,” *Proc. IEEE*, vol. 69, no. 1, pp. 14–47, 1981.

[6] B. Pradhan and S. Lee, “Delineation of landslide hazard areas on Penang Island, Malaysia, by using frequency ratio, logistic regression, and artificial neural network models,” *Environ. Earth Sci.*, vol. 60, no. 5, pp. 1037–1054, Jul. 2009.

[7] K. Y. Ng, “Rainfall-induced landslides in Hulu Kelang area, Malaysia,” Universiti Tunku Abdul Rahman, 2012.

[8] A. Rahimi, H. Rahardjo, E. Leong, and M. Asce, “Effect of Antecedent Rainfall Patterns on Rainfall-Induced Slope Failure,” no. May, pp. 483–491, 2011.

[9] H. Rahardjo, E. C. Leong, and R. B. Rezaur, “Effect of antecedent rainfall on pore-water pressure distribution characteristics in residual soil slopes under,” vol. 523, no. October 2007, pp. 506–523, 2008.

[10] L. M. Lee, N. Gofar, and H. Rahardjo, “A simple model for preliminary evaluation of rainfall-induced slope instability,” *Eng. Geol.*, vol. 108, no. 3–4, pp. 272–285, Oct. 2009.

[11] M. Budhu, *Soil mechanics and foundations*. John Wiley and Sons, 2007.

Chapter 5

STATIC AND DYNAMIC ANALYSIS ON SLOPES

5.1 Introduction

Landslide is a part of a geomorphologic movement of earth that changes the landscape of earth surface. It occurs in many ways such as mudflow, slope failure and rock/soil movement. It may affect directly or indirectly to human and their activities depending on its size and location. The massive and uncontrollable land-use has increase the susceptibility of landslide. Of course this cannot be denied when it comes to urbanization especially in city area.

Most of the locations where landslides occur are in developing countries where regulations are insufficient and management is hard to sustain. All landslides have few things in common that is they are the result of soil/rock movement controlled by gravity and this can occurs due to several factors such as earthquakes, volcanic eruptions, soils saturated by heavy rain or groundwater rise, and river undercutting. Earthquake shaking of saturated soils creates particularly dangerous conditions. Although landslides are highly localized, they can be particularly hazardous due to their frequency of occurrence.

Analysis of landslide and slope stability is not new in geotechnical engineering. Initially slope stability was analyzed using limit equilibrium method and in earlier time, it can be calculated by hand-calculations. The idea to analyze slope stability started in 20th century. In 1936, Ordinary Slice Method or also known as Swedish method was

introduced by Fellenius. In mid 1950s, Janbu and Bishop developed advances in the analysis method. More rigorous methods were introduced after the advancement in computers. Morgenstern and Price (1965) as well as Spencer (1967) introduce these rigorous methods.

In limit equilibrium analysis, a single constant factor of safety is produced. The factor of safety is widely used by engineers to determine whether slope is safe or unsafe. Estimation of safety of slope can be done easily using limit equilibrium method but users usually do not understand the limitation of the method. Therefore it is said to be able to analyze slope stability, the dynamic analysis gives better outcome and more precise in representing behavior of slope.

Dynamic analysis is used to determine the response and behavior of slopes when it is subjected to dynamic motion such as earthquakes. In dynamic analysis, the motion, movement during shaking is checked and the generation of excess pore-pressures is determined. It is known that when pore pressure increases, the shear strength of the soil reduces and this can lead to slope failure.

Both analyses are important in order to assess slope stability but it is important to understand which analysis gives the outcome needed for judgment or countermeasures to be taken. The static analysis (limit equilibrium) is a simple method that can easily be used without to many inputs or unknown assumptions but there is limitations that need to be understood and the dynamic analysis can provide better result and more precise

outcome on slope behavior especially when there is dynamic motion input but it may take longer time and needed more rigorous analysis.

In this study, both analyses were done to provide better insight on Penang Island slope. The main objective in this chapter is to be able to determine the slope safety on Penang Island slope with regards to earthquake and rainfall effects. Using both static and dynamic method, the safety factor and total displacement on several slopes in Penang Island were done and presented in proceeding sub-chapters.

5.2 Chapter Overview

Evaluation of slopes on Penang Island was done in this chapter. The analyses include static and dynamic analysis of slopes with regards to earthquake and rainfall effects. At the end of this chapter, we hope to be able to check and predict stability or failure of slopes on Penang Island with regards with the effects mentioned earlier.

In this chapter, results from previous chapter 2, 3 and 4 are used for the analysis. The peak ground acceleration for probability of earthquake occurrences in 98 years, 475 years, 975 years and 2500 years return period are used as inputs for earthquake effects. The water height due to accumulated antecedent rainfall of 1.25 years, 2 years, 5 years and 10 years return periods are used as rainfall effect input.

A number of slopes were selected for the analysis. In chapter 4, several locations on Penang Island were classified as higher possibility of slope failure based on the slope

angles. One of the locations is Batu Ferringhi. In this chapter, one site from Batu Ferringhi was chosen for static and dynamic analysis. The reason to choose this site was based on the input parameters needed for the analysis. This location is a housing development and soil investigation was done by local consultant to determine the soil characteristics and is important for the analysis. Fig. 5.1 and Fig. 5.2 show the location of analysis for this chapter.

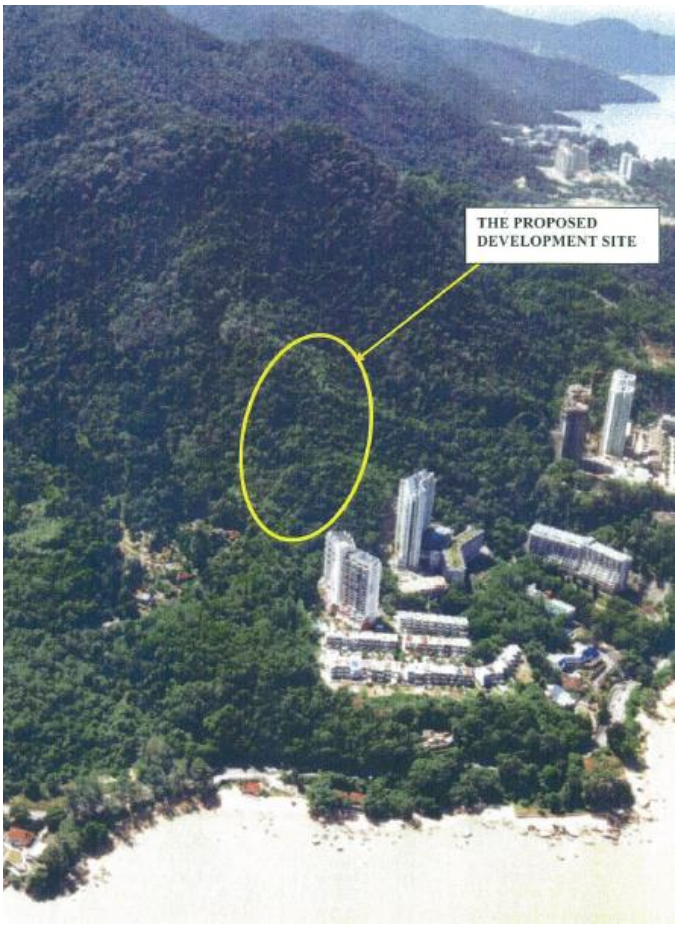

Fig. 5.1 Location of study in Batu Ferringhi, Penang

Fig. 5.2 Proposed site location

In the first part of the analysis, a slope was selected based on the consultant record. Using the same soil layer and its characteristics, a slope was selected using spatial analyst function in ArcGIS. Static and dynamic analyses for these slopes were done. At the end of the chapter, deformation of slope based on several return periods of

earthquakes and rainfall is constructed and the effect of slope failure to nearby areas can be seen. Fig. 5.3 shows the flowchart of this chapter.

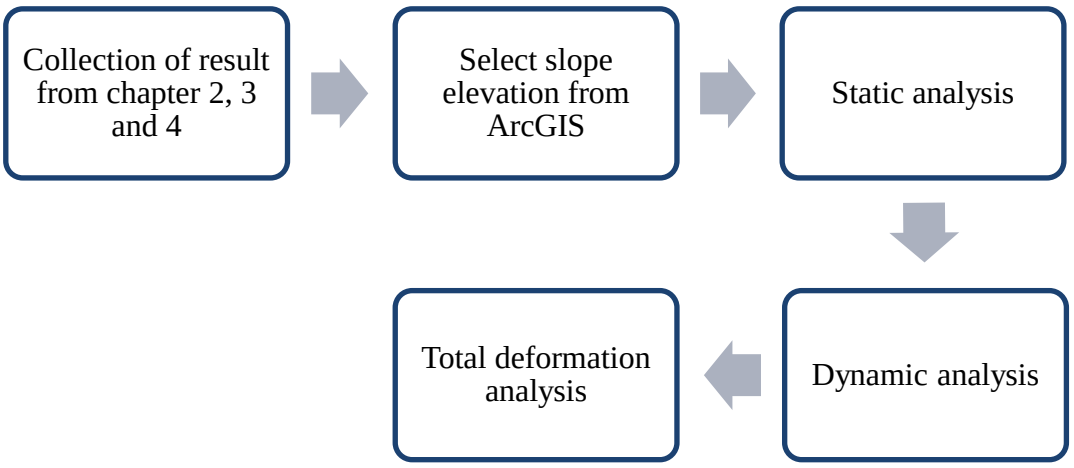

Fig. 5.3 Flowchart of chapter 5

5.3 Static Analysis for Slope

Slope failures can occur due to natural forces or development activities. For example, the slope may fail at a continuously erode slopes whether it is natural or man-made slopes. Erosion changes the slope geometry and resulting in slope failure. Another cause of slope failure is rainfall. Long periods of rainfall increase the water level in soil and reduce the soil strength and this will lead to slope failure.

The earthquakes also may cause slope failure. The dynamic force especially dynamic shear force reduces the shear strength of the soil, and porewater pressures in saturated soil may rise to value equal to total means stress and causing soil to behave like viscous

fluid – which is called dynamic liquefaction[1]. Other than that, external loading from building of public structure like roads or drainage also may add gravitational loads and will increase mobilized stress and will reduce the factor of safety of slope and lead to slope failure.

Slope failure depends on the soil characteristics and its physical geometry. Soil characteristics include the soil stratification, groundwater level and seepage. There are several common types of slope failure for example, failure across weak zone of soil is called translational slide. This type of slide is common in coarse-grained soil and the movement can travel long distance before coming to rest.

The most common type of failure for fine-grained soil is the rotational slide. This type of failure has point of rotation on imaginary axis parallel to the slope. Rotational slides can occur in several different ways such as base slide where the critical arc engulfs the whole slope, toe slide where the slope failure passes through the toe and the slope slide where failure passes through the slope. There are also the wedge or block slides that can occur along joints, seams, fissures and weak zone. The shattered mass moves as blocks and wedges from the slope[1].

In each analysis, the critical slope surface type must be chosen upfront. Although each type of critical slip surface is chosen based on the soil types, there are other effects that must be taken into account too. In order to determine the position of the critical slip surface with lowest factor of safety, it involves trial and error procedure. The process is repeated for many possible slips and the slip with lowest factor of safety is chosen.

In limit equilibrium method, each trial surface is divided into slices and forces acted on these slices are analyzed and summation of all forces acted on each slices are combined to determine the equilibrium. The importance of interslice force functions depends on the amount of contortion needed for the sliding mass to move.

The factor of safety is a single empirical result that determines whether the slope is safe or not. Commonly, if the factor of safety is lower than 1.0, it is considered as unsafe. The factor of safety is usually calculated by dividing resisting forces over driving forces. If earthquake is taken into consideration, the static and pseudo-static conditions are analyzed and the seismic forces are added as additional forces in the analysis.

To solve the forces acting on the slip surface, there are many methods for analysis as mentioned in the introduction of this chapter. Basically, all methods are similar and the differences between each method only depends on the equation of statics included and satisfied, which interslice forces included and the relationship between the interslice forces and normal forces[2].

The first method developed to solve limit equilibrium analysis of slope stability was the Ordinary method or sometimes called as Fellenius method (1936). At that time the analysis was done by hand calculations and the method uses circular slip surface. The Fellenius method neglects all interslice forces and only satisfied the moment equilibrium. This assumption makes the calculation simpler and can be done manually.

In 1955, Bishop introduced a method that include interslice normal forces but ignored the shear forces. The Bishop’s Simplified method satisfy only moment equilibrium and

by including normal interslice forces, the factor of safety equation became nonlinear and interative procedure is required to solve the factor of safety[2]. Janbu's Simplified method that was created in 1954 is similar to Bishop's Simplified method and it includes the normal interslice forces and ignores the interslice shear forces. The Janbu's Simplified method only satisfies horizontal equilibrium and not moment equilibrium.

After introduction of computers, solving iterative procedures becomes easier and this lead to more rigorous mathematical equation been introduced to represent detail process of slope stability analysis. In 1965, Morgenstern-Price introduces another method and followed by Spencer in 1967. Both of these methods include all interslice forces and satisfy all equation of static.

5.4 Static Analysis Method

5.4.1 Background theory

In this study, the Morgenstern-Price analysis method is chosen. This method was introduced by Morgenstern and Price in 1965. Prior to the method introduced by Morgenstern and Price, slip surfaces were analyzed using circular slip surface. But, researchers realized that based on documented cases shows that slope failures occurred in non-circular surfaces. The degree of surface disturbance of sliding mass provides visual method to distinguish between circular and non-circular movement[3]. Severe case of surface disturbance is usually occurred when failure occurs on a non-circular slip. The normal circular slip surface analysis takes into account homogeneity of soil

and the strength and parameter of soil and its pore-pressures vary considerably. Analysis based solely on circular slip most probably over-estimates the factor of safety. Problem occurs when several conditions are different such as present of soft layer in foundation and different types of soil or rock in the potential failure surface with different strength. In this case, non-circular slip surface should be chosen for analysis of stability of slope.

The aim of Morgenstern and Price was to develop a method that able to calculate factor of safety for non-circular slip surfaces and can consider wide variety of surfaces with different shear strength properties. They also wanted to introduce a method that can combine all equation of equilibrium and solve moment equation of equilibrium. The method uses the same concept initially introduced in the Ordinary slope method that is by creating a slip surface and slicing it into several individual blocks. It can be represented in Fig. 5.4. Each forces acting in the figure are assumed to be vertical and the weight of the block, W acted at the center of the slice, the normal force, N acted at the center of the block and lateral forces, E acted at the side of the blocks.

Fig. 5.4 shows all forces acting on a certain slice in a non-circular slip surface. The variables associated with the slice are defined by Morgenstern and Krahn[4] as follows:

W = total weight of slice with width, b and height, h

P = total normal force on the base of the slice over length l

S_m = shear force mobilized on the base of the slice. It is a percentage of the shear strength as defined by Mohr-Coulomb equation which is

$$S_m = \left(c' + \left(\frac{P}{l} - u\right)\tan \emptyset'\right)/F \tag{5.1}$$

with c'= effective cohesion parameter

ϕ' = effective angle of internal friction

F = factor of safety

u = porewater pressure

l = length of slice base

R = radius of the moment arm associated with mobilized shear force, S_m

f = perpendicular offset of the normal force from the center of rotation

α = angle between the tangent to the center of the base of each slice and the horizontal line

E_L, E_R = horizontal interslice forces. L and R is left and right side of the slice

X_L, X_R = vertical interslice forces. L and R is left and right side of the slice

k = seismic coefficient for dynamic horizontal force.

e = vertical distance from the centroid of each slice to center of rotation

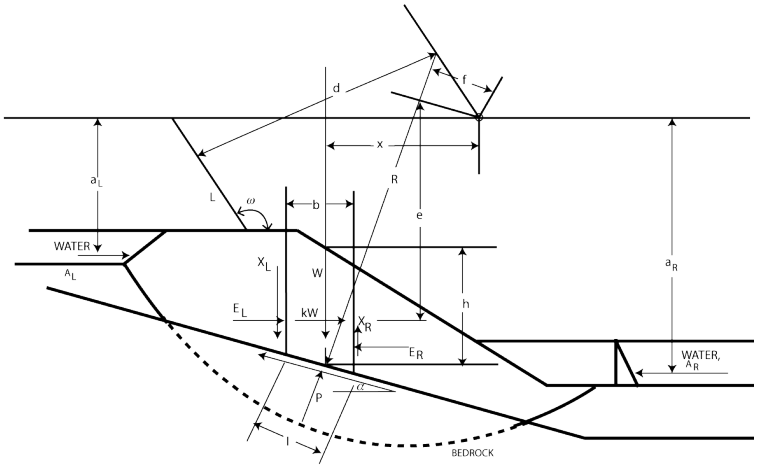

Fig. 5.4 Forces acting on slices for slope analysis

Morgenstern-Price method assumes an arbitrary mathematical function to describe the direction of the interslice forces[5].

$$\lambda f(x) = X/E \tag{5.2}$$

Where λ = a constant to be evaluated when solving the factor of safety.

f(x) = functional variation with respect to *x*

In this analysis, the half-sine function is used for *f(x)* and the λ used for the analysis is shown in Fig. 5.5 and at the bottom picture shows how to designate the direction of the interslice forces[5].

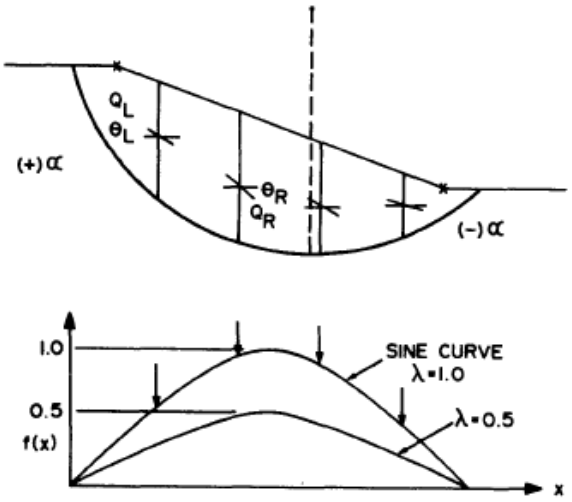

Fig. 5.5 Side force designation for Morgenstern-Price method[4]

The solution for this method is based on the summation of tangential and normal forces to each of the slices. Then the force equilibrium equations are combined and moment and force equations are solved for factor of safety and lambda.

The normal force is derived from vertical force equilibrium equation as below[5]:

$$\mathrm{P} = \frac{W-(X_R-X_L)-\frac{c'-l-\sin\alpha}{F}+\frac{u-l-\tan\phi'\sin\alpha}{F}}{m_\alpha} \tag{5.3}$$

with $m_\alpha = \cos\alpha + \frac{\sin\alpha\tan\phi'}{F}$

Fredlund and Krahn[5] details out that two factor of safety equations are computed, one with respect to moment equilibrium and one with respect to force equilibrium.

The moment equilibrium equation is taken with respect to a common point and this common point can be used even if the slip surface is composite.

The summation of moments at a common point is given as

$$\sum M_o = 0; \quad \sum Wx - \sum S_m R - \sum Pf + \sum kWe \pm Aa + Ld = 0 \tag{5.5}$$

Factor of safety with respect to moment equilibrium is

$$F_M = \frac{\sum\{c' lR + (P - ul)R \tan \phi'\}}{\sum Wx - \sum Pf + \sum kWe \pm Aa + Ld} \tag{5.6}$$

The factor of safety with regards to force equilibrium is

$$F_F = \frac{\sum\{c' l \cos \alpha + (P - ul) \tan \phi' \cos \alpha\}}{\sum P \sin \alpha + \sum kW \pm A - L \cos \omega} \tag{5.7}$$

In first step to solve the interslice shear forces, the first iteration of vertical shear force is set to zero and the horizontal interslice forces are obtained by combining the summation of vertical and horizontal forces on each slice.

$$(E_R - E_L) = [W - (X_R - X_L)] \tan \alpha - \frac{S_m}{\cos \alpha} + kW \tag{5.8}$$

The horizontal interslice forces are obtained by integration from the entry of slip surface to the exit (left-to-right or right-to-left). Then, the vertical shear forces are computed using assumed lambda value and side force function.

$$X_R = E_R \lambda f(x) \tag{5.9}$$

The side forces are computed for each iteration. The moment and force equilibrium factors of safety are solved for a range of lambda values and a specified side force function.

The factor of safety equation can be visualized as consisting of the following components as shown in Table 5.1.

Table 5.1 Components in factor of safety equations

	Moment Equilibrium	**Force Equilibrium**
Cohesion	$\Sigma c'.l.R$	$\Sigma c'.l.\cos\alpha$
Friction	$\Sigma(P-u.l).R.\tan\phi'$	$\Sigma(P-u.l).R.\tan\phi'.\cos\alpha$
Weight	$\Sigma W.x$	----
Normal	$\Sigma P.f$	$\Sigma P.\sin\alpha$
Earthquake	$\Sigma k.W.e$	$\Sigma k.W$
Partial submergence	$A.a$	A
Line Loading	$L.d$	$L.\cos\omega$

5.4.2 Input properties

The static analysis for slope stability in this chapter is done using a commercial software name GeoStudio Slope/W Version 2012. Input parameters for soil were taken from the same data from borelog used in previous chapters. To simplify the analysis, a slice were chosen with 3 borehole records and data from that slice are used for all slopes at the site shown in Fig. 5.1.

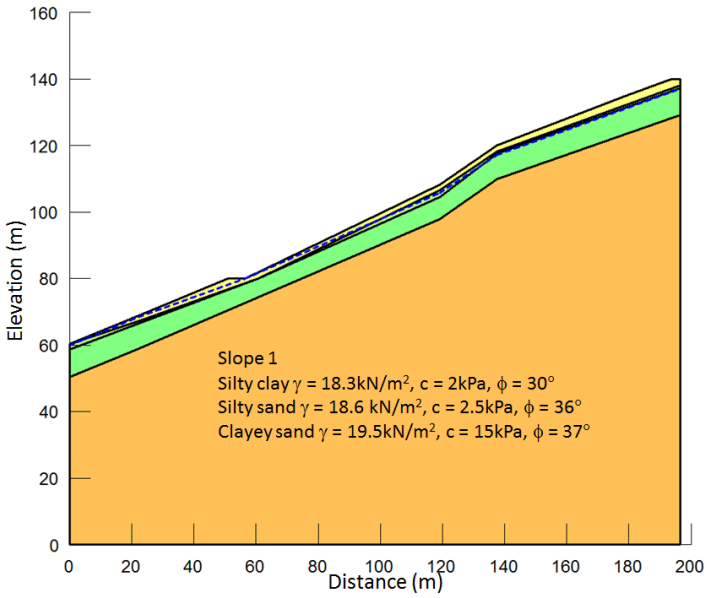

Fig. 5.6 Slope chosen from site investigation report

Fig. 5.6 shows the slope from the site investigation report. The same layer locations are used in the static analysis for the next step. Details of all parameters used in the static analysis are shown in Table 5.2. The soil model is based on Mohr-Coulomb condition and to simplify the next proses, all parameters for each layer are assumed to be the same as in the table.

Table 5.2 Soil parameters for static analysis

Characteristics	Silty sand (layer 1)	Silty clay (layer 2)	Clayey sand (layer 3)
Unit weight (kN/m^3)	18.3	18.6	19.5
Cohesion	2	2	15
Friction angle	30	30	37

Bedrock is assumed as impenetrable layer and no input was given for bedrock. These data represents the soil parameters for fully saturated condition (S = 100%).

In order to analyse soil layer in unsaturated condition, data from Sokhanvar and Kassim[6] was used. The data provided is tabulated as in Table 5.3 below. It comes from unconsolidated undrained tests done for local soil in Johor, Malaysia. The volumetric water content for saturation condition (S = 100%) is 0.44 and suction is 0.1kPa, at air-entry value the volumetric water content (S = 90%) is 0.405 and suction is 9kPa.

Table 5.3 Unsaturated data taken from local researcher

Matric Suction	Friction angle	Cohesion
0.1	23	9
20	26.62	19.02
50	36.13	45.50

These data are then plot into the graph as shown in Fig. 5.7. Linear regression can be seen here for both friction angle as well as cohesion. In the paper, it was shown that for 90% saturation, the matric suction is 9.0 and when the value is substituted into the graph, new cohesion and friction angle for 90% saturation rate can be seen in Table 5.4.

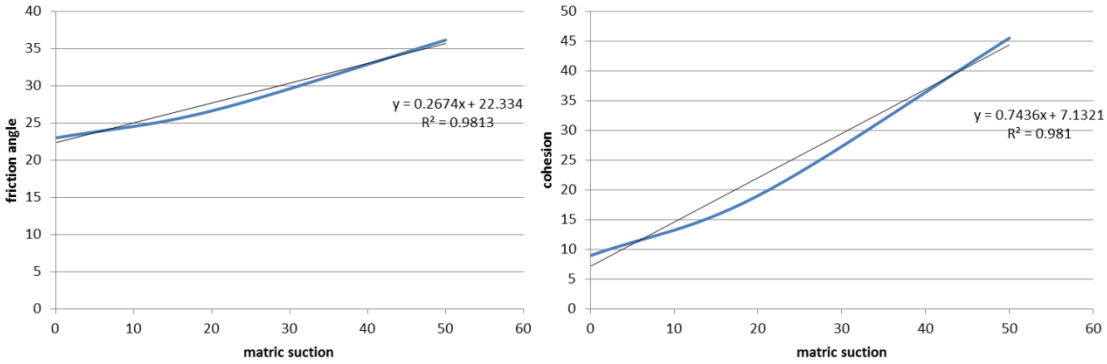

Fig. 5.7 Friction angle vs. matric suction (left) and cohesion vs. matric suction (right)

Table 5.4 Unsaturated soil parameters for saturation 90%

Soil parameter	S = 100%, matric suction = 0.1	S = 90% matric suction = 9	Ratio
Cohesion	9	13.8	1.53
Friction angle	23	24.7	1.07

From the calculated ratio in Table 5.4, the parameters for all soil layer under unsaturated condition is calculated again and shown in Table 5.5.

Table 5.5 Soil parameters for unsaturated soil condition in static analysis

Characteristics	Silty sand (layer 1)	Silty clay (layer 2)	Clayey sand (layer 3)
Unit weight (kN/m^3)	18.3	18.6	19.5
Cohesion	3.1	3.1	23
Friction angle	32.1	32.1	40

The next step is choosing the slope for analysis. Using ArcGIS map as in chapter 4, three slopes were chosen using Spatial Analyst command. The location of the

slopes chosen is the same as in Fig5.1 in the initial pages of this chapter. The three slopes locations are shown in Fig. 5.7.

Data used for horizontal earthquake acceleration and the ground water level are shown in Table 5.3. Data used are taken from previous chapters and compiled in the table. For each slices shown in the table above, calculation of factor of safeties are done.

Table 5.6 Earthquake and water height input used in the static analysis

Peak ground acceleration	Water height input Initial water level from ground (14.5m)
98 years return period – 0.11g	1.25 years return period – 13.557m from ground
475 years return period – 0.19g	2 years return period – 13.512m from ground
975 years return period – 0.23g	5 years return period – 13.465m from ground
2500 years return period – 0.29g	10 years return period – 13.429m from ground

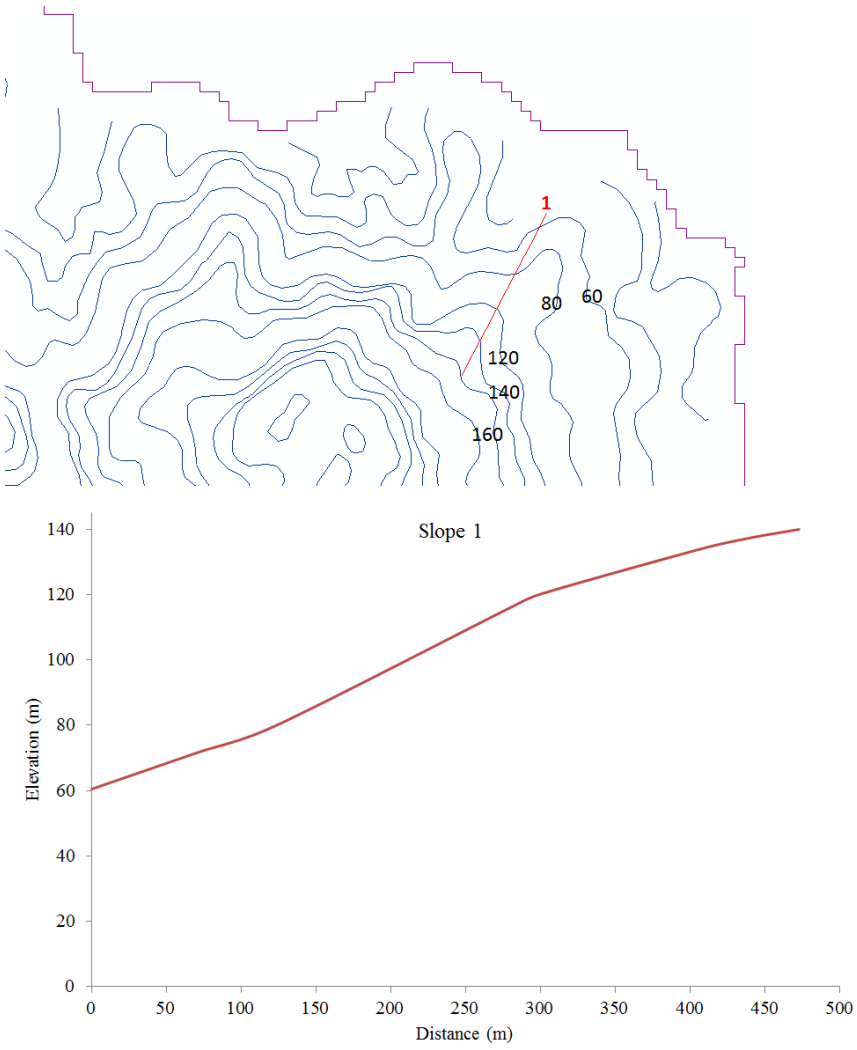

Fig. 5.8 Location of the slice used in analysis

5.4.3 Static analysis procedure

In this analysis, the Geoslope Slope/W software was used where Morgenstern-Price method with half-sine function was selected for static analysis method. The slip surfaces were determined using the entry and exit method where the entry and exit of slip surface were chosen manually. The slip surface chosen for the slope is

local slope (marked red) where only a certain portion of the area is analysed for failure (Fig. 5.9).

This also makes it possible to see the effect between the static analysis and dynamic analysis which will be describe later.

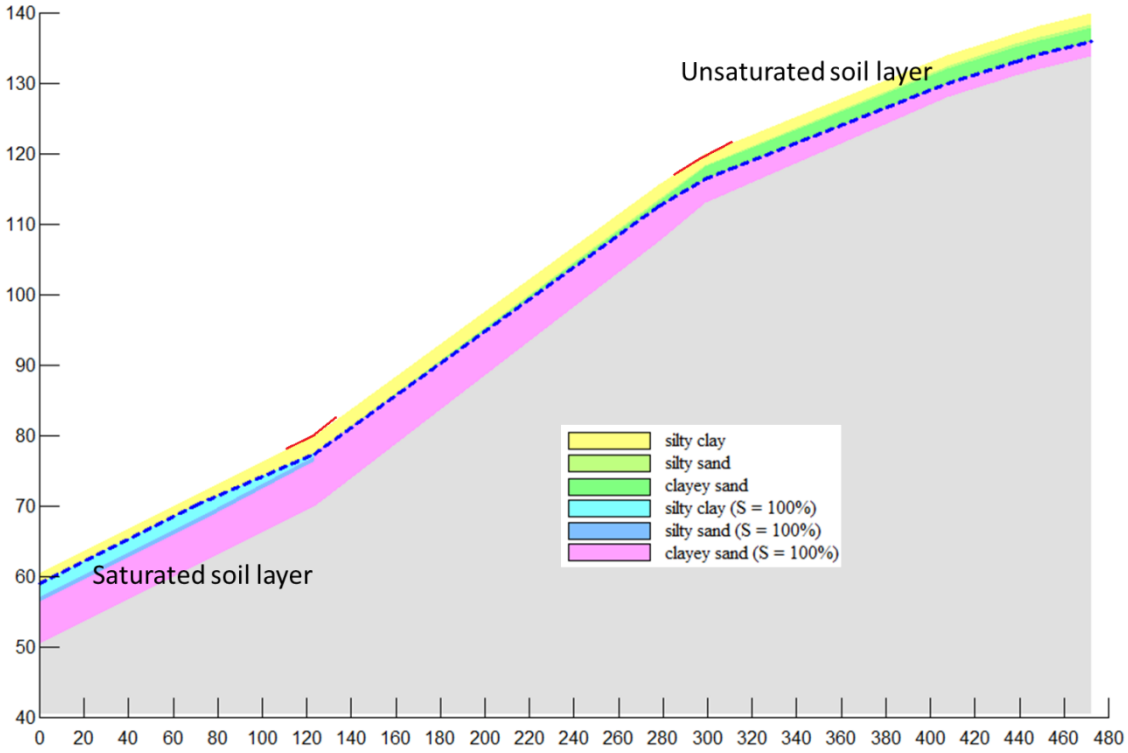

Fig. 5.9 Cross-section of slope 1

5.4.4 Static analysis result

Result for analysis of the slope is shown in Table 5.7. It can be seen that, when the water table increases and without any earthquake input, the factor of safeties are above 1.0 which is the minimum threshold, and any number below 1.0 means the slopes are not in equilibrium condition and there is high possibility of slope failure.

But, when the earthquake inputs are used, the factor of safeties started decreasing with increase of groundwater table. In this case, the factor of safeties started to fell below 1.0 for 0.19g earthquake input and continuously decreasing after that with increase of groundwater level.

Table 5.7 Factor of safeties for static analysis

Earthquake input (g)	Initial groundwater level	1.25 years return period groundwater level	2 years return period groundwater level	5 years return period groundwater level	10 years return period groundwater level
0.0g	1.761	1.574	1.570	1.562	1.555
98 years r.p– 0.11g	1.158	1.030	1.025	1.019	1.015
475 years r.p – 0.19g	0.912	0.814	0.809	0.804	0.801
975 years r.p – 0.23g	0.823	0.734	0.730	0.725	0.722
2500 years r.p – 0.29g	0.717	0.638	0.634	0.630	0.627

Note: r.p = return period

In this analysis, the slope chosen from the DEM map catered as many contour lines as possible within the site area. Therefore, the distances are very wide and some slope has flat surface between several inclinations of height. From the result seen in the previous tables, it can be concluded that although earthquake and water level gives effect with changes in factor of safeties.

5.5 Dynamic Slope Analysis

In dynamic analysis of slope stability, the ground motion of bedrock was imposed to the slope and the slope is subjected to the ground motion. The behavior or movement of the slope during that time is analyzed. The limit equilibrium method

provides the factor of safety which is an empirical number only to represent whether the slope safe of not and there is no information on deformation associated with the slope failure. Slope deformation is important to determine the serviceability of the slope after the event of failure.

Kramer[7] mentioned that pseudostatic factor of safety varies throughout the earthquake because the earthquake-induced accelerations vary with time. If the inertial forces acting on potential slip surface become large enough that total driving forces including static and dynamic forces exceed available resisting forces, factor of safety will be lower than 1.0. This concept was considered by Newmark in 1965 where when the factor of safety is lower than 1.0, the failure surface is no longer in equilibrium and it will be accelerated by unbalanced force. Newmark assumed this condition as same as a block sitting on an inclined plane and this analogy is used to predict permanent displacement of slope subjected to any ground motion[7].

In order to determine the displacement of the slope, the behavior of slope during earthquake shaking must be understood. These include motion, movement and inertial forces that occur during shaking, reduction in shear strength of soil and changes in porewater pressure. The inertial forces occur during earthquake shaking causes the stresses in soil to oscillate and along the potential slip surface, the mobilized shear strength changes (increase and decrease) with response to the inertial forces. At some point during the shear strength to exceed the shear resistance, the factor of safety may reduce than 1.0 and the ground may experience

some displacement. Accumulation of these movements becomes permanent displacement.

5.6 Dynamic Analysis Method

Before we are able to determine the permanent displacement of a certain slope, finite element numerical methods need to be done to see the behavior of slope under cyclic loading. The concept of finite element numerical methods come from dividing a continuum into small pieces and describe the behavior of each pieces before reconnecting it again to determine the behavior of the continuum as a whole. This process is known as discretization or meshing and the small pieces are known as finite elements.

The first step to solve finite elements is by defining the geometry of the model prior consideration of mesh. The geometry of slope is drawn as same as the geometry in the static analysis only with different soil model. After defining the geometry, the mesh is drawn on the slope then followed by defining the material properties and boundary conditions. The simplest model is the linear-elastic model where the stress is directly proportional to the strain and the constant of proportionality is Young's modulus, *E*. The linear relationship does not related to the material strength and there is no iterative procedure required. In reality the linear-elastic model may be not useful for field problem because the stress-strain relationship is almost non-linear.

The next model used in dynamic analysis is the equivalent model and this model is similar to linear-elastic model. The difference between the models with linear-elastic model is that the soil stiffness, *G* is modified with respond to computed strain. The analysis started with a specified *G* value and then steps through entire ground motion record and identifies peak shear strains at each Gauss numerical integration point in each element. The shear modulus is then modified according a specified shear modulus reduction function (G_{max} reduction function) and process is repeated. The iterative procedure continues until required *G* modifications are within specified tolerance. The *G* is constant through earthquake record and the *G* value may be modified for each pass through record but remains constant during one pass. When plotted in σ vs ε space, each iterations gives different slope and the changes in slope for each iteration reflects reduction in *G* between iterations.

The non-linear model can show dynamic response at particular site when it is affected with the generation of excess pore-pressures during shaking. To capture the behavior in a numerical model, true non-linear analysis is required where excess pore-pressures are calculated and soil properties are modified during shaking. The increase in pore-pressures changes the effective stresses thus lead to changes in soil properties. This is referred to as dynamic effective stress analysis.

The difference between equivalent linear model and non-linear model is that the excess pore-pressures are calculated based on the peak dynamic shear stresses. The peak values are not known until the end of the dynamic analysis therefore the effective stresses does not changed during the shaking. In this study, the equivalent

linear model was chosen for analysis method and the changes of water level for different return period remains constant during initial stress analysis.

The shear modulus *G* in the analysis is designated as G_{max}. It is considered to be a small-strain shear modulus and in this software, the G_{max} values can be specified as functions. Generally, soil stiffness increases with increase in confining or overburden stress therefore by specifying the behavior of G_{max} in a function will make it easier.

5.6.1 Input properties

A soil subjected to dynamic stresses tends to 'soften' in response to cyclic shear strain. In equivalent linear model, the softening is described as ratio relative to G_{max} and is called as G-reduction function. The cyclic shear strain comes from finite element analysis. The computed shear strain together with the function and the specified G_{max} are used to compute new *G* values for each iterations. The G_{max} for each layer values used for this study are calculated using the following equation:

$$G_{max} = v_s^2 . \rho \tag{5.10}$$

Where v_s is the shear wave velocity as calculated in chapter 2 and ρ is the bulk density of soil.

Other data used for dynamic analysis in this chapter is shown in Table 5.8 below. The soil layer is the same as used in static analysis in previous sub-chapter.

Table 5.8 Data used for dynamic analysis

Characteristics	Silty sand	Silty clay	Clayey sand	Bedrock
Unit weight (kN/m^3)	18.3	18.3	19.5	26.5
Poisson's ratio	0.33	0.3	0.28	0.2
Gmax (kPa)	70,000	120,000	140,000	260,000

For every soil layer, the unsaturated condition is taken into account. The ground motion record use for earthquake input is the same as in chapter 2. The peak ground motion of the record is modified based on the value of Probabilistic Seismic Hazard Analysis map for Penang Island bedrock as in Fig. 2.7. The input for peak ground acceleration and water level for every return period is shown in Table 5.9. The values are based on the location of the slope on Penang Island.

Table 5.9 Earthquake and water height input used in the dynamic analysis

Peak ground acceleration (modified value for ground motion)	Water height input Initial water level from ground (14.5m)
98 years return period – 0.05g	1.25 years return period – 13.557m from ground
475 years return period – 0.085g	2 years return period – 13.512m from ground
975 years return period – 0.115g	5 years return period – 13.465m from ground
2500 years return period – 0.15g	10 years return period – 13.429m from ground

5.6.2 Dynamic analysis procedure

The dynamic analysis for slope to determine the permanent displacement using Newmark's method must go through several processes. The first step is the initial static analysis then followed by dynamic analysis using the result from initial static stress as initial condition and finally the Newmark's displacement analysis.

In initial static stress analysis, the groundwater level inputs are the same value used for each return period; the material uses the equivalent linear model as mentioned in Table 5.8. Then dynamic analyses were done for all earthquake and groundwater level inputs. The initial boundary condition is shown in Fig.5.10.

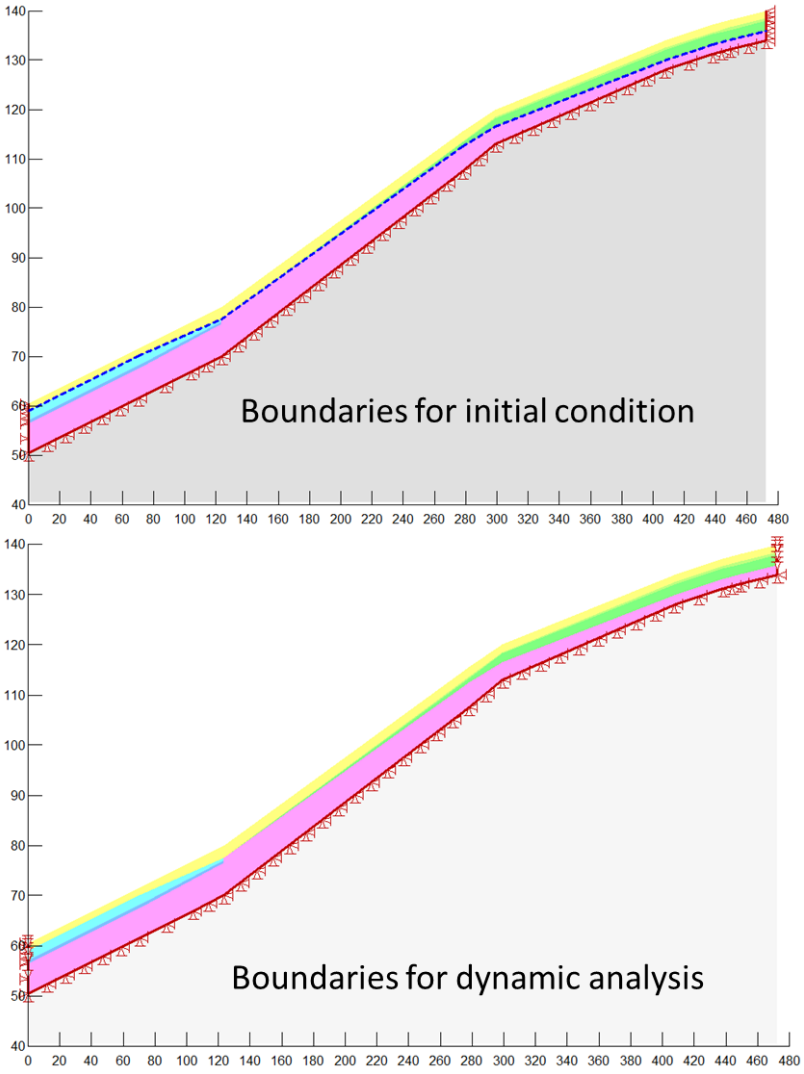

Fig. 5.10 Boundaries condition for initial condition and dynamic analysis

5.6.3 Dynamic analysis and Newmark's deformation analysis result

The results of dynamic analysis were collected for every period of 0.01sec. For each time histories, the ground motions with the modified peak accelerations (Table 5.9) were imposed on the slope and the movement of slope can be seen. The ground motion input are imposed at the bottom part of the slope where bedrock lies and are then amplified upward until it reaches the surface of the slope.

Then, Newmark's deformation analyses were done for every return period and for all groundwater level return period. An example shown in the following procedures is from the case in slope. For the analysis, on each trial slip surface, the initial stress condition from the previous analysis is used to establish static stress of the slope. It is then followed by implying dynamic stress at every time steps to compute the dynamic shear stress of the slope and the factor of safety for all time steps during shaking process. The total mobilized shear arising from the dynamic inertial forces is then determined. Average acceleration is determined from the ratio of driven mobilized shear over total slide mass. The average acceleration is sometimes referred to as the yield acceleration that reflects the acceleration value that affect the stability of slope at certain time.

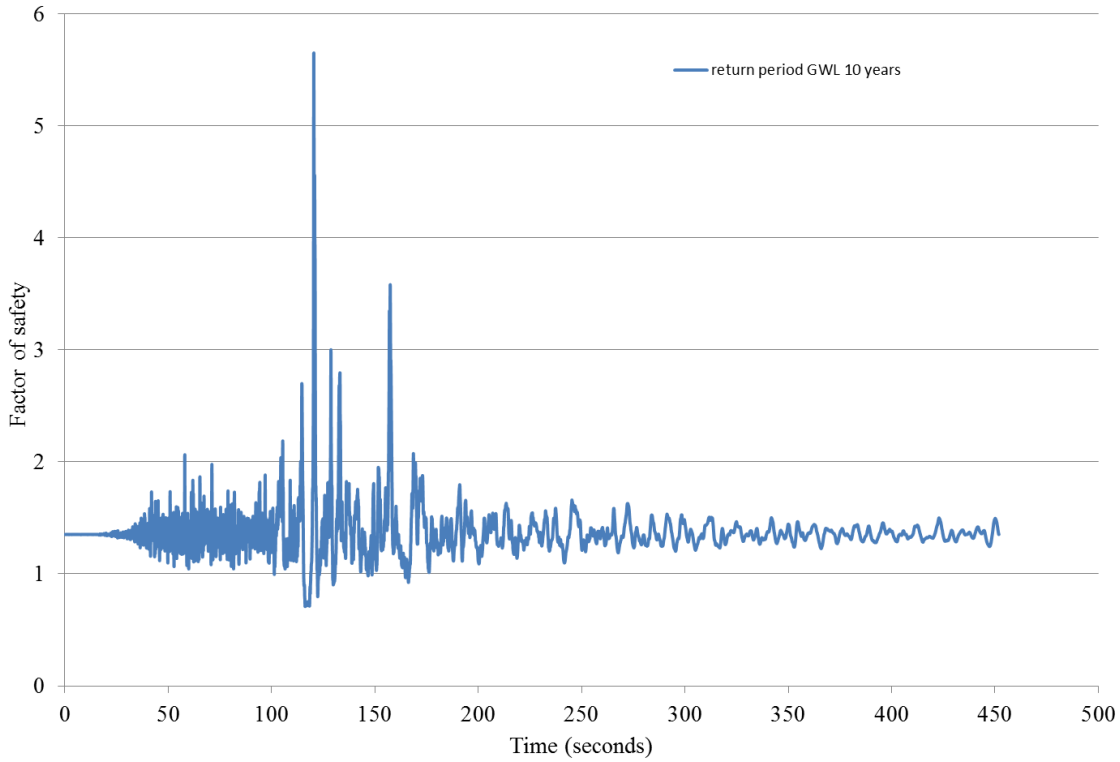

Fig. 5.11 Factor of safety vs. time

Fig. 5.11 shows the factor of safety at the most critical slip surface during the shaking for slope with PGA of 0.15g with 10 years return period groundwater level. The highest factor of safety for critical slip surface for PGA of 0.15g is about 5.58 at about 120.4seconds and the lowest factor of safety for the slip surface is about 0.7 at 116.2seconds. When factor of safety reach lower than 1.0, total deformation occurred and it can be seen in the following figures. In this case, there are few points that are lower than 1.0 so large deformation can be expected.

Fig. 5.12 shows the relationship between factors of safeties with average acceleration for the slope. It can be seen that the average accelerations that produce

FOS lower than 1.0 is at about 0.06g and this value is considered as the yield acceleration value.

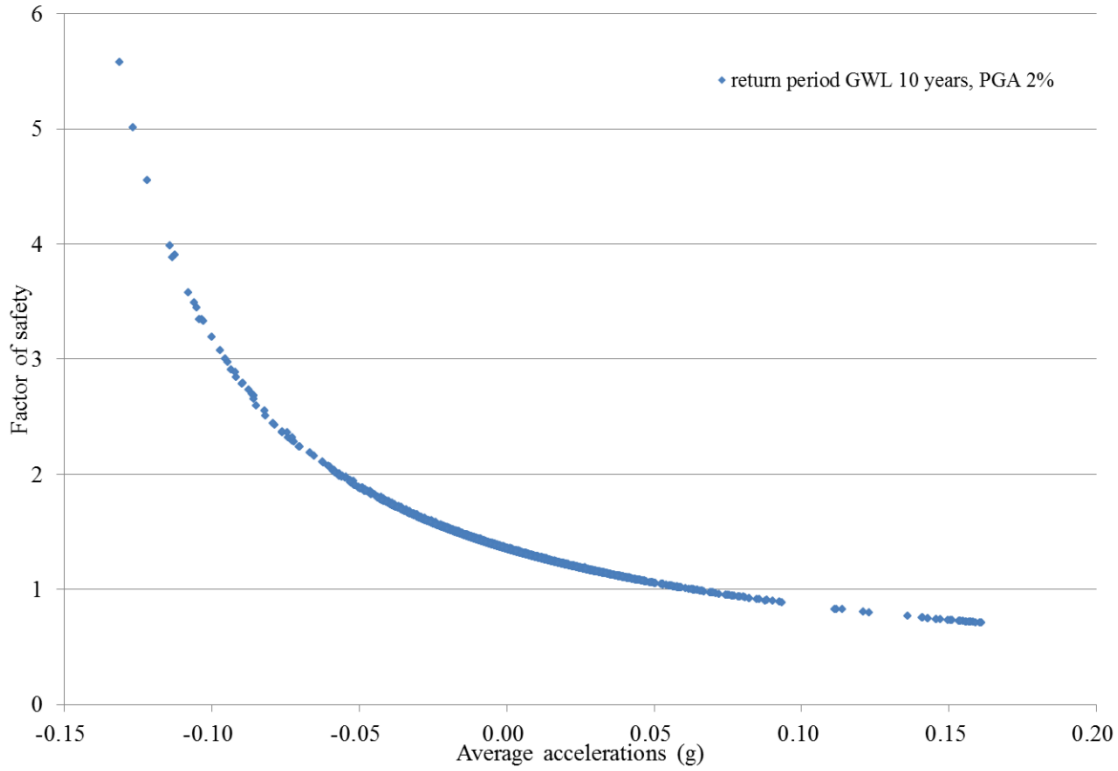

Fig. 5.12 Factor of safety vs. average accelerations

Fig. 5.13 shows the average acceleration vs. time and Fig. 5.14 shows the velocity vs. time for the slope. To calculate the amount of deformation, the area under Fig, 5.14 must be integrated. The area under Fig.5.14 comes from integration of area below the yield acceleration values in Fig.5.13 which in this case is 0.06g. The yield acceleration for every cases are different based on the input earthquake and this will give changes in the total deformation amount.

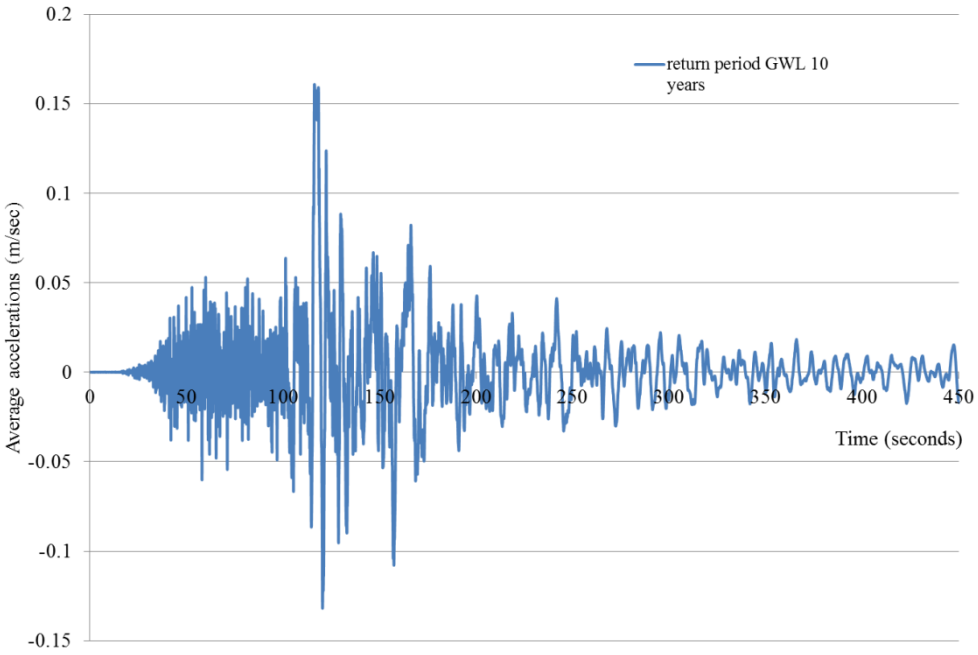

Fig. 5.13 Average acceleration vs. time

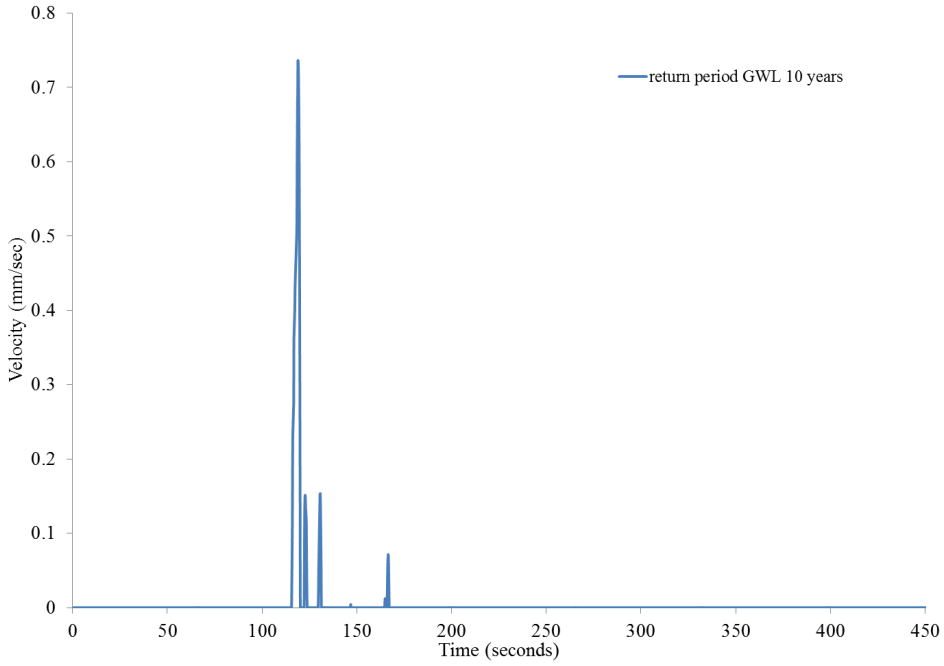

Fig. 5.14 Velocity vs. time

To determine the total deformation, area under Fig. 5.14 is integrated. Comparison can be seen in Fig.5.15 below. This graph shows the total deformation for earthquake input 0.15g but for different groundwater level. The initial groundwater level when imposed with 0.15g earthquake gave deformation on 0.214m. But when the groundwater level increases, the total deformation increases significantly until it reach 1.564m for groundwater level in 10 years return period.

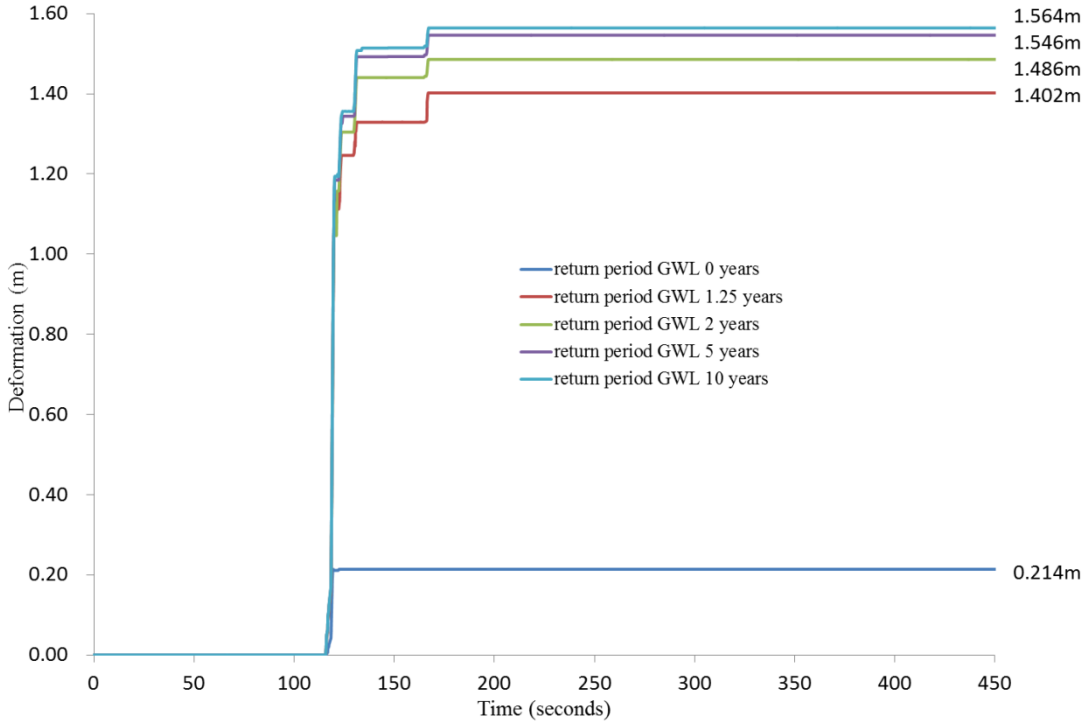

Fig. 5.15 Deformation vs. time for different ground water level (PGA 0.15g)

Fig. 5.16 shows the deformation of the same groundwater level but different PGA input. In this figure, the case is for 10 years return period of groundwater level. It can be seen that for PGA input for 40% probability of occurrences (0.05g), there is no deformation recorded.

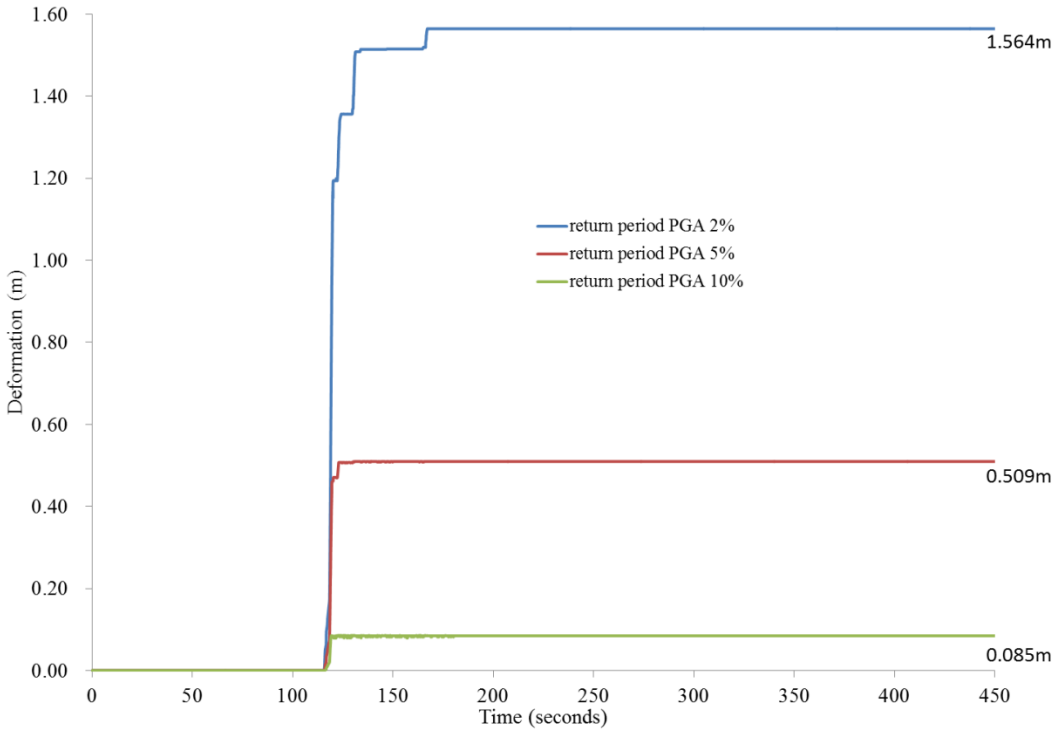

Fig. 5.16 Deformation vs. time for same PGA input

Total deformation recorded for this slope can be seen in Table 5.10. It can be seen here that for PGA of 0.05g and lower, there will be no deformation recorded. Total deformation started to increase from PGA input of 0.085g onwards. This table if compared with Table 5.7 where result of factor of safeties for static analysis, there are some similarities where the factor of safeties are lower than 1.0 for cases of earthquake input with 40% probability of exceedance and lower. The difference can only be seen in the case of PGA input with 10% probability of exceedance with initial groundwater level. In static analysis, the FOS is already lower than 1.0 but for dynamic analysis, there is no deformation recorded. This is probably due to the earthquake input, because, the earthquake input for static analysis comes from PGA values of surface map and this

surface map was analysed using 1-dimensional linear analysis where else for dynamic analysis in this chapter, we use the equivalent linear analysis.

Table 5.10 Total deformation for dynamic analysis

Earthquake input (g)	Initial groundwater level	1.25 years return period groundwater level	2 years return period groundwater level	5 years return period groundwater level	10 years return period groundwater level
0.0g	0	0	0	0	0
98 years r.p– 0.05g	0	0	0	0	0
475 years r.p – 0.085g	0	0.066m	0.076m	0.083m	0.085m
975 years r.p – 0.115g	0.018m	0.414m	0.445m	0.468m	0.509m
2500 years r.p – 0.15g	0.214m	1.402m	1.486m	1.546m	1.564m

Note: r.p = return period

5.7 Conclusions

The static and dynamic analyses on slopes on Penang Island were done in this chapter. This is part of the procedures to understand the behavior of slopes on Penang Island when it is influenced by several earthquake inputs with different groundwater level which directly resulted from different return periods of heavy rainfall (accumulated antecedent rainfall). This aim of study is achieved by analyzing each cases related to the cases of earthquake and rainfall.

In static analysis, all slopes were analyzed using the Morgenstern-Price analysis method which include the moment and force equilibrium. The aim of Morgenstern-Price method is to calculate factor of safety for non-circular slip surfaces and can

consider wide variety of surfaces with different shear strength properties. The earthquake input is considered as horizontal forces acting on the slip surface. The analysis produces the factor of safety which is an empirical number that represent whether slopes are safe or not. The threshold value of factor of safety is 1.0 where any value lowers than 1.0 means that the slope is unstable.

From the results, it can be seen that for slopes at the site of interest, when there is no earthquake effect even though increases of groundwater is visible, the slopes stay safe. But, when earthquake effects are included, the factor of safeties started to reduce significantly with increase of earthquake input (PGA). Changes in factor of safeties are also influenced by the shape of slope with different slope angle and the length of slope. It can also be seen in the analysis that there is no specific pattern to determine overall behavior of slopes at the location of interest. Each slope gives different outcomes and therefore analysis should be done in detail for each slope and overall or generalize assumption on behavior of slope when earthquake and rainfall occur simultaneously should be forbidden.

The second part of this chapter covers dynamic analysis for the slope. The dynamic analysis for a certain slope is done to determine the permanent displacement using Newmark's method and must go through several processes. The first step is the initial static analysis then followed by dynamic analysis using the result from initial static stress as initial condition and finally the Newmark's displacement analysis.

In initial static stress analysis, the groundwater level input is the same value used for each return period; the material uses the equivalent linear model. Then dynamic analysis was done for all earthquake and groundwater level input.

References

[1] M. Budhu, *Soil mechanics and foundations*. John Wiley and Sons, 2007.

[2] J. Krahn, "Stability Modeling with SLOPE/W An Engineering Methodology," no. August. 2004.

[3] N. . Morgenstern and V. . Price, "The Analysis of The Stability of General Slip Surfaces," *Geotechnique*, vol. 15, pp. 79–93, 1965.

[4] D. . Fredlund and J. Krahn, "Comparison of Slope Stability Methods of Analysis," in *29th Canadian Geotechnical Conference*, 1976.

[5] D. . Fredlund and J. Krahn, "Comparison of Slope Stability Methods of Analysis," in *29th Canadian Geotechnical Conference*, 1976.

[6] M. Sokhanvar and I. A. Kassim, "Unsaturated Shear Strength Behavior under Unconsolidated Undrained Tests," *Electron. J. Geotech. Eng.*, vol. 18, pp. 601–612, 2013.

[7] S. L. Kramer, *Geotechnical Earthquake Engineering*. 1996, pp. 438–439.

Chapter 6

CONCLUSIONS

Recent development on hillside as well as mountainous are sometimes resulted on landslides and slope failure. Landslides are associated with movement of soil with respect to gravity due to several causes such as heavy rainfall, earthquakes as well as reduction on soil strength due to human activities. It may occur in many ways such as mudflow, slope failure or soil/rock movement depending on its location. This disaster may affect not only directly to human lives but also to community surrounding depending on the size and location of the landslide.

In this study Penang Island was selected as the location of interest. In order to understand the behavior of slope under the effects of earthquake and landslide, several objectives were set prior to the study which include seismic hazard analysis of Penang Island, Malaysia, rainfall distribution on the island then followed by combination of probabilistic analysis of earthquake and rainfall on Penang Island, Malaysia. Final part of this study evaluates on the effect of earthquake and rainfall on Penang Island slopes and at the end of the day, all works must satisfy the objectives of this study. The study covers several topics which at the end are used to combine all of the analysis. Results obtained from the study are summarized as follows.

(1) In the second chapter of this study, behavior of seismicity on Penang Island was assessed. Using Probabilistic Seismic Hazard Analysis, peak ground acceleration (PGA) map for Penang Island were mapped based on 40%, 10%, 5%, and 2% probabilities of events in 50 years (98-, 475-, 975-, and 2,500-year return periods, respectively). Analysis in this chapter uses the historical data since Malaysia earthquake records are very scarce. Then, suitable attenuation relationship was chosen to be used in producing the PGA map. The PGA bedrock map was done by using results from total probability theorem. The next part in the second chapter covers the ground motion analysis using a nearby ground motion record. The ground response analysis is used to determine surface motion influenced by the soil layer beneath the surface. Then the PGA map for ground surface was made. The final results for the second chapter shows that the distributions of peak ground accelerations are highly concentrated in the lowlands, especially near the coast.

This is because amplifications on lowlands are higher than on hillsides. It can be seen that the implications are less than those in highly seismic regions. Lowland areas are at higher risk; they contain softer soils that amplify earthquake motion more than do the soil types of higher ground. This is because the soil layer are shallow, and the bedrock (granite) is located at shallow depths (high level) on the tops of hills, yielding lower amplification factors, which in turn yield lower PGA values.

(2) In the third chapter, this study tries to determine the probability rainfall analysis for Penang Island. In order to accomplish that, several steps of procedure were done which include collection of rainfall data for Penang Island, determine the suitable distribution functions that can best represent the rainfall pattern on Penang Island, test the distribution functions and finally selecting the best function.Five distribution functions were selected and they are Normal distribution and extreme condition distributions (Gumbel, Frechet, Weibull and Generalized Extreme Value). The extreme condition distribution is chosen since the data used for analysis represent extreme rainfall condition for Penang Island. To determine the best distribution function that can represent accumulated antecedent rainfall for Penang Island, goodness-of-fit tests were done. The Kolmogorov-Smirnov test, Anderson-Darling test and Chi Squared test were chosen for the analysis. These tests are most commonly used and are accepted as appropriate tests for the analysis based on previous researchers works. The most suitable distribution functions that can represent accumulated antecedent rainfall for Penang Island are GEV distribution and Frechet distribution. However, from previous researchers' work, it can be concluded that GEV is the best distribution functions to be used for Penang Island condition. The GEV distribution function is considered suitable for this study since GEV represent extreme condition and is based on combination of other three distribution functions (Gumbel, Frechet and Weibull) and will be used in the next chapter analysis.

(3) The fourth chapter provides the identification of areas that are critical with most numbers of slopes; Geographical Information System (GIS) method was used. By using ArcGIS10, Digital Elevation Model (DEM) and TIN (Triangulated Irregular Network) model were created and spatial analysis was done to produce map that shows the slopes

in degrees and in percentage (%). Slope maps for Penang Island with different cell size were created. Smaller cell represents ideal condition of the slope formation. 2 cell sizes were chosen for this study to represent Penang Island slope, 10-unit and 50-unit. The map for 10-unit cell size shows better prediction on Penang Slope than 50-unit. From the map, it can be seen that the highest angle on Penang Island is 86.6° and this is almost the same as reported by previous researcher. It can also be seen that almost 70% of the total area on Penang Island is governed with slopes with more than 16° angle and reach up to 86.6° angle. Second part of chapter four discussed about the relationship between 5-days accumulated antecedent rainfall with water heights. Using piezometer data and rainfall data from local rainfall station, a graph has been plotted and provided regression equation that will gave idea on water height when a certain rainfall amount occurred. Combining result from probability rainfall analysis in Chapter 3, gives water height result to be used in next chapter. Cumulative Distribution Function analysis was also done in this chapter and the most suitable method to represent the water height changes is GEV method. At the last part of the chapter, combination for probabilities of earthquake and groundwater level were calculated and tabulated.

(4) The static and dynamic analyses on slopes on Penang Island were done in chapter 5. In static analysis, the slope was analyzed using the Morgenstern-Price analysis method which include the moment and force equilibrium. The analysis produces the factor of safety which is an empirical number that represent whether slopes are safe or not. The threshold value of factor of safety is 1.0 where any value lowers than 1.0 means that the slope is unstable. From the results, it can be seen that for slopes at the site of interest, when there is no earthquake effect even though increases of groundwater is visible, the slopes stay safe. But, when earthquake effects are included, the factor of safeties started to reduce significantly with increase of earthquake input (PGA). Changes in factor of safeties are also influenced by the shape of slope with different slope angle and the length of slope. It can also be seen in the analysis that there is no specific pattern to determine overall behavior of slopes at the location of interest. Each slope gives different outcomes and therefore analysis should be done in detail for each slope and overall or generalize assumption on behavior of slope when earthquake and rainfall occur simultaneously

should be forbidden. The second part of this chapter covers dynamic analysis for the slope. The dynamic analysis for a certain slope is done to determine the permanent displacement using Newmark's method and must go through several processes. The first step is the initial static analysis then followed by dynamic analysis using the result from initial static stress as initial condition and finally the Newmark's displacement analysis. From the results, it can be seen that for slope at the site of interest, when there is no earthquake effect even though increases of groundwater is visible, the slopes stay safe. But, when earthquake effects are included, the factor of safeties started to reduce significantly with increase of earthquake input (PGA) and in this study, deformation can be seen to occur after the slope is imposed with ground acceleration of more than 0.085g. Changes in factor of safeties are also influenced by the shape of slope with different slope angle and the length of slope.

There are several limitations in this study which should be considered thoroughly in the future. For example, analysis of PSHA in chapter 2 was only done using 1-dimensional linear analysis since at the beginning of the research, the time was limited and to analyze whole area would be a big problem. However in chapter 5, the dynamic analysis was done using Equivalent Linear method and therefore gave a little different result when compared. In chapter 4, the location of rainfall gauge and piezometer can be considered quite far from each other and therefore assumption was made. This was supposed to be avoided in order to have a good result. Next is soil type. In chapter 5 analysis, the soil type was limited to 1 type although on Penang Island there are a lot of different soil types that can be considered in the analysis. This is due to limitation of soil data. Relevant assumptions must also be made in the case where limited records of soil layer can be found especially on hilly terrain.

APPENDIX A –List of boreholes used in analysis

Batu Ferringhi											
Borehole number	**Depth (m)**	**N-number**	**Description**	**Unit weight (g/cm^3)**	**V_s (m/s)**	**Borehole number**	**Depth (m)**	**N-number**	**Description**	**Unit weight (g/cm^3)**	**V_s (m/s)**
BH1	3.6	12	Gravelly sand	1.92	183	BH6	2.4	11	Clay	1.8	178
	6.6	28	Gravelly sand	1.94	243		2.4	50	Granite boulder	2.65	368
	8.25	35	Gravelly sand	1.95	262		1.8	20	Sandy clay	1.85	271
	9.45	44	Gravelly sand	1.97	282		0.65	32	Sandy clay	1.88	317
	5.45	50	Granite	2.65	295		5	50	Granite	2.65	368
BH2	2.4	9	Clayey sandy gravel	1.86	166	BH7	2.55	13	Sandy clay	1.85	235
	4.35	19	Sandy silt	1.88	267		3.9	24	Sandy clay	1.87	288
	6.55	33	Gravelly sand	1.92	257		7.35	50	Granite	2.65	368
	2.65	37	Gravelly sand	1.95	267	BH8	5.7	16	Sandy clay	1.79	252
	6.45	50	Granite	2.65	295		1.55	11	Silty clay	1.83	222
BH3	3	20	Silty clay	1.8	271		1.4	24	Sandy silt	1.85	288
	1.5	38	Clayey sand	1.86	336		6.6	50	Granite	2.65	368
	6.5	50	Granite	2.65	295	BH9	2.7	18	Silty clay	1.83	262
BH4	5.4	21	Gravelly sand	1.9	221		5.4	38	Clayey sand	1.86	269
	6.6	23	Gravelly sand	1.94	228		6.05	50	Granite	2.65	368

	12.3	50	Granite	2.65	295		5.7	15	Silty clay	1.83	247
BH5	2.4	11	Silty clay	1.8	178	BH10	1.8	32	Sandy silt	1.86	317
	1.8	22	Clayey sand	1.86	224		7.8	50	Granite	2.65	368
	9.3	50	Granite	2.65	295						

Batu Ferringhi

Borehole number	**Depth (m)**	**N-number**	**Description**	**Unit weight (g/cm^3)**	**V_s (m/s)**	**Borehole number**	**Depth (m)**	**N-number**	**Description**	**Unit weight (g/cm^3)**	**V_s (m/s)**
BH11	2.7	10	Clay	1.9	215	BH15	1.5	11	Clayey silt	1.87	222
	1.5	40	Clayey sand	1.88	342		4.5	16	Sandy silt	1.8	202
	7.2	50	Granite	2.65	295		3	39	Sandy silt	1.85	271
BH12	4.35	16	Gravelly sandy clay	1.93	202		4	40	Gravel sand	1.9	274
	0.95	23	Sandy silt	1.95	228		6	50	Granite	2.65	295
	6	50	Granite	2.65	295	BH16	1.5	7	Silty sand	1.8	153
BH13	1.5	10	Sandy silt	1.88	172		1.5	12	Silty clay	1.83	183
	1.2	13	Sandy gravel	1.91	188		3	14	Clayey silt	1.93	241
	2.7	28	Sand	1.95	243		3.5	25	Sandy silt	2	234
	6.6	50	Granite	2.65	295		3	50	Gravelly sand	2.1	295
BH14	1.5	5	Clayey silty sand	1.87	171		3.3	50	Very dense gravelly sand	2.3	295
	4.5	8	Clayey silt	1.73	160						
	0.6	17	Sandy silt	1.8	206						
	3	50	Granite boulder	2.65	295						
	2.4	40	Dense gravel sand	2.1	274						
	4.8	50	Sandy silt	2	368						

Tanjung Bungah											
Borehole number	**Depth (m)**	**N-number**	**Description**	**Unit weight (g/cm^3)**	**V_s (m/s)**	**Borehole number**	**Depth (m)**	**N-number**	**Description**	**Unit weight (g/cm^3)**	**V_s (m/s)**
BH1a	1.5	50	Very dense sand with gravel	1.9	295	BH6a	2	8	Loose silty sand with gravel	1.95	160
	1.5	38	Silty sand with gravel	1.85	269		1.45	7	Loose silty sand with gravel	1.99	191
	3	50	Granite	2.65	295		1.5	10	Loose silty sand with gravel	1.84	191
BH2a	2	33	Silty sand	1.8	257		2	13	Medium silty sand with gravel	1.83	191
	8	50	Silty sand with gravel	2	295		2	17	Medium silty sand with gravel	2.03	191
	3.5	50	Granite	2.65	295		1.5	21	Medium silty sand with gravel	2.01	191
BH3a	2	15	Silty sand with gravel	1.99	197		5	50	Granite	2.65	191
	1.45	16	Silty sand with gravel	2	202	BH7a	2	5	Loose silty sand	1.95	191
	1.5	32	Silty sand with gravel	2	254		1.5	8	Loose silty sand	1.95	191
	3	50	Granite	2.65	295		1.5	11	Loose silty sand	1.95	191

BH4a	2	8	Loose silty sand with gravel	2	160		5	15	Medium silty sand	2.05	191
	1.45	10	Loose silty sand with gravel	1.94	172		1	20	Medium silty sand	2.05	191
	1.5	17	Medium silty sand with gravel	1.9	206		2	25	Medium silty sand	2.05	191
	2	23	Medium silty sand with gravel	1.93	228		3	28	Medium silty sand	2.05	191
	3	50	Medium silty sand with gravel	2	295		6	50	Dense silty sand	2.15	191
	3	50	Granite	2.65	295		3	50	Granite	2.65	191
BH5a	2	10	Loose silty sand with gravel	1.95	172						
	2	12	Medium silty sand with gravel	2.03	183						
	3	50	Granite	2.65	295						

APPENDIX B – Amplification factors for all boreholes

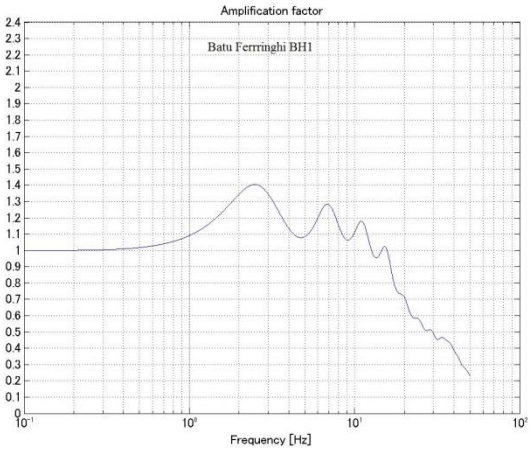

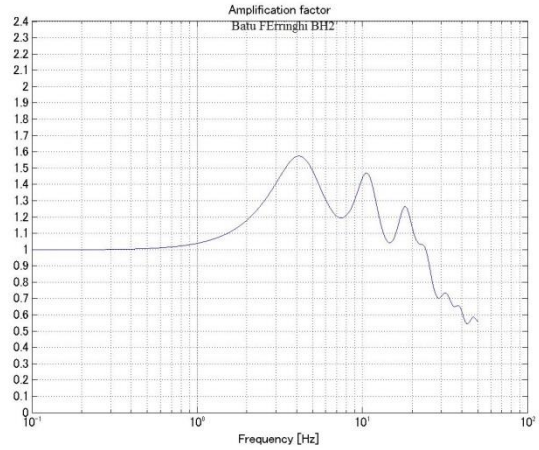

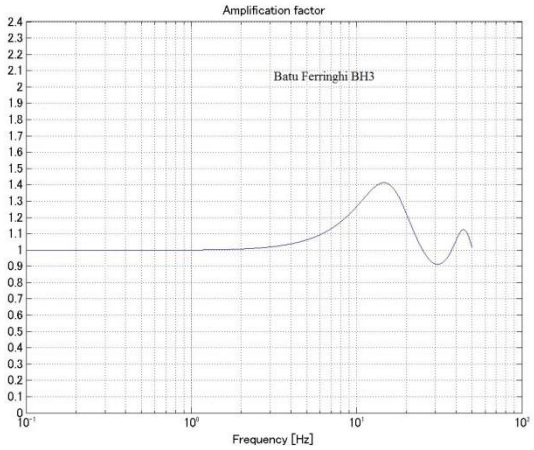

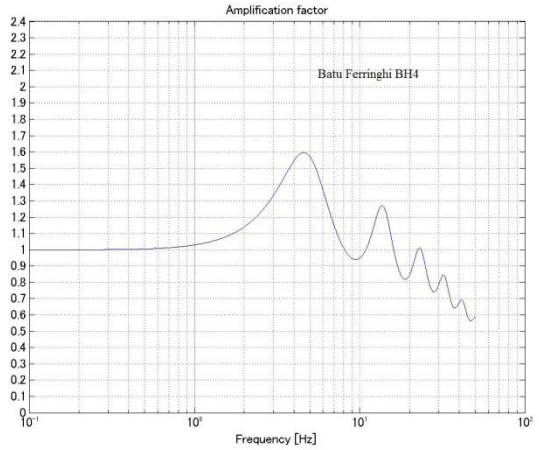

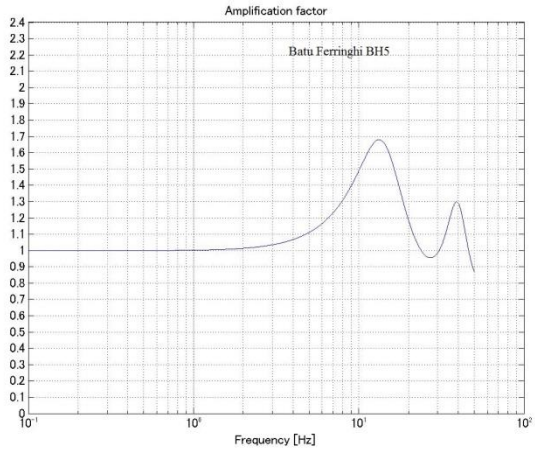

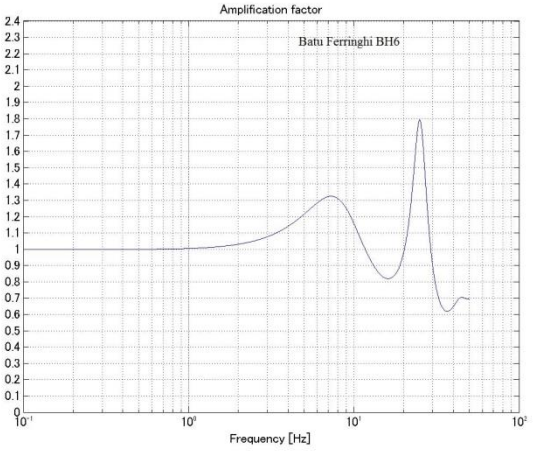

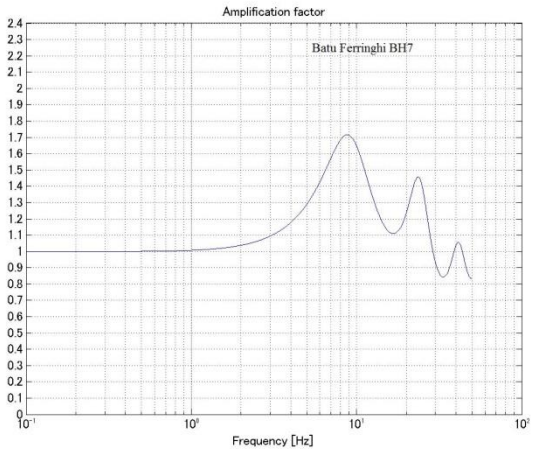
Amplification factor
Batu Ferringhi BH7
Frequency [Hz]

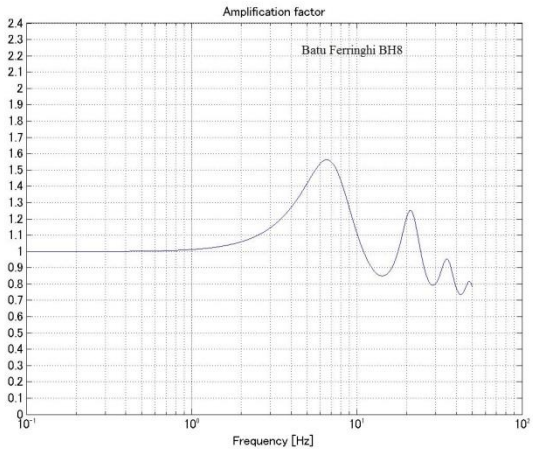
Amplification factor
Batu Ferringhi BH8
Frequency [Hz]

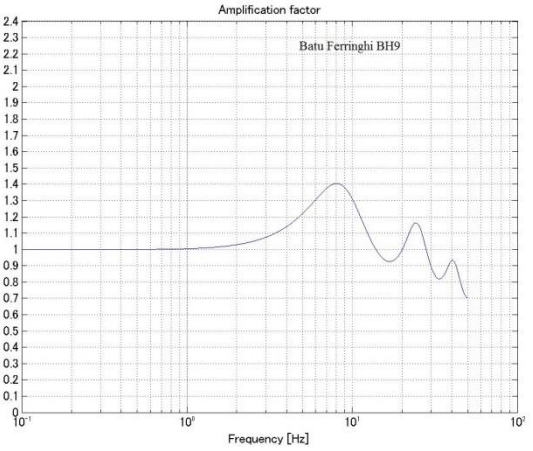
Amplification factor
Batu Ferringhi BH9
Frequency [Hz]

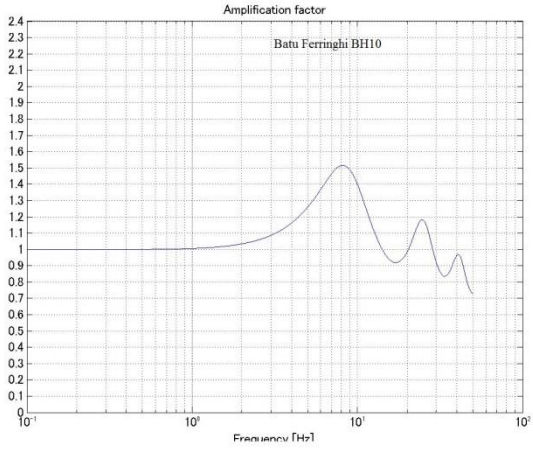
Amplification factor
Batu Ferringhi BH10
Frequency [Hz]

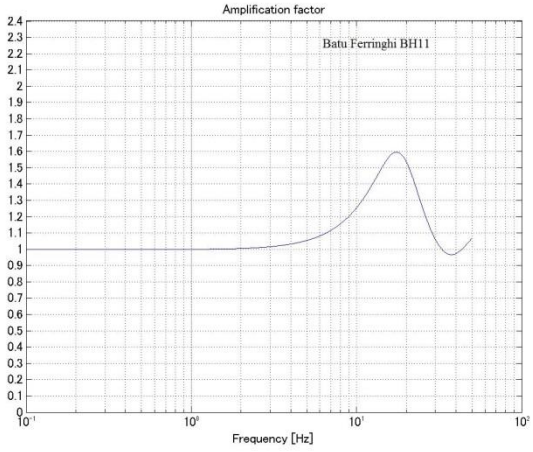
Amplification factor
Batu Ferringhi BH11
Frequency [Hz]

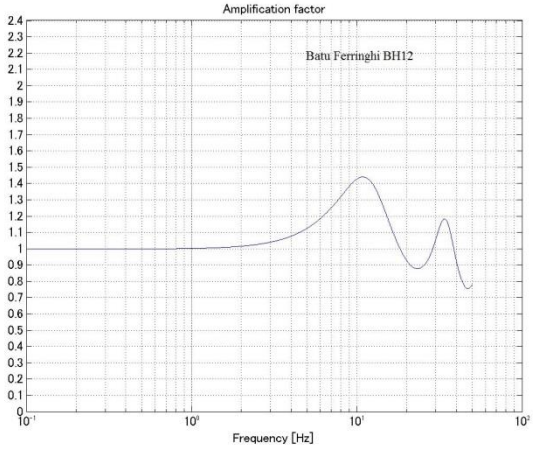
Amplification factor
Batu Ferringhi BH12
Frequency [Hz]

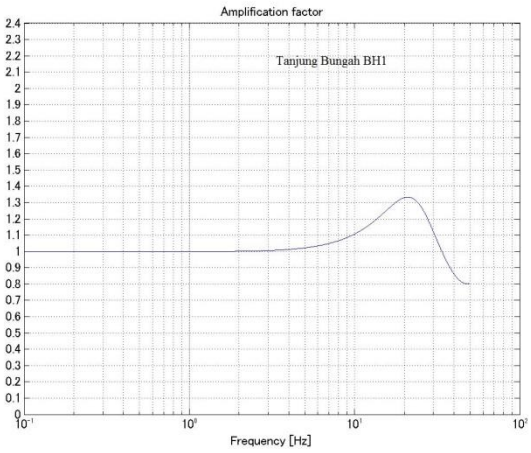
Amplification factor
Tanjung Bungah BH1
Frequency [Hz]

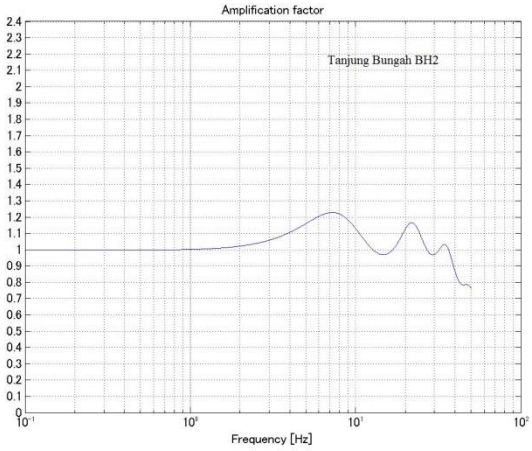
Amplification factor
Tanjung Bungah BH2
Frequency [Hz]

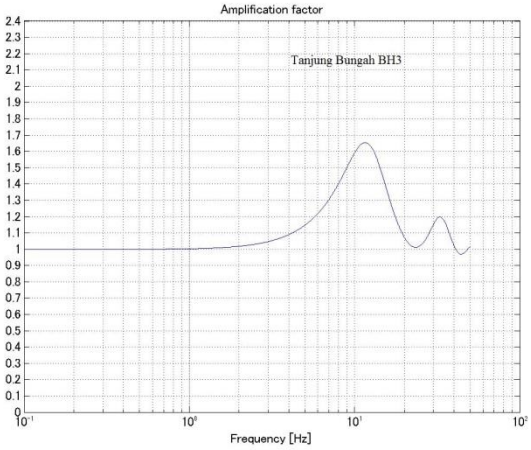
Amplification factor
Tanjung Bungah BH3
Frequency [Hz]

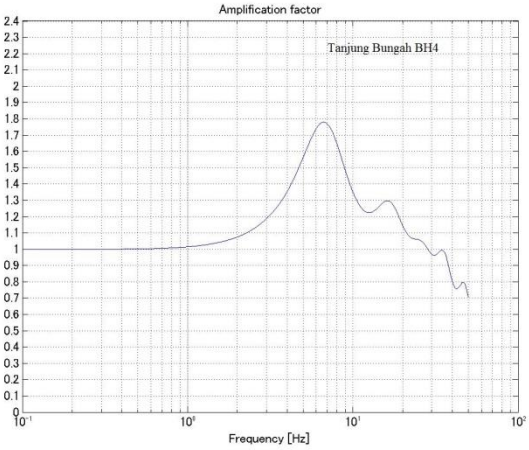
Amplification factor
Tanjung Bungah BH4
Frequency [Hz]

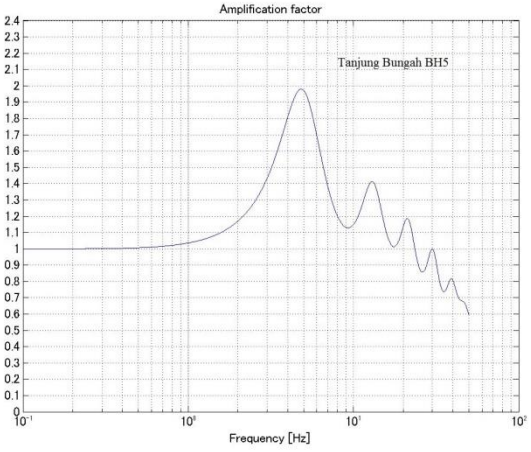
Amplification factor
Tanjung Bungah BH5
Frequency [Hz]

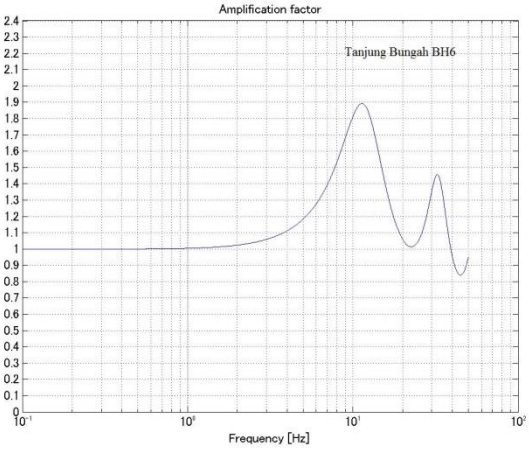
Amplification factor
Tanjung Bungah BH6
Frequency [Hz]

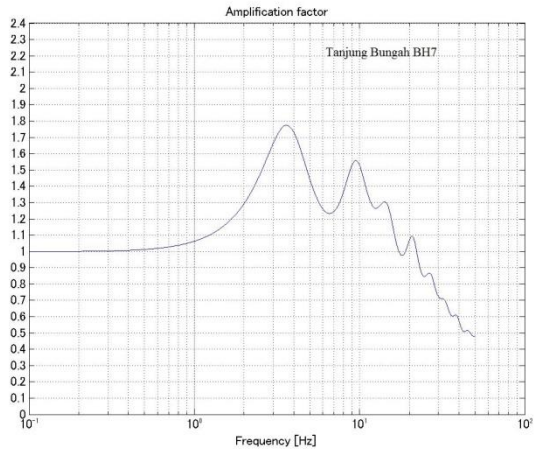
Amplification factor
Tanjung Bungah BH7
Frequency [Hz]

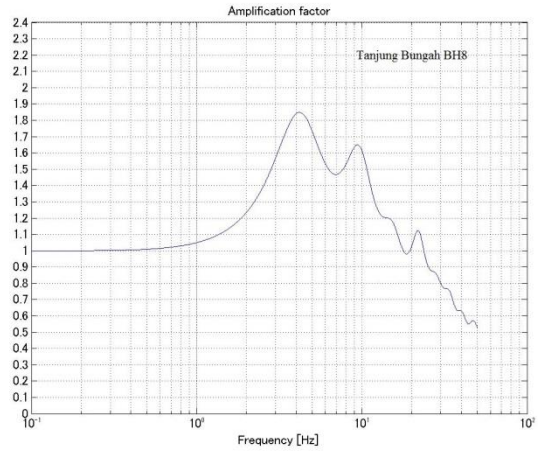
Amplification factor
Tanjung Bungah BH8
Frequency [Hz]

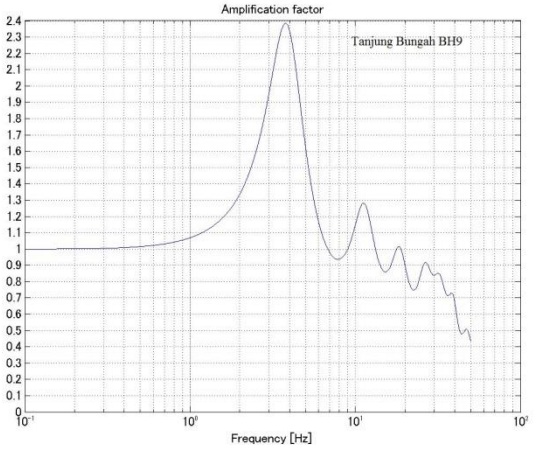
Amplification factor
Tanjung Bungah BH9
Frequency [Hz]

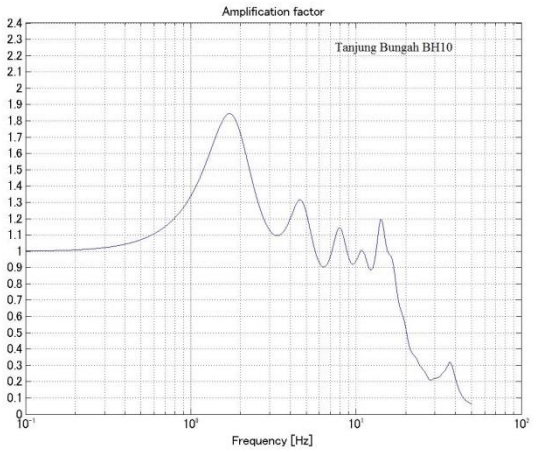
Amplification factor
Tanjung Bungah BH10
Frequency [Hz]

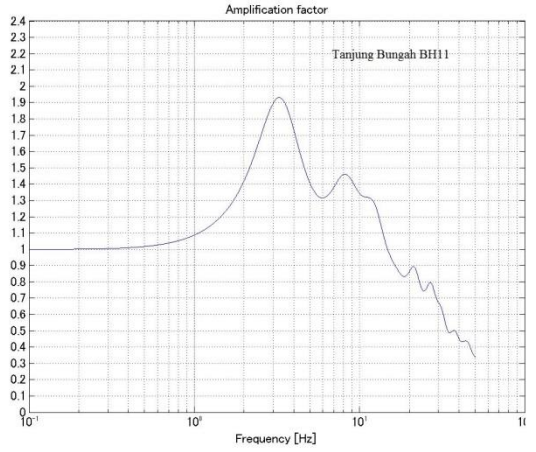
Amplification factor
Tanjung Bungah BH11
Frequency [Hz]

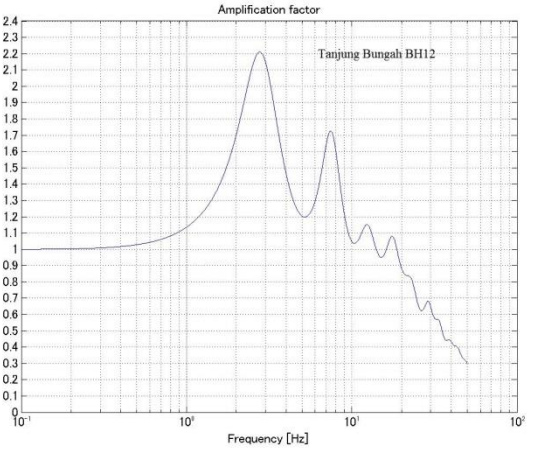
Amplification factor
Tanjung Bungah BH12
Frequency [Hz]